Towards Secure and Intelligent Diagnosis: Deep Learning and Blockchain Technology for Computer-Aided Diagnosis Systems

A Thesis Submitted to the
College of Graduate and Postdoctoral Studies
in Partial Fulfillment of the Requirements
for the degree of Doctor of Philosophy
in the Department of Computer Science
University of Saskatchewan
Saskatoon

By
Sara Hosseinzadeh Kassani

Permission to Use

In presenting this thesis/dissertation in partial fulfillment of the requirements for a Postgraduate degree from the University of Saskatchewan, I agree that the Libraries of this University may make it freely available for inspection. I further agree that permission for copying of this thesis/dissertation in any manner, in whole or in part, for scholarly purposes may be granted by the professor or professors who supervised my thesis/dissertation work or, in their absence, by the Head of the Department or the Dean of the College in which my thesis work was done. It is understood that any copying or publication or use of this thesis/dissertation or parts thereof for financial gain shall not be allowed without my written permission. It is also understood that due recognition shall be given to me and to the University of Saskatchewan in any scholarly use which may be made of any material in my thesis/dissertation.

DISCLAIMER

Reference in this thesis/dissertation to any specific commercial products, process, or service by trade name, trademark, manufacturer, or otherwise, does not constitute or imply its endorsement, recommendation, or favoring by the University of Saskatchewan. The views and opinions of the author expressed herein do not state or reflect those of the University of Saskatchewan, and shall not be used for advertising or product endorsement purposes. Requests for permission to copy or to make other uses of materials in this thesis/dissertation in whole or part should be addressed to:

Head of the Department of Computer Science
University of Saskatchewan
176 Thorvaldson Building, 110 Science Place
Saskatoon, Saskatchewan S7N 5C9 Canada

Or

Dean
College of Graduate and Postdoctoral Studies
University of Saskatchewan
116 Thorvaldson Building, 110 Science Place
Saskatoon, Saskatchewan S7N 5C9
Canada

Abstract

Cancer is the second leading cause of death across the world after cardiovascular disease. The survival rate of patients with cancerous tissue can significantly decrease due to late-stage diagnosis. Nowadays, advancements of whole slide imaging scanners have resulted in a dramatic increase of patient data in the domain of digital pathology. Large-scale histopathology images need to be analyzed promptly for early cancer detection which is critical for improving patient's survival rate and treatment planning. Advances of medical image processing and deep learning methods have facilitated the extraction and analysis of high-level features from histopathological data that could assist in life-critical diagnosis and reduce the considerable healthcare cost associated with cancer. In clinical trials, due to the complexity and large variance of collected image data, developing computer-aided diagnosis systems to support quantitative medical image analysis is an area of active research. The first goal of this research is to automate the classification and segmentation process of cancerous regions in histopathology images of different cancer tissues by developing models using deep learning-based architectures. In this research, a framework with different modules is proposed, including (1) data pre-processing, (2) data augmentation, (3) feature extraction, and (4) deep learning architectures. Four validation studies were designed to conduct this research. (1) differentiating benign and malignant lesions in breast cancer (2) differentiating between immature leukemic blasts and normal cells in leukemia cancer (3) differentiating benign and malignant regions in lung cancer, and (4) differentiating benign and malignant regions in colorectal cancer.

Training machine learning models, disease diagnosis, and treatment often requires collecting patients' medical data. Privacy and trusted authenticity concerns make data owners reluctant to share their personal and medical data. Motivated by the advantages of Blockchain technology in healthcare data sharing frameworks, the focus of the second part of this research is to integrate Blockchain technology in computer-aided diagnosis systems to address the problems of managing access control, authentication, provenance, and confidentiality of sensitive medical data. To do so, a hierarchical identity and attribute-based access control mechanism using smart contract and Ethereum Blockchain is proposed to securely process healthcare data without revealing sensitive information to an unauthorized party leveraging the trustworthiness of transactions in a collaborative healthcare environment. The proposed access control mechanism provides a solution to the challenges associated with centralized access control systems and ensures data transparency and traceability for secure data sharing, and data ownership.

Publications

Research presented in this thesis has resulted in the following publications:

Journal papers:

1. **Sara Hosseinzadeh Kassani**, Peyman Hosseinzadeh Kassani, Michal J. Wesolowski, Kevin A. Schneider, and Ralph Deters. "Automatic Detection of Coronavirus Disease (COVID-19) in X-ray and CT Images: A Machine Learning-Based Approach". (Accepted)

2. **Sara Hosseinzadeh Kassani**, Peyman Hosseinzadeh Kassani, Michal J. Wesolowski, Mark Eramian, Kevin A. Schneider, and Ralph Deters. "An Ensemble-based Deep Learning Method for Leukemic B-lymphoblast Classification". (Under Review)

3. **Sara Hosseinzadeh Kassani**, Peyman Hosseinzadeh Kassani, Michal J. Wesolowski, Kevin A. Schneider, and Ralph Deters. "Deep Transfer Learning Based Model for Colorectal Cancer Histopathology Segmentation: A Comparative Study of Deep Pre-trained Models". (Under review)

4. **Sara Hosseinzadeh Kassani**, Peyman Hosseinzadeh Kassani, Michal J. Wesolowski, Kevin A. Schneider, and Ralph Deters. "Revisiting Deep Skip Connections and Transfer Learning for Lung Cancer Segmentation in Histology Images". (In preparation)

Conference papers:

1. **Sara Hosseinzadeh Kassani**, Peyman Hosseinzadeh Kassani, Michal J. Wesolowski, Kevin A. Schneider, and Ralph Deters. Automatic polyp segmentation using convolutional neural networks. In Canadian Conference on Artificial Intelligence, pages 290-301. Springer, 2020.

2. **Sara Hosseinzadeh Kassani**, Peyman Hosseinzadeh Kassani, Reza Khazaeinezhad, Michal J. Wesolowski, Kevin A. Schneider, and Ralph Deters. Diabetic retinopathy classification using a modified xception architecture. In 2019 IEEE International Symposium on Signal Processing and Information Technology (ISSPIT), pages 1-6. IEEE, 2019.

3. **Sara Hosseinzadeh Kassani**, Peyman Hosseinzadeh Kassani, Michal J. Wesolowski, Kevin A. Schneider, and Ralph Deters. Depthwise separable convolutional neural network for skin lesion classification. In 2019 IEEE International Symposium on Signal Processing and Information Technology (ISSPIT), pages 1-6. IEEE, 2019.

4. **Sara Hosseinzadeh Kassani**, Peyman Hosseinzadeh Kassani, Michal J. Wesolowski, Kevin A. Schneider, and Ralph Deters. Classification of histopathological biopsy images using ensemble of deep learning

networks. In CASCON 2019 Proceedings - Conference of the Centre for Advanced Studies on Collaborative Research - Proceedings of the 29th Annual International Conference on Computer Science and Software Engineering, 2020. arXiv:1909.11870.

5. **Sara Hosseinzadeh Kassani**, Peyman Hosseinzadeh Kassani, Michal J. Wesolowski, Kevin A. Schneider, and Ralph Deters. A hybrid deep learning architecture for leukemic b-lymphoblast classification. In 2019 International Conference on Information and Communication Technology Convergence (ICTC), pages 271-276. IEEE, 2019.

6. **Sara Hosseinzadeh Kassani**, Peyman Hosseinzadeh Kassani, Michal J. Wesolowski, Kevin A. Schneider, and Ralph Deters. Breast cancer diagnosis with transfer learning and global pooling. In 2019 International Conference on Information and Communication Technology Convergence (ICTC), pages 519-524. IEEE, 2019.

7. **Sara Hosseinzadeh Kassani**, Kevin A. Schneider, and Ralph Deters. Leveraging protection and efficiency of query answering in heterogenous rdf data using blockchain. In Data Management and Analysis, pages 1-15. Springer, 2020.

8. Uchi Ugobame Uchibeke, **Sara Hosseinzadeh Kassani**, Kevin A. Schneider, and Ralph Deters. Blockchain access control ecosystem for big data security. In 2018 IEEE International Conference on Internet of Things (iThings) and IEEE Green Computing and Communications (GreenCom) and IEEE Cyber, Physical and Social Computing (CPSCom) and IEEE Smart Data (SmartData), pages 1373-1378. IEEE, 2018.

Statement of Contributions

Chapter 3 is based on Conference Paper [106], which describes a three-path ensemble method to extract features from histology images of breast cancer. Four publicly available datasets including BreakHis [193], Patch Camelyon (PCam) benchmark dataset [209, 37], Bioimaging 2015 [2] and ICIAR 2018 [32] are used to validate the performance of the proposed architecture in this chapter. My contributions to this manuscript were: 1) deep neural network method design and development 2) conducting the image pre-processing 3) implementation of the experimental design and 4) writing and editing the manuscript and figures.

Chapter 4 is based on Conference Paper [105], which describes an automated deep learning-based method to distinguish between immature leukemic blasts and normal cells. Data used in preparation of this chapter were obtained from ISBI 2019 provided by SBILab which is available for public at [4]. My contributions to this manuscript were: 1) model development and technical design, 2) conducting the image pre-processing, 3) implementation of the experimental design, and 4) writing and editing the manuscript.

Chapter 5 describes a deep learning-based encoder-decoder architecture to automatically segments out the lung tumor from histology images. Data used in preparation of this chapter were obtained from ACDC-

LungHP [126] dataset available at [1]. My contributions to this manuscript were: 1) model development and technical design, 2) conducting the image pre-processing, patch extraction, and data cleaning, 3) implementation of the experimental design, and 4) writing and editing the manuscript and figures.

Chapter 6 describes a comparison study of performances and characteristics of a wide variety of deep learning-based architectures for tumor segmentation of colorectal tissue samples. The effectiveness of incorporating deep modules and transfer learning in the encoder part of a segmentation architecture is highlighted in this study to test the generalization ability of the proposed approach in histology image analysis. Data used in this manuscript were obtained from DigestPath [123] available at [5]. My contributions to this manuscript were: 1) model development and technical design, 2) conducting the image pre-processing, patch extraction, and data cleaning, 3) implementation of the experimental design, and 4) writing and editing the manuscript and figures.

Acknowledgements

I would like to express great appreciation to my supervisors, Dr. Ralph Deters and Dr. Kevin Schneider for their supports on this PhD research throughout the duration of my PhD. They allowed me to pursue my interests in my study and research for the last three years.

I would like to especially thank Dr. Mike Wesolowski for his continuous support, valuable advice, and mentorship throughout my graduate studies. Without his support, my achievement would not be so much in the journey of pursuing my Ph.D.

I also would like to express my sincere gratitude to Dr. Behrouz Shabestari (NIBIB) for introducing me to the field of deep learning and medical image analysis.

A deep and heartfelt thanks, to Ifeoma and Farhad, for all the help and guidance they provided me.

I also appreciate the helps and collaborations of my colleagues, friends and family during my PhD studies. A lot has happened during these last few years as a graduate student and their love and support has been unwavering.

Finally, I am grateful to my committee supervisory members for reviewing this dissertation especially Dr. Gordon McCalla and also Dr. Kevin Schneider for their time and helpful comments.

Dedication

This thesis is dedicated in memory of my father, Mehdi (1955-2017).

Contents

List of Tables

List of Figures

List of Abbreviations

1D	One dimensional
2D	Two Dimensional
ABE	Attribute-based Encryption
ACC	Accuracy
ACL	Access Control List
AdaBoost	Adaptive Boosting
ALL	Acute Lymphoblastic Leukemia
AML	Acute Myelogenous Leukemia
ANN	Artificial Neural Network
AUC	Area Under the Curve
CAD	Computer Aided Diagnosis
CLL	Chronic Lymphocytic Leukemia
CNN	Convolutional Neural Network
CML	Chronic Myeloid Leukemia
CBC	Complete Blood Count
CP-ABE	Ciphertext-Policy Attribute-Based Encryption
CRC	Colorectal Cancer
CT	Computed Tomography
ConvNet	Convolutional Neural Network
DT	Decision Tree
EHR	Electronic Health Record
EMR	Electronic Medical Record
FCN	Fully Connected Network
FN	False Negative
FP	False Positive
FPN	Feature Pyramid Network
GPU	Graphic Processing Units
H&E	Hematoxylin and Eosin
HIBE	Hierarchical Identity-based Encryption
ILSVRC	ImageNet Large Scale Visual Recognition Challenge
kNN	K nearest neighbor
ML	Machine Learning
MLP	Multi-Layer Perceptron
MR	Magnetic Resonance
MRI	Magnetic resonance imaging
MSE	Mean Squared Error
NoSQL	Not only SQL
PET	Positron Emission Tomography
PHR	Personal Health Record
PKI	Public Key Infrastructure
POET	Proof of Elapsed Time
PoS	Proof of Stake
PoW	Proof of Work
ReLU	Rectified Linear Unit
RF	Random Forest
RGB	Red-Green-Blue
ROI	Region of Interest
SE	Squeeze-Excitation
SVD	Singular Value Decomposition
SVM	Support Vector Machines

TN	True Negative
TP	True Positive
WHO	World Health Organisation
WSI	Whole Slide Image
XGBoost	eXtreme Gradient Boosting

1 Introduction

1.1 Motivation

Cancer is the second leading cause of death across the world after cardiovascular disease, with 9.6 million deaths in 2018, according to the annual report provided by world health organization (WHO) [3]. Cancer is responsible for about 1 in 6 deaths globally and approximately 70% of cancer-related deaths is in low- and middle-income countries. Cancer happens when normal cells transformed into tumor cells leading to abnormal cell division. The progress of cancer is in a multistage form, generally from a pre-cancerous lesion to a malignant tumor. The formation of cancer can happen by the interaction of a person's genetic factors and three categories of external agents, including physical carcinogens, chemical carcinogens, and biological carcinogens. More than 90% of high-income countries reported treatment services are generally available compared to less than 30% of low-income countries in the public sector. The economic impact of cancer also is significant and is increasing. The costs of cancer care for the year of 2020 were estimated and projected to be $207 billion with a rapidly growing trend. This estimate represents a 66% increase from 2010, which is considered highly significant [139].

Obtaining an early and reliable cancer diagnosis from medical images plays an essential role towards the effective treatment planning of cancer and patient care. With the advancement of technology over the past few decades, a variety of medical imaging modalities, including X-ray, computed tomography (CT), Cardiac Magnetic Resonance (CMR) imaging, magnetic resonance imaging (MRI), echography, histology, ultrasound scanning, etc, are available for early detection, diagnosis and prognosis of cancer [43].

Taking biopsy samples from abnormal or suspicious tissue is a pre-requisite step in diagnosing many different types of cancer with a more precise examination and studying the manifestations of disease. The histology assessment of biopsy slides is considered as the current gold standard for cancer diagnosis. Histology, also known as microscopic anatomy or micro-anatomy, is the study of microscopic examination of tissue samples through a microscope. However, interpretation and an accurate diagnosis from histopathology images taken from patients depends on experienced pathologists. With the recent advances of techniques in automated tissue processing and imaging of slides, the speed for producing histology slides has increased dramatically. The large-scale histopathology images need to be analyzed promptly for early cancer detection which is critical for improving the patient survival rate and proper treatment planning.

Modern digitizing allows pathologists to observe digital biopsy slides on a computer with a high magnification level for tissue analysis rather than through a microscope. Also, digitized histology images provides

the advantage of employing image processing and machine learning methods for different medical image analysis tasks, including quantitative analysis, segmentation and detection, to assist pathologists in the diagnostic pathology workflow [50, 65, 88]. The manual searching and examination process of cancerous tissue from large-scale histopathological images through the conventional methods is a challenging task since it is expensive, labor-intensive, error-prone, time-consuming and also requires expert pathologists [158].

Hand-crafted features, based on limited low-level information, are easily vulnerable to different variations of noise and artifacts present in the input images. Extracting low-, mid- and high-level contextual information [86] by deep learning methods helps build a more robust computer-aided diagnosis (CAD) systems to assist in accurate detection of disease and treatment of patients. Nowadays, designing sophisticated hand-crafted features that requires domain expertise is replaced by automatically feature extraction approaches using deep learning-based methods.

Deep learning is an improvement to classical artificial neural networks where deep architectures formed by a sequential convolutional layers are able to learn non-linear hierarchically discriminative representations from input data [26, 177]. Deep learning offers an end-to-end learning mechanism that learns directly from input data through a self-learning paradigm without the need of designing hand-crafted features. Compared to traditional hand-crafted feature-based approaches, deep learning methods can rapidly learn informative features in a task-driven manner and obtain improved performance. Accurate detection and segmentation of cancerous regions from large-scale histopathology slide images using deep learning methods are highly demanded in digital pathology to aid and accelerate the diagnosis process. Some examples of Hematoxlin & Eosin-stained tissues of lung cancer, colorectal cancer and breast cancer is illustrated in Figure 1.1.

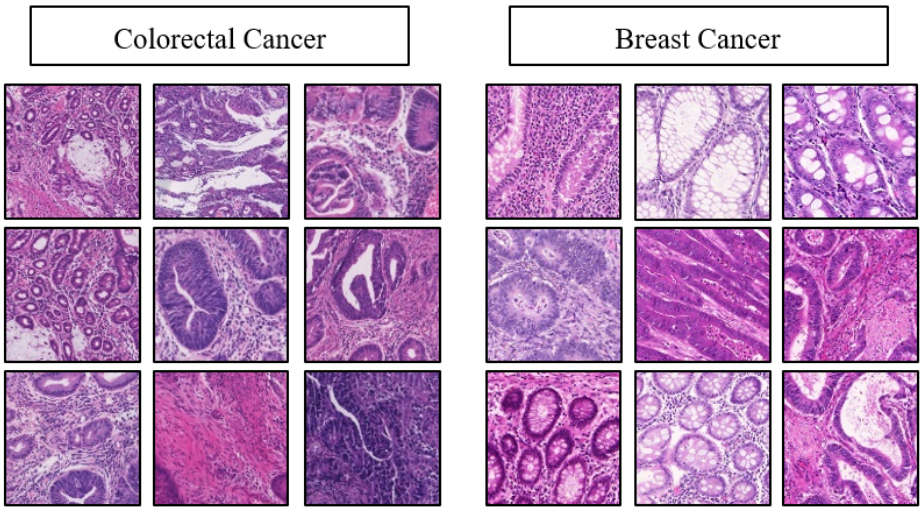

Figure 1.1: Hematoxlin & Eosin-stained samples of two types of tissue; colorectal and breast cancer. Histology images are adapted from [193], [209], [37], [32], [123].

1.2 Problem Statement

Due to the advancement in modern technologies in medical imaging acquisition systems, large amounts of medical data are generated in recent years. Medical image analysis is currently experiencing a paradigm shift due to deep learning. Deep learning, an extension to classical neural networks, achieved the state-of-the-art performance in different visual recognition tasks. Although deep learning techniques achieve promising results in finding hidden patterns in different medical applications, the current deep learning state-of-the-art methods face some serious challenges in developing computer-aided diagnosis systems. In this section, the major challenges faced in the era of applying deep learning methods for medical image analysis tasks are discussed.

1.2.1 Lack of Annotated Data

The robustness of the state-of-the-art deep learning models usually depends on the training of millions of parameters, specifically very deep networks with more layers and modules. However, designing deep models with a large number of parameters raises the need for large annotated datasets. Training deep models using a small number of labelled training samples is prone to the over-fitting problem, resulting in poor generalization ability. Deep learning models are highly sensitive to the weights or the number of training samples that adequately cover data characteristics. However, providing adequate annotated medical data requires a high level of specific expertise, which is a difficult and time-consuming task [215] [28].

1.2.2 Imbalanced Data

Another challenge in medical image analysis is the problem of class imbalance of data samples which commonly occurs in medical image analysis tasks. For example, a dataset collected for training a model of lung cancer detection may contain a limited number of malignant samples while a large number of images are benign or healthy samples. Training deep networks with data that is skewed towards one class can cause an unstable model which is biased towards the class with a large number of samples. Considering the limited number of occurrences of positive samples (cancerous cases), the class imbalance issue has a negative impact on training deep learning models. In this case, trained models tend to have a better performance on the classes with a large number of samples, and poor performance for the classes with a small number of samples. Several methods have been proposed in the literature to address the class imbalance problem and ensure a uniform class distribution including i) balancing class distribution using data augmentation techniques to increase samples of the minority classes, ii) developing methods based on weighted loss function to penalty the misclassified minority class samples [28] [148].

1.2.3 Medical Data Management

Another major challenge in medical image analysis is to deal with the heterogeneity of medical data. In recent years, the digital world has experienced a massive amount of data being captured with many different formats. Accordingly, medical data management has emerged for storing, managing and extracting valuable knowledge from collected data. Hence, developing a framework to manage the issue of data heterogeneity collected from multiple sources is a critical need for a robust automated analysis tool.

1.2.4 Security and Privacy Issues

The large amount of data available in healthcare settings also have made security critically important. The gap between data processing and security requirements has given rise many issues and concerns. An attacker may attempt to obtain unauthorized read/write permissions against the stored data objects or attempt to reveal or derive the credentials of account owners. Authorization is highly important when private and sensitive data is stored in a multi-user environment, as insufficient authorization and access management system allows attackers to gain access to data and compromise the consistency of the system [215] [125]. The traditional access control systems suffer from the problem of central authority as a third-party is responsible to delegate or revoke access to multiple entities. Considering the rise of cloud computing platforms for collaborative healthcare ecosystems and the increasing number of participants, Blockchain technology with decentralization and transparency features can enable a secure data ownership and management system. However, Blockchain applications in healthcare are an extremely fast-moving and at initial stage of maturity—a number of potential research limitations and challenges discussed below.

- Most of the studies implemented the Blockchain was limited to laboratory or simulation testing. However, real-world demonstrations are needed for the evaluation of the proposed solution for large-scale healthcare data management.
- Blockchain employs hashing to protect data, however, for a secure medical data sharing between patients and healthcare providers, access control methods such as identity, role or attribute-based access control designed on the top of Blockchain can ensure data is not falsified, modified or accessed incorrectly while being transferred between participants.
- Interoperability between different healthcare centers (e.g. hospitals) is another challenge that need to be addressed as each hospital uses different standards for data structure and security policy implementation. This issue complicates the data access verification across the nodes in the cross-organizational networks. Defining unified standards and protocols for data modelling and access policies can facilitate interoperability across networks.

Motivated by the advantages of Blockchain technology in healthcare data sharing frameworks, an artificial intelligence (AI) framework integrated with Blockchain technology would be a solution to address the current

challenges in a healthcare network. Integrating Blockchain technology with AI systems not only provides an opportunity to advance deep learning and transfer learning techniques to develop an effective and secure distributed predictive analytics but also solves issues such as:

- **Identity and Data Ownership Management**

  Identity management and authenticity verification of users is critical for protecting medical data. For example, an organization should be able to verify the identity of an entity to determine if it is the rightful owner of data or an authorized user to have access to data. Ownership management is mainly used for proving true ownership and traceability of data access rights. In current systems, data ownership management has several major problems: (1) data verification and management ownership, (2) transaction security and reliability, (3) privacy protection [133], and (4) repudiation of data or transaction. Using Blockchain, ownership of data or transaction is written on the blocks that are provably immutable. In this way, Blockchain audits and tracks the ownership through hashing algorithms and timestamps.

- **Privacy Protection**

  Privacy issues are another main challenge that hinders the development of big data. Sharing data between multiple entities complicates the process of maintaining privacy. Privacy issues involving healthcare and personal data need to be carefully addressed to protect the integrity and confidentiality of sensitive data from major losses. The integration of AI with privacy protection and trust mechanisms supported by Blockchain could improve the advancement of automation in big data platforms enabling to effectively preserve data privacy of patients in real-world healthcare solutions. Furthermore, Blockchain can solve the problem of anonymity on the identification of the users of the conventional system without a third-party intervention.

- **Data Provenance**

  Establishing provenance of data is another challenge of the current systems as data access in healthcare platforms has become more complicated due to the numerous entities in the patient's diagnosis and treatment process. The current computer-aided diagnosis systems focused more on developing novel predictive models. However, it is necessary for a medical data owner to be aware of its data access requests, i.e. history of transactions (how data is used), and data movements through one user to healthcare providers (who used data) to further enhance the trustworthiness as well as the security of the access control scheme. Utilizing the distributed ledger with an immutable access log of transactions enables to trace data provenance.

- **Access Control Management**

  Another primary challenges of data sharing is access control management. The central point of failure is one of the main issues in the current centralized systems that should be avoided as a single entity

manages access control policies that might become a bottleneck for security. This challenge becomes even more important when it comes to the sensitive and personal data as the violator needs to breach on only a single central third-party validator. All these highlights the need for robust and resilient security solutions to specify fine-grained access control policies. To emphasize these considerations, decentralized solutions without any trusted central authority are proposed for granting access rights and permissions to overcome the risks associated with centralized architectures. The main idea behind of adopting decentralized services is to avoid relying on third-parties for authorizing and granting access to a user to have access the system. Blockchain as a distributed ledger by benefiting from smart contracts allows a data owner to enforce the access control policies and grant permission. In this manner, the patient takes full responsibility for the preservation of the privacy and security of its own medical and personal records. The miner nodes in the Blockchain network check the identity and attributes of data requester and if it matches the patient-defined smart contract, the permission to access an data entity will be granted. Furthermore, the trained AI models can act as the predictive engine and be deployed on web services for providing online predictions (such as aiding doctors in their diagnosis, and so forth) which is also necessary to protect trained models from misuse and theft.

1.3 Research Questions

In the previous studies published in the literature, automatic cancerous tissue segmentation and detection methods are often based on transfer learning, pre-trained networks and also custom-designed architectures. Development of models by employing hand-crafted features also is discussed in a variety of studies. Considering the large variation of structures in color, and heterogeneous textures in histopathology images, employing hand-crafted features, which are often based on low-level features, are computationally intensive and require elaborate fine-tuning that could introduce complexity to the model. Besides, a number of visual characteristics such as variations in the sources of acquisition device and different protocols in stain normalization can adversely affect the performance of a deep convolutional neural network (CNN). The first part of this research aims to address the following research questions:

- What deep CNN architecture can efficiently extract features of shape, heterogeneous textures and morphological characteristics from the histopathology images collected across multiple sources?
- Given the reliability of digital pathology imaging, what margins of accuracy are necessary for a deep learning model to predict the malignancy level of cancer?
- Since the feature extraction is an important step in medical image analysis, how accurately can tumor regions be distinguished from non-cancerous areas using extracted features?

Traditional healthcare data sharing schemes mainly have relied on the architecture of the network and

also storage providers. Both network architectures and storage providers need a centralized trusted third-party to manage data. For example, a hospital stores a large amount of patients' personal and health data in its data center or using cloud storage. The transfer of data between different parties such as patient, doctors, researchers, and other healthcare providers is enabled by a central hub node and if the hub node is attacked, patients' data are compromised. Another main challenge of the existing architecture is the issue of single point of failure when the central party is unavailable to operate correctly and provide timely services. Therefore, the second aim of this research is to address research questions related to data availability, provenance and access control management:

- How to provide a flexible attribute-based access control to users to fully control their own data without the involvement of a trusted third-party validator to avoid bottleneck and single point of failure?
- How to manage keys and data in a dynamic collaborative environment with healthcare providers and patients using a decentralized approach to achieve improved security and enhanced privacy?
- How to guarantee fine-grained access control over data using an attribute-based scheme for electronic health record management and also trained deep learning models?
- How to ensure that the patient's data are stored securely and can be accessed only according to the patient policies in a fast manner?

1.4 Thesis Objectives and Contributions

With the recent advances of techniques in the area of deep learning and medical image processing, the new opportunities for automated tissue processing from histology slides have increased dramatically. CAD systems, integrated with medical image processing and machine learning methods, could be considered as the second opinion to decrease misdiagnosis (false positive or false negative) error rates and also considerably reduce the heavy workload of manual diagnosis on pathologists. Over the past decade, developing automated CAD systems using deep learning approaches has drawn considerable attention by achieving more and more success on various biomedical image analysis tasks [176] [31] [124] and even outperforming the performance of physicians [19] [42]. However, the process of cancer detection from stained Whole Slide Images (WSIs) is challenging. The primary challenges are due to inter- and intra-observer variability and operator dependency, inter-region similarity, and intra-regional variability within the images, which adversely affects the reproducibility of a diagnosis. The advances of deep learning methods can facilitate the extraction and analysis of high-level features from histopathology data and alleviate the aforementioned challenges. To do so, a pipeline with different modules including (1) data pre-processing, (2) data augmentation, (3) feature extraction, and (4) deep learning architectures is designed. First, the efficiency of standard deep learning architectures is evaluated based on the

performance of various feature extractors such as InceptionV3, Xception, ResNet, VGGNet, MobileNet, and DenseNet, as well as SE-ResNeXt. Then, based on the obtained results, deep ensemble models are developed and the depth and layers of different convolution modules of the proposed architecture is optimized. To improve the performance of the proposed model, different techniques such as hyper-parameter optimization and grid-search is employed. To evaluate my findings, four validation studies were designed to conduct this research, including: (1) differentiating benign and malignant lesions in breast cancer (2) differentiating between immature leukemic blasts and normal cells in leukemia cancer (3) differentiating benign and malignant regions in lung cancer, and (4) differentiating benign and malignant regions in colorectal cancer.

Another significant challenge in healthcare applications is responding to cyber-based attacks and securely processing data without revealing sensitive data to an unauthorized party. To address the problem of access control management, a fine-grained attribute-based access control scheme is proposed to allow data owner securely share data using access rules defined based on users' attributes and only users whose attributes match the policies is able to have access to the patient data and trained deep CNN models. In the proposed model, the actual personal health records are stored in the health center distributed database and the access log and meta-data are stored in Blockchain. This research is conducted in three phases.

- **Phase 1:** Create an automatic image analysis pipeline for four typical histopathology medical analysis tasks, including colorectal, breast, bone marrow and lung cancer. The proposed pipeline includes:

  i Necessary image pre-processing steps required for generating relevant features in regard to the challenges of crowded nuclei and massive background clutter;

  ii Design, train, and validate automated detection and segmentation models using deep learning-based architectures to investigate the tumor properties and different grades of tumor (benign and malignant tumors).

- **Phase 2:** Design and develop an end-to-end computer-aided diagnosis tool for digital pathology image analysis using the models trained from Phase 1. The proposed CAD tool include different modules for data preparation, data augmentation, data normalization, deep learning model, and data visualization.

- **Phase 3:** The attribute-based access control scheme integrated with Blockchain technology to leverage the trustworthiness of transactions in healthcare setting and address the issues of privacy, provenance and data access for patients' personal and medical data.

1.5 Outline of the Thesis

This thesis is divided into eight chapters. Chapter 1 provides the overall introduction to this thesis which includes motivation and background of this research.

Chapter 2 provides a detailed literature review of deep learning applications in medical image processing. Convolutional neural networks techniques and machine learning approaches used for computer-aided diagnosis, including image classification and segmentation is discussed. Also, the background related to Blockchain technology is provided, focusing on the motivations, the literature in this field, and summary of studies on Permissioned, Consortium and Permissionless Blockchain.

Chapter 3 to 6 presents four validation case studies conducted. In respective order, these chapters review studies related to breast cancer (chapter 3), leukemia B-lymphoblast cancer (chapter 4), lung cancer (chapter 5) and finally, the colorectal cancer (chapter 6). Each chapter follows the format required for publication e.g. abstract, introduction, motivation and the goal of the study, contributions, and the methods to conduct the study are highlighted. Also a detailed description of results, a discussion of the findings and conclusion is discussed.

Chapter 3 presents technical details of methodological pipeline proposed for breast cancer classification. In this chapter an ensemble deep learning-based method is proposed using three pre-trained CNNs, namely VGG19, MobileNet, and DenseNet for automatic binary classification of breast histology images. The features extracted from the proposed method then fed into a multi-layer perceptron classifier to carry out the classification task. This chapter provides a description of different pre-processing steps including stain-normalization, data augmentation, hyper-parameter tuning, and fine-tuning to train the model. The performance of the proposed method is validated on four publicly available datasets, namely, ICIAR, BreakHis, PatchCamelyon, and Bioimaging.

Chapter 4 presents the proposed solution for computer-aided leukemia cancer diagnosis. The proposed deep learning-based method is a hybrid method using VGG16 and MobileNet architectures to distinguish between immature leukemic blasts and normal cells. Different methods such as transfer learning and various data augmentation is employed to accelerate the learning process and further improve the performance of the proposed network.

Chapter 5 presents the proposed solution for segmenting lung cancer from histopathology tissue images. To perform the segmentation task, a CNN-based encoder-decoder architecture with skip-connections is designed for lung cancer tissue segmentation to delineate the fine-grained structure of the histopathology images. On the proposed backbone, four skip-connections with concatenation operation are established to link the lower layers and upper layers of network. The integration of batch normalization technique helps alleviate internal covariant shift and over-fitting issues. The feasibility of transfer learning strategy of 14 state-of-the-art feature extractors are introduced to the encoder part of the proposed architecture.

Chapter 6 investigates the performance of a wide variety of deep learning-based architectures for automatic tumor segmentation of colorectal tissue samples. The proposed approach highlights the utility of incorporating CNN modules and transfer learning in the encoder part of a segmentation architecture for histopathology image analysis. Transfer learning strategy is employed to accelerate the learning process and further improve the performance of the proposed network. A comparative and extensive experiment was conducted on a challenging histopathological segmentation task to demonstrate the effectiveness of the incorporating deep modules in the segmentation encoder-decoder network as well as the contributions of its components.

Chapter 7 highlights the challenges related to access control management, provenance and data privacy of medical data using attribute-base encryption and Blockchain technology. Motivated by the advantages of Blockchain technology in healthcare data sharing frameworks, the focus of the second part of this research is to integrate Blockchain technology in computer-aided diagnosis systems to address the problems of managing access control, authentication, provenance, and confidentiality of sensitive medical data. This chapter discusses a hierarchical identity and attribute-based access control mechanism using smart contract and Ethereum Blockchain to securely process healthcare data without revealing sensitive information to unauthorized party leveraging the trustworthiness of transactions in a collaborative healthcare environment. The proposed access control mechanism provides a solution to the challenges associated with centralized access control systems and ensures data transparency and traceability for secure data sharing, and data ownership.

Finally, Chapter 8 provides the conclusions of this research and proposes directions for future work.

2 Literature review

This chapter aims at presenting an overview of recent studies on different components of this research. The first part of this review focused on medical image classification, and segmentation tasks using deep learning methods in computational pathology. This is followed by blockchain studies targeting healthcare are also reviewed.

2.1 Deep Learning Methods in Cancerous Tissue Recognition

2.1.1 Classical Neural Network

An artificial neurons network (ANN), inspired by a biological neuron, consists of layers of neurons wherein the neurons receives inputs from the input layer and compute output values. A neuron (sometimes called a node or unit) is the fundamental computational element. ANNs are constructed of one or more layers of neurons, called hidden layers. When a neuron receives inputs, internal parameters including weights and bias are learned and adjusted during training process. Figure 2.1 illustrates the architecture of a multi-layer neural network. The first layer in the input layer. The next two layers are hidden layers and the last layer is the output layer.

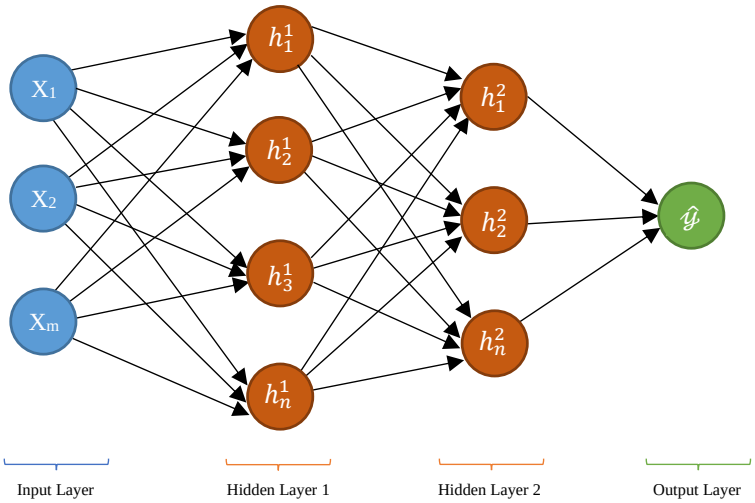

Figure 2.1: An example of the architecture of a multilayer neural network.

The basic structure of a neural network is composed of five components:

– The input layer

– A number of hidden layers of neurons

– The output layer

– Activation function for each hidden layer of neurons to decide information of which neurons should be passed to the subsequent layers.

– A loss function to minimize the error of the network

2.1.1.1 Perceptron

The perceptron, invented in 1957 by Frank Rosenblatt [179], is a linear model for binary classification tasks. The perceptron uses the Heaviside step function as the activation function with a threshold value of 0.5, which is a binary value (0 or 1) to produce the final output. Figure 2.2 demonstrate the diagram of a basic perceptron.

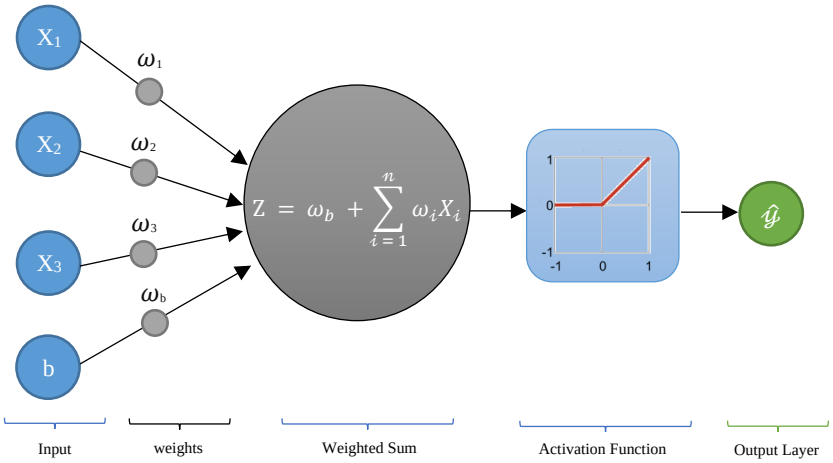

Figure 2.2: The basic structure of a perceptron.

As can be can seen in the Figure, a perceptron can take one or more inputs, a bias, an activation function, and a single output. The perceptron applies some weight to the given inputs and produce the output from the received weighted inputs by the activation function. Multi-layer perceptron can be modelled by including more hidden layers to the single-layer perceptron.

The Heaviside step function is used in perceptron as shown in the equation 2.1, where x is the weighted combination of the input features:

$$f(x) = \begin{cases} 0 & if \;\; x < 0 \\ \\ 1 & if \;\; x \geq 0 \end{cases} \tag{2.1}$$

2.1.1.2 Input layer

The input layer receives input data and fed into hidden layers in neural network. This layer consist of neurons unit the same number as the input features. The input neurons could be connected to the all of the neurons of the next layer, which is called a fully connected layer.

2.1.1.3 Hidden layer

In the structure of neural network, the input layer is connected to one or more hidden layers. In other words, hidden layers are stacks of hidden nodes between input and output layers. The role of neurons in hidden layers is to take input signals and converts them into corresponding output using an activation function. Hidden neurons in convolutional neural networks focus on image processing task to accurately find objects, contours or edges in the given input images. In recurrent neural networks, hidden neurons act as memory or forget neurons to control model input and output. Figure 2.3 shows the diagram of an ANN with four hidden layers.

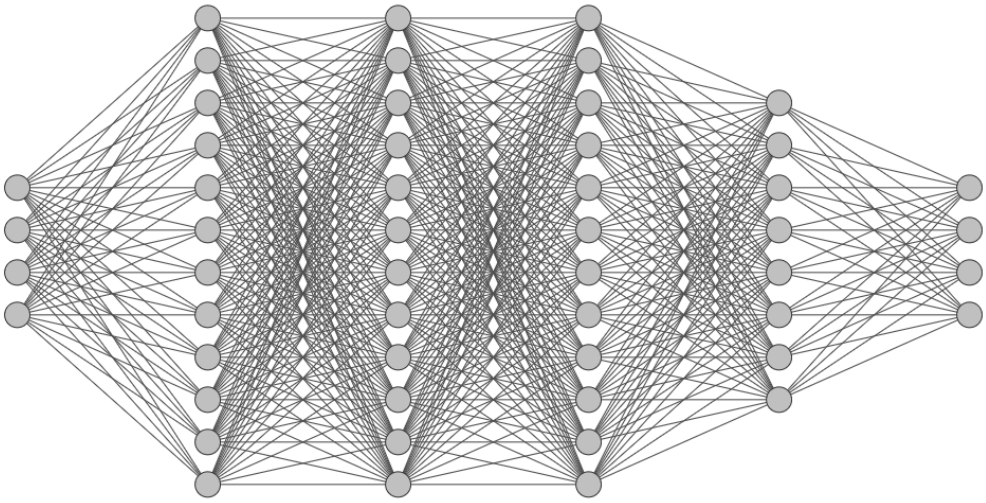

Figure 2.3: An ANN with four hidden layers. The figure is designed with [10].

2.1.1.4 Output layer

The output layer is the last layer in the network that receives information from the last hidden layer and produce the final result. Depending on the type of the activation function in the presented neural network, the final answer of the output layer may be a real-value in a regression task or a set of probabilities in a classification task or a predicted mask in a segmentation task.

2.1.1.5 Bias

A Bias is a constant scalar value added to the input layer in order to trigger initial learning in case when the input signal is low. Bias as an additional parameter allows to shift the activation function to either left or right to increase the flexibility of the neural network to fit the data.

2.1.2 Convolutional Neural Networks

LeCun et al. [116] devised the modern Convolutional Neural Network (CNN), also called ConvNets. Although this network structure was first created by Fukushima in 1988 [80], due to the limitation of computation power, it was not widely used. LeCun et al. [116] applied a gradient-based learning algorithm with weights updated by backpropagation and developed LeNet architecture as the first CNN in 1998. This approach achieved promising results for the handwritten digit classification problem [115] to read zip codes, digits, etc. After that, with further improvement, AlexNet architecture proposed by Krizhevsky et al. [111]. AlexNet has a similar architecture to LeNet but includes more convolutional layers and parameters and outperformed the performance of other CNN models. In 2014, Simonyan and Zisserman proposed VGGNet [189] with different depth and parameters for image classification task. VGGNet demonstrated that deeper networks could result in a better performance when training samples are large enough. In 2015, Inception module was introduced by Szegedy et al. [198]. The proposed module reduces the number of parameters in the architecture and leading to less computational resource workloads. Szegedy's proposed approach is very useful for tasks with small training samples. Today's, CNNs have been widely used and achieved promising results in the field of pattern recognition for different tasks such as image and video recognition, object detection, and semantic segmentation. The general architecture of a CNN is illustrated in Figure 2.4.

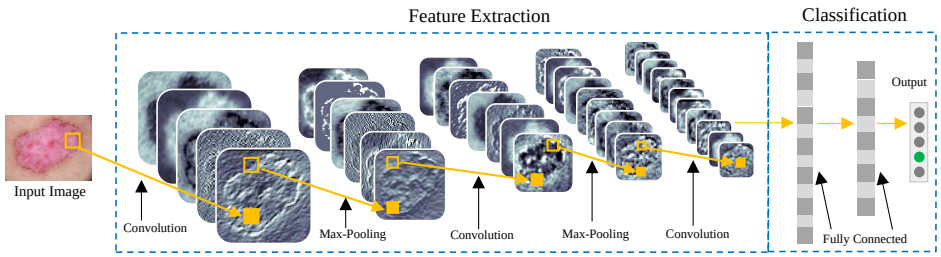

Figure 2.4: The schematic representation of the conventional CNN model. The medical image is adapted from [59, 204].

A typical deep convolutional neural network generally refers to a structure of the following fundamental layers: convolutional layers for generating feature maps, pooling layers for reducing the dimensionality of feature maps, fully connected layers for classifying the extracted features, activation functions, loss function, output layer and dropout layer [77]. Different type of CNN models can be formulated by

stacking these layers [186].

2.1.2.1 Convolutional Layer

The core component in a CNN model is convolutional layer. As illustrated in Figure 2.5, an input image transforms into locally trained filters through a convolution-based procedure to extract visual feature maps. Next, the size of feature maps has been reduced by pooling operation, and then these reduced-sized feature maps feed to the next convolution as input [185].

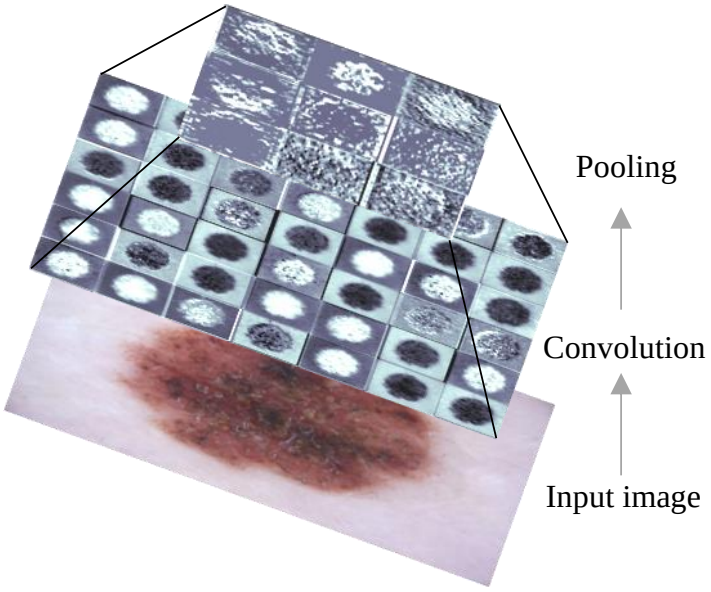

Figure 2.5: Example of a convolution and pooling operations. The medical image is adapted from [59, 204].

2.1.2.2 How convolution sees the world

CNNs have evolved from traditional ANNs. The two main processes in CNNs are extraction and feature classification. CNN is an end-to-end feature learning method that has been recently used and achieved great success in different computer vision tasks such as image classification, object detection, and semantic segmentation. CNNs can learn a hierarchical of features from an input image in a fully automated manner as shown in Figure 2.6. Each convolutional layer is composed of two stages: convolution and detection. In the first stage, a number of fixed-size convolution kernels or filters convolves sequentially on the given training sample to create different visual patterns and preserve the spatial relationships [185]. After generating feature maps using convolution operation, an element-wise non-linear activation function is applied to the produced feature maps in order to form the final output feature maps [241] [205] [216]. The visual patterns extracted from each convolution operation can be elementary and simple, but the combination of these simple patterns in intermediate or last

convolutional layers allows for the recognition of sophisticated class-level features and characteristics such as motifs, parts, or objects [173] [156]. An example of convolution operation is given in Figure 2.7.

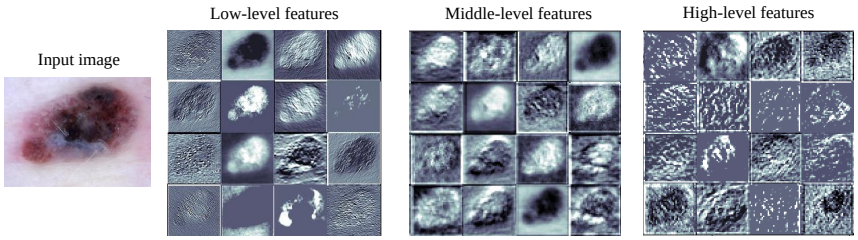

Figure 2.6: Feature visualization of convolutional operation. The medical image is adapted from [59, 204].

Each kernel has the same weight and bias values during the feature extraction process. This weight sharing properties have made CNNs to significantly reduce the number of parameters compared to a fully connected neural network. The key aim of weight sharing mechanism is to make CNNs to be invariance to translation [185] and provide the ability to represent the same feature as is convolved on the whole image [156].

A feature map consists of multiple neurons. Each neuron of a feature map is connected to the neurons of the previous layer which is called receptive fields through a set of weights of a convolution kernel. The receptive field of the neuron represents the region which the neuron is connected in previous layer. Size of the receptive field is defined by the size of the kernel [185].

2.1.2.3 Pooling layer

A pooling layer, also referred to as the subsampling layer, is generally utilized after a convolutional layer or block of convolutional layers with the aim to reduce the spatial dimensionality of the feature map. This reduction operation preserves important features while discarding irrelevant details, thus significantly reduces the number of network parameters [76] [185]. If the pooling operation is removed in a CNN architecture, the amount of computation increases exponentially in the subsequent layers as the number of feature maps increases. Hence, the pooling operation results in faster processing. Another advantage provided by the pooling operation is to increase the robustness of the model by reducing the sensitivity to small transformations, variations, distortions and translations in the input data [241]. Pooling is defined by two parameters: (1) the pooling kernel size and (2) the stride, which indicates the size of the step that pooling kernel slides over feature map [157]. The two most common pooling strategies are max-pooling (taking the maximum value of the input), and average-pooling (taking the averaged value of the input) to compute the maximum or average in a local window of the input feature map, respectively [240].

Figure 2.8 shows two examples of max-pooling and average-pooling for a 2×2 kernel with stride step

size 2 on an input feature map of 4×4. As demonstrated in this figure, the output feature map size is down-sized to the output feature size of 2×2. Max-pooling operation takes the maximum value from the input values, while average-pooling operation output the average value from the input values.

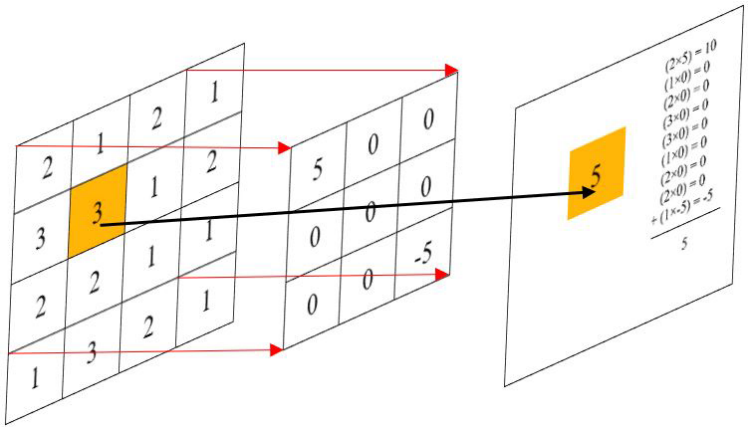

Figure 2.7: Diagram of a convolution operation.

At this point, two options are available: i) summarize the extracted feature maps through one or more fully connected layer or ii) repeat the process of passing the outputs into alternately stacked convolutions and pooling layers for deeper convolution architectures.

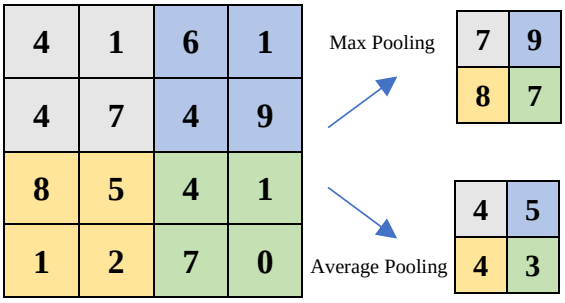

Figure 2.8: Two examples of max-pooling and average-pooling.

2.1.2.4 Fully Connected Layer

The advantage of the CNN models is to extract features from low-level information to produce high-level reasoning. After extracting abstract features from input data through alternately stacked convolutions and pooling layers, two approaches can be used to make inference from extracted features:

- Train extracted features maps using a machine learning classifier such as Support Vector Machine(SVM), decision trees (DT), random forest (RF), etc.
- Feed the extracted set of features maps to fully connected (FC) layers and perform the final classification [231] [92].

A fully connected layer is a one-dimensional vector similar to the basic structure of a conventional artificial neural network (ANN) or a multi-layer perceptron. In the fully connected layer, every neuron in one layer has a connection to all of the neurons in its adjacent layer, similar to multi-layer perceptron. The difference between a CNN architecture and FC layer is that not all neurons have full connectivity in convolutional layers [186]. The main function of a FC layer is to convert an extracted 2D summarized feature map into a 1D feature vector by a flattening operation and pass the learned high-level feature maps extracted from the previous convolutional and pooling layers to output layer and predict the corresponding classes [241]. As demonstrated in Figure 2.4, one or more FC layers are connected to the feature extractor. The input-output operation in a neuron of the FC layer defined in Eq. 2.2 [240]. In each neuron unit, the learned weights are multiplied by the corresponding data from previous layer and added the bias value. The calculated value transmitted to the activation function before being passed to the next layer [185].

$$fc = f(b + \sum_{i}^{m} \omega_i x_i) \tag{2.2}$$

where f represents an activation function such as ReLU, SoftPlus, Tanh, and etc., w is the weight vector, x is the input feature vector of the i^{th} neuron, m is the number of feature maps, and b is the bias vector [185].

2.1.2.5 Activation functions

The activation function introduces non-linearities to each convolution operation to extract non-linear characteristics from input data. Based on the obtained weighted sum, an element-wise nonlinear activation operation determines if a given neuron should be activated or not [240]. Activation functions are applied to the outputs of neurons as is presented below:

$$h(x) = g(y(x)) \tag{2.3}$$

where the function g is the activation function, h is the output of the activation function, and $y(x)$ is an output of a neuron, which is the input of the activation function [192]. Several kinds of activation functions have been proposed for training CNNs. Mostly used activation functions are ReLU, ELU and Tanh [129] [205]. The mathematical shapes of different types of activation functions is shown in 2.9.

2.1.2.6 Rectified Linear Units (ReLU)

ReLU is one of the widely-used activation function in the training of CNN architectures. ReLU activation function converts all negative input values to zero and keeps positive values the same, hence, allows extra weight to all of the non-negative neurons.

$$f(x) = \max(0, x) \tag{2.4}$$

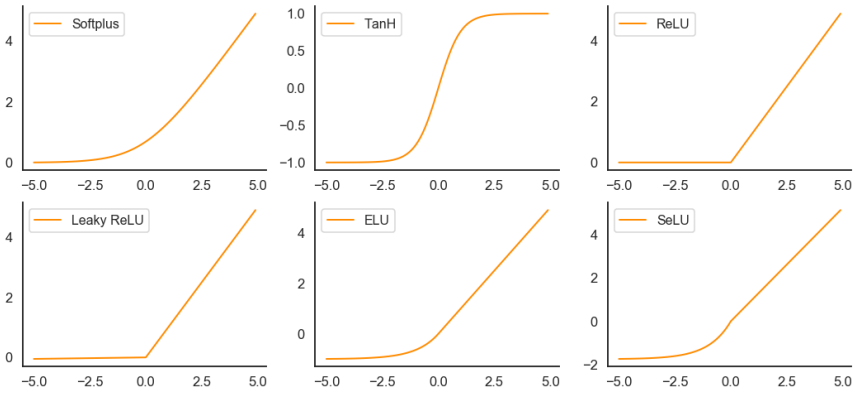

Figure 2.9: Different Activation Functions.

2.1.2.7 Leaky ReLU

Leaky ReLU is a variant of ReLU activation function that allows some negative values to exist. Unlike ReLU activation function that truncates every negative values to zero and pass through to the next layer, Leaky ReLU approach prevents the network get stuck in a dying situation [49] [130]. Leaky ReLU is expressed as follows:

$$LeakyReLU(x) = \begin{cases} \alpha x & \text{if } x \leq 0 \\ x & \text{if } x > 0 \end{cases} \tag{2.5}$$

The value of α is typically set to a small number such as 0.01. This small slope of α fixes the saturation region.

2.1.2.8 Tangent Hyperbolic Function (Tanh)

Tanh [83] is a hyperbolic tangent which outputs a real-valued number to the range between [1, 1]. Therefore, The output of Tanh non-linearity is zero-centered [75] and is expressed as follows:

$$Tanh(x) = \frac{2}{(1 + e^{-2x})} - 1 \tag{2.6}$$

2.1.2.9 Softplus

Softplus or SmoothReLU function is a smooth version of the rectifying non-linearity [228] and is defined as follows:

$$softplus\,(x) = log\,(1 + e^{x}) \tag{2.7}$$

2.1.2.10 Exponential linear unit (ELU)

ELU [58], defined by Eq.(2.8), is similar to Leaky ReLU. This activation function uses a small value of α of exponential function to solve variance and bias problem of the negative part of the input value [35].

$$ELU(x) = \begin{cases} \alpha(e^x - 1) & \text{if } x \leq 0 \\ x & \text{if } x > 0 \end{cases} \tag{2.8}$$

2.1.2.11 Scaled exponential linear unit (SELU)

The SELU activation function, as defined in equation 2.9, proved to has advantages over the traditional ReLU activation function due to its self-normalizing properties [109].

$$SeLU(x) = \lambda \begin{cases} \alpha(e^x - 1) & \text{if } x \leq 0 \\ x & \text{if } x > 0 \end{cases} \tag{2.9}$$

2.1.2.12 Loss Function

The loss function (also called the objective function or cost function) helps the network to update trained weights during training producer to achieve the best weight vector through measuring the error. Loss function is usually computed as follows:

$$L(W) = p - \hat{p} \tag{2.10}$$

Where L measures the difference between the prediction (weights, biases) and the actual value. It is essential for the algorithm to reach the minima of the loss function between the predicted value and the actual value during the training process.

2.1.2.13 Output Layer

The last component of the CNN architecture is output layer. The output of obtained feature vector from the last fully-connected is fed into the softmax activation function to calculate the probability score of each class for classification purposes. The class with the highest probability score will be the final classification result [241] [240]. The softmax activation function can be shown as Eq. 2.11:

$$x_j = \frac{e^{y_j}}{\sum_{k=1}^{n} e^{(y_k)}} \qquad for\ j = 1,\ 2,\ 3,\ \ldots,\ n \tag{2.11}$$

where x_j corresponds to the specific j^{th} class in the softmax output vector, y_j is the j^{th} value in the final output vector, and n is the number of classes. Softmax activation function ensure the sum of all

class probabilities be equal to 1 even when the predicted value of y is negative since the e^y is always positive [114].

2.1.2.14 Dropout Layer

Dropout technique, introduced by Hinton et al. [194] in 2012, is used to randomly eliminate some neurons at a certain probability from the network during training process [240]. Using a dropout layer, excessive adaptation can be prevented from the model and therefore, improve the generalization ability. The dropout technique has been widely used in different deep learning tasks because the learning producer becomes more robust to the over-fitting issue, which is a common issue in training deep CNN models [185].

2.2 Access Control Management Systems Based on Blockchain

Blockchain is a shared, immutable, distributed ledger of all transactions or events, which are recorded permanently into blocks. These blocks are linked sequentially in a chain to secure data from possible attacks and misbehavior, ensuring data integrity and security. Each block consists of the hash of the previous transaction and public key of the next owner that arranged chronologically and linked together in the Blockchain as illustrated in Figure 2.10. Blockchain technology provides an infrastructure for keeping track of provenance of data and confirms the actual owner of digital asset among all parties involved. Blockchain was first developed in 2008 as the foundational technology to secure and facilitate the exchange of Bitcoin cryptocurrency without the involvement of the third party. Further opportunities exist for institutions to use Blockchain technology in order to enhance security against data breaches or detect illegal activities. Development of protection mechanisms have become crucial for threat detection and having a Blockchain-based infrastructure provides a more proactive approach that could be strategically significant in gaining a competitive advantage over rivals.

By using Blockchain technology, institutions can prevent fraud of each transaction since it is permanent and impossible to alter or delete a transaction that is stored on the ledger. There is no single point of failure in Blockchain since each participant node has a full copy of transactions. The process of creating a new block is called mining, and every new block has to receive a consensus from a majority of the network peers before it gets added to the chain. The transactions are irreversible after confirmation, and when a block is verified, the new block propagates to all participant nodes on the network, and every block in the Blockchain should be re-validated.

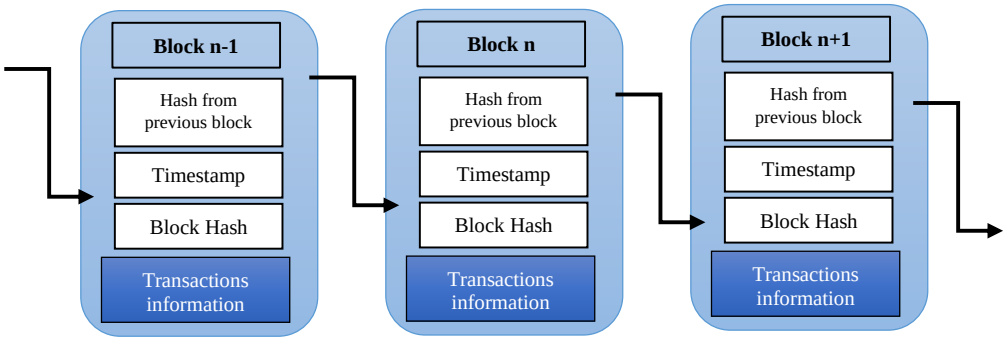

Figure 2.10: The structure of Blockchain.

2.2.1 Smart Contracts

One of the significant advantages of Blockchain is smart contract [62]. Smart contracts are self-executing contracts that allow users to control access of data by writing a pre-determined set of criteria and agreements, which are stored inside of a hosting Blockchain [190]. When a smart contract is triggered by Blockchain transactions by a node on the network, the terms of the contract will automatically be executed [187]. Moreover, smart contracts can leverage trusted transactions by enabling a secure transfer of the various types of ownership of data assets and assist the automation of a state without supervision or an external third-party [53]. Smart contracts' information is distributed throughout the Blockchain nodes at a low data interaction cost [144]. The smart contracts could be written with domain-specific languages, such as Solidity, Pact, Liquidity or general-purpose languages such as Kotlin, Go, and Java [190].

2.2.2 Consensus Mechanisms in Blockchain

Different consensus protocols are employed by different Blockchain systems to provide integrity of information with participants who do not trust each other [48]. Proof of work, proof of stake and proof of elapsed time are some of the most popular ways to reach a consensus without central authorities.

2.2.2.1 Practical Byzantine Fault Tolerance (PBFT)

Practical Byzantine Fault Tolerance (PBFT) consensus algorithm, proposed by Miguel Castro and Barbara Liskov, is the foundational consensus solution in distributed systems such as consortium blockchain platforms. It is based on a Byzantine agreement protocol and achieves consensus with a voting mechanism. PBFT reduces the complexity of the original BFT algorithm with an overall overhead of about 3% to the system, which is significantly less computationally intensive in comparison to the PoW consensus-based systems. This algorithm requires a minimum of 3f+1 node to tolerate in a system

off Byzantine failing nodes. Hyperledger Fabric uses the PBFT protocol to achieve consensus among participant nodes in a Permissioned blockchain [119].

2.2.2.2 Proof of work

Proof-of-Work (PoW) is one of the most widely used consensus mechanisms for reaching consensus on a Blockchain network [150] to protect the network from threats. PoW procedure ensure that each node that adds a block to the network must prove that it has done a certain amount of work before adding the block to the network. The PoW main mechanism is through mining by performing computationally expensive mathematics operations in order to add a new block to the Blockchain. It should be noted that the block is added to the Blockchain network when other miners agree that the given solution is correct. The longest chain in the Blockchain network is considerate as the legitimate and the most updated one because it has proof of having done the most work and majority decisions in a Blockchain network. PoW is most notably used by Bitcoin and Ethereum [45] [175].

2.2.2.3 Proof of stake

Proof of stake (PoS) is proposed as the most common alternative to PoW for verifying the transactions on the block. POW is a computationally expensive consensus mechanism and demands increased difficulty of the puzzles to prevent an attack attempt to happen, leading to spend more hardware resources and time to mine only a single bitcoin. Aiming to solve this issue, PoS reaches consensus by using ownership, instead of using a mathematical puzzle, which is an energy-efficient approach. The PoS algorithm requires participant node to prove their ownership of the coins in the system with a digital signature as it cuts out the mining process. The rationale behind POS consensus algorithm is that a miner who stake more coins has more power to mine or validate transactions, and therefore is less likely to attack the network. There are different variants of PoS such as delegated proof of stake [236] [226] [188].

2.2.2.4 Proof of elapsed time

Proof of Elapsed Time (POET) [11] is a relatively recent consensus mechanism was developed by Intel and adopted by the Hyperledger Sawtooth project [14]. POET is not based on reward system for validating nodes; therefore, is not computationally intense [90]. In PoET, each validator is requested to generate blocks after a randomly generated period of waiting time. The node with shortest wait time determines the first validator to add the block to the Blockchain [46]. This consensus is an efficient alternative to PoW as it provides a secure and fast mechanism for block validation. [235].

2.2.3 Opportunities of Blockchain Technology

The following section highlights an overview on the benefits provided by Blockchain technology.

- **Security:** Blockchain achieves a highly secure transaction system using cryptography. Every transaction is inserted into the Blockchain network by solving a complex mathematical process. Each block is cryptographically secured with digital signatures. Also, every node on the network should verify that the new transaction is valid. Each participant node in the network has its own private key that is associated to a transaction or any update of an existing transaction. Hence, security vulnerabilities are identified and prevented.
- **Decentralization:** Decentralization is the core concept of Blockchain in storage, communication, and computation. The trust between distributed nodes is built through a peer-to-peer setup of mathematical process rather than centralized organizations; therefore, there is no need for any central authority or a trusted third party to control the network and validate transactions. A consensus mechanism is used to perform validation of transactions without the need of a central trusted party. Unlike conventional centralized systems using such decentralized systems, the bottleneck issues such as single point of failure, server cost or information delay problems can be avoided.
- **Reliability:** Blockchain provides reliability since every transaction should be validated before being added to the ledger. And then, it is distributed and replicated to all nodes across the network to provide transaction reliability and reduce the brokerage costs. Also, no single point of failure or single point of control exists in this scheme.
- **Transparency:** Blockchain technology provides transparency to each participant node in the network, so that a shared level of trust can be ensured to all participants. Based on the permissions that are delegated in a private or public Blockchain-based network, a full copy of transactions or token activities ever executed in the system are visible to all participant in the network without being controlled by a third party. Transparency is derived from the openness feature of the Blockchain, preventing transactions from being hidden or manipulated, as any change to the recorded data is visible to all of the peers on the network.
- **Immutability:** Immutability of transactions is one of the critical characteristics of Blockchain. Blockchain, as a shared distributed ledger, is designed to be immutable, which means data is written once and no update or delete operations of existing records is allowed, which makes a Blockchain an immutable and permanent data structure. Immutability makes it very difficult to delete, fake or alter the recorded data of a block leading to guarantee data integrity. When transactions are broadcast to the network, almost every participant node has a copy of data. The immutability increases with time when more and more blocks are added to the Blockchain.

- **Auditability:** Auditability is automatically derived from the transparency and immutability properties of Blockchain technology. All transactions are validated and stored in a chain of blocks. Cryptographic hashes and a timestamp are employed to link the blocks together. Therefore, the auditability of data already exists and can be verified with its previous records across the network.
- **Traceability:** Traceability means the flow of all transactions are arranged in chronological order using the cryptographic hash function. Each transaction record should be traced and tracked along the Blockchain mining process. An effective traceability system can track the complete transaction path and cannot be tampered. Therefore, the traceability can be achieved through a forwards and backwards direction during the entire history of transactions records. The traceability mechanism can help prevent fraudulent activities.

2.2.4 Challenges of Blockchain Technology

Blockchain is an emerging technology that ensures the integrity and availability of data. However, some concerns exist that need to be addressed in order to build robust Blockchain-based applications. Some of the challenges in developing Blockchain-based applications are summarize as follows [131].

- **Data privacy:** The main problem in adapting Blockchain technology for financial institutions and healthcare environments are privacy and confidentiality of transactions, which is not provided due to the requirements of transparency.
- **Network latency:** Read/write transaction latency in achieving consensus by nodes participating in Blockchain network is another drawback. This delay is necessary to detect any kind of intrusion of transactions. For example, in Bitcoin, almost 30 minutes is needed to verify a transaction validity and feasibility.
- **51% Attack:** The risk of majority attack, also known as 51% attack, is another problem in Blockchain. Based on the Blockchain mechanisms, if 50% of the participating nodes confirm a fraudulent transaction, that will become true. By verifying a manipulated transaction, the illegitimate nodes can gain control of the entire network, and the entire network can be compromised [40]. Also, studies in the literature reported that the 50% control is not sufficient for the network security [146] [20] [138].
- **Private key management:** The primary authentication mechanisms in Blockchain are the hash function, digital signature, public and private keys. The private key of the senders is used to digitally sign and validate the transaction messages. The only way to decrypt a private key is by the corresponding public key. However, if private key of a wallet is compromised or stolen, the hacker can have access or steal the assets of respective account [131] [117]. Mt.Gox is an example of attacking a Bitcoin wallet company and leaking of their customers' private keys [95] [60].

2.2.5 Types of Blockchain

Blockchain exists in three types in terms of deployment, including public Blockchain, consortium Blockchain, and private Blockchain.

2.2.5.1 Public Blockchain

Public or open Blockchains, such as Bitcoin, is accessible to anyone who can participate in the consensus process [200]. However, using a public Blockchain does not mean that the content is available to the public. A public Blockchain requires substantial computational resources to achieve consensus for stored transactions and blocks of the Blockchain since each node in a network must solve a cryptographically complex, resource-intensive problem. Examples of open Blockchain are Bitcoin and Ethereum [131] [146].

2.2.5.2 Private Blockchain

Private Blockchain, also referred as closed Blockchain, restricts network participation. This characteristic allows businesses to develop and customize decentralized systems based on their business models. In pivate Blockchain, network participants are carefully controlled. In these types of Blockchain, registering transactions, accessing the ledger and viewing data are allowed only by trusted members or groups of members within a organization or multiple divisions of an organization [138] [146]. Private Blockchain also allows transparent network transactions without the need for mining that is approved by a specific central party [117]. Therefore, a private Blockchain provides more transaction privacy in compare to public Blockchain, which is essential for sensitive data transactions such as medical or financial data. Examples of private Blockchains include Hyperledger Fabric and Corda [23].

2.2.5.3 Consortium Blockchain

Consortium Blockchains is an extension of the private Blockchain that also benefits from the decentralized property (not centrally controlled) provided by public Blockchain [234]. Consortium Blockchain [66] is a type of Blockchain that is based on a group of pre-selected authentication nodes [152] instead of allowing anyone to validate the transactions. Proof-of-Authority consensus mechanism is widely used in consortium Blockchains. New blocks are added to the Blockchain by the network members that are joined to the network by invitation only, thereby significantly increasing efficiency by saving time and network workload [79].

2.2.5.4 Permissioned Blockchain

At the network level, Blockchain systems can be divided into two types of Permissionless and Permissioned Blockchain. In Permissioned Blockchain, several nodes are selected as pre-authorized nodes to have full authority, control the consensus process and grant permissions [182]. In Ripple, as an example of Permissioned Blockchain, the roles of the individuals that can play within the network is controlled. Therefore, the Permissioned Blockchain can address the issue of network latency and network scalability through limited participation while maintaining a decentralized structure [117] [131].

2.2.5.5 Permissionless Blockchain

In contrast, entities in Permissionless Blockchain do not require permission to participate in the Blockchain network. Anyone can anonymously join the network and participate in the process of block verification to add a new block to the ledger. Ethereum is a popular example of this type of Blockchain; also, cryptocurrencies such a Bitcoin are based on Permissionless Blockchains. The consensus mechanism in Permissionless Blockchains is based on Proof-of-Work (PoW) algorithm for mining a new block. PoW requires solving a complex mathematical problem using brute force, which, in practice, is computationally intensive and results in high latency of transaction verification [99] [212].

All types of Blockchain use cryptography to allow each participant on any given network to manage the ledger in a secure way without the need for a central authority to enforce the rules. The removal of central authority from the database structure is one of the most important and powerful aspects of Blockchains.

2.2.6 Enhancing Blockchain Security with Cryptography

Asymmetric (Public-key) cryptography and hash functions with the distributed consensus mechanisms are the main cryptographic primitive in Blockchains for securing data sharing between participants.

2.2.6.1 Public-Key Cryptography

Public-key cryptosystems are the primary mechanism for the secure exchange of information between parties in Blockchain. In this approach, transactions are authenticated through digital signatures. The private key is kept secret while the public key is shared publicly among all other participant nodes. In other words, the public key is used as the address of the node to interact with other nodes on the Blockchain network. Private key is used to initiate the signature process by signing a transaction. Then, the corresponding public key is used to i) exchange information between parties, ii) verify the validity of signature iii) verify the identity of the transaction creator using its public key [101].

2.2.6.2 Digital Signature

The concept of the digital signature was introduced by two researchers, White Diffie and Martin Hellman, in 1976 [67]. Diffie-Hellman key exchange protocol, as an underlying primitive of cryptography, generate a shared key of a combination of a private key and public key [140]. Digital signatures were envisaged by Diffie-Hellman key exchange protocol. A secure digital signature algorithm ensures that only the rightful owner of data or transaction can sign with a private key and the corresponding public key to verify the signature and guarantee the authentication, non-repudiation and integrity of the messages/transactions [213][78]. For instance, ECDSA [44] and EdDSA [39] are the two widely used digital signature schemes in Blockchain systems. Popular Blockchain systems such as Ethereum and Bitcoin adopt the ECDSA (Elliptic Curve Digital Signature Algorithm) to generate the public key [208]. EdDSA (Edwards-curve Digital Signature Algorithm) is an alternative to ECDSA with a further scheme based on a twisted Edward curve. The Edward curve is a class of an elliptic curve that significantly outperforms the general elliptic curve with high security, performance, and verification [237].

2.2.6.3 Hash Functions

Hash functions like SHA-256 and Public Key Infrastructure (PKI) are essential parts of Blockchain systems. Hash functions can create a hash string of fixed length from any input but are irrecoverable and complicated to forge. For example, in Bitcoin, all transactions are encrypted by Secure Hash Algorithms (SHA) such as SHA-256, and the process of mining verifies the authenticity of the transaction. Hash functions are also used to link blocks of Blockchain in chronological order. Each block contains the hash of the previous block, which is calculated with the SHA-256 hash function [170] [213].

Blockchain is an emerging and promising technology in providing a decentralized trust and management system. Numerous studies have investigated the application of Blockchain for secure medical data sharing and management.

2.3 Related Work

The next section summarizes the previous works on applications of convolutional neural networks on automated histology image analysis systems, which has successfully been applied to classification and segmentation tasks.

2.3.1 Deep Learning for Histopathological Image Classification

A magnification independent classification approach with deep CNN applied by Bayramoglu et al. [36] on BreakHis dataset. Two different architectures were used: i) single task CNN for malignancy predic-

tion, ii) a multi-task CNN for both malignancy and image magnification level detection simultaneously. To increase dataset size, different data augmentation strategies such as flipping, rotation with angles of 90˚, 180˚, and 270˚ were employed and finally, all images are center cropped to obtain a square patch. The second CNN model was a multi-task model with two branches; the first branch classifies each input image into its corresponding benign/malignant class. The second branch determines the magnification factor of the input image (40×, 100×, 200×, and 400×). The CNN model employed for this study contains three convolutional layers; each layer followed by a pooling layer. Bayramoglu's experiment demonstrated the single CNN approach outperformed the performance of magnification model and the previous state-of-the-art studies.

In a study conducted by Kieffer et al. [108], the performance of deep classification CNN is measured based on features extracted from pre-trained convolution neural networks with/without transfer learning. In their first approach, the pre-trained CNN was used as a feature extractor without fine-tuning. The extracted features then were fed into a linear SVM to be trained for the classification task. For the second approach, authors employed fine-tuned CNNs as a classifier. In this method, the extracted bottleneck features were used as input to a Multi-layer perceptron (MLP). Kieffer's study demonstrated that models trained by features extracted from a pre-trained network on ImageNet dataset achieved competitive performance with CNN trained from scratch. VGG16 and InceptionV3 architectures were used as pre-trained models. Kieffer's experimental results also demonstrated that the fine-tuning does not seem to contribute in the performance improvement of VGG16 but resulted in considerable improvement in InceptionV3 architecture.

The problem of intra-class classification of breast histopathology images was addressed in a study conducted by Adeshina et al. [22]. Adeshina's approach employed a Deep CNN architecture combined with an ensemble of Adaboost classifier for binary classification on BreakHis histopathology dataset. The feature extractor component of the proposed method consists of seven convolutional layers followed by two fully connected layers. All input images were normalized by subtracting the mean value from each pixel intensity to remove the bias from features. The Adaboost classifier optimized the predictions by adding more weights to samples with high error rate.

In a similar study conducted by Bejnordi et al. [74], two VGGNet architectures were employed to extract global features from H&E-stained breast biopsies. The first model classifies the input WSI into one of the three classes (epithelium, stroma, and fat). And at the next stage, the second model use the output of the first stage to classify the stromal regions as healthy stroma or cancerous stroma. Finally, a RF classifier was used to classify each WSI into cancer or non-cancer class. Patches of the size of 224×224 pixel extracted from input WSI biopsies. Different data augmentation methods, including random flips, rotation and color transformation were utilized to increase the dataset size and improve the proposed method performance. The experimental results of Bejnordi's study demonstrated that the presented two-stage CNN model achieved higher performance than each CNN model individually.

Chang et al. [52] adopted a pre-trained Google's InceptionV3 architecture for binary classification of breast cancer from histopathology images. The feasibility of transfer learning strategy was also investigated for medical diagnosis. The performance of the proposed method validated on BreaKHis dataset with magnification factor of 40×. Data augmentation methods, i.e. rotations (with angels of 90°, 180° and 270°), mirroring (flipped left-right, top-bottom), and random distortion was also employed to overcome insufficient training data samples. Chang's experiment indicated that transferring knowledge learned from a cross-domain dataset can be beneficial for training histopathology images.

Wu et al. [217] proposed a deep attentive feature learning for H&E-stained histopathology image classification. VGG19 architecture integrated with two different attention modules was used as the base model for this study to learn more discriminative features. Authors fine-tuned the weights of the convolutional blocks in VGG19 model while the attention modules were trained from scratch. All of the input images are resized to 224×224 and augmented using random flip and rotation methods. Attention modules, by generating attention maps of different dimensions, enabled to focus on critical regions and discriminative feature channels and discard irrelevant information. BreakHis dataset is used to evaluate the performance of the proposed method. Wu's experimental results showed the effectiveness of attention modules in histopathology image classification task.

Khan et al. [107] used three widely-used pre-trained deep CNN architectures, i.e. VGGNet, GoogLeNet and ResNet as feature extractors. The extracted features combined together and fed into a fully connected layer to classify breast cancer from histopathological images. Authors also compared the performance of the proposed method with each of the employed CNNs separately. The Macenko et al. [135] method was used for stain-normalization of digitized tissues. Different data augmentation methods such as color processing, translating, scaling, rotation, flipping and noise perturbation were employed to increase dataset size and prevent over-fitting problem. The results demonstrated that proposed ensemble model achieve better results than those individual architectures.

Araújo et al. [31] used a CNN-based architecture similar to VGGNet to classify H&E-stained histology images. The proposed architecture can capture feature information from different scales applied on both image-wise and patch-wise (patches of 512×512 pixels size, with 50% overlap) images. The proposed CNN architecture consists of five convolutional layers alternated by max-pooling layers and followed by three fully connected layers. The extracted features also fed into an SVM classifier to calculate the final output. The proposed CNN model was trained on the augmented patch dataset and tested on image-wise dataset. Araújo's study showed that both CNN model and SVM classifier achieved comparable results, however, higher sensitivity achieved for carcinoma cases by proposed CNN architecture.

Jannesari et al. [103] applied fine-tuned pre-trained deep learning approaches for breast cancer subtypes detection. The performance of the proposed method also validated on histopathological images on different tissues of lung, breast, lymphoma, and bladder cancer. Several data augmentation methods such as horizontal and vertical flipping, brightness, saturation and contrast adjustment employed.

Different depths of Inception (V1, V2, V3 and V4) and ResNet (50, 101 and 152) architectures selected to investigate the performance of models. Authors concluded the ResNets achieved better performance as being deeper and wider networks for large and complex dataset than Inception models in all cancer datasets.

2.3.2 Deep Learning for Histopathological Image Segmentation

Chen et al. [55] presented a deep learning model and image processing methods for nuclei detection and segmentation from microscopy images. A multi-layer convolutional neural network employed for feature extraction from both spatial and color information. The proposed U-Net model has been implemented using H&E-stained microscopy images containing seven different tissue samples for segmenting the boundary and detecting the geometric center of the nuclei.

BenTaieb et al. [38] designed a multi-loss convolution network that performs both classification and segmentation for colon adenocarcinomas diagnosis. In BenTaieb's method two distinct loss functions employed to optimize a single deep CNN. The proposed CNN architecture composed of two components organized symmetrically. For the first stage, the classification component determines the type of tumour using stacked layers of convolution and subsampling operations. Then, at the second stage, the segmentation component performs deconvolution and up-sampling operations to segment out the identified glands from the first stage. To integrate the feature maps from the first part (classification stage) to the segmentation stage, cross-network spatial activation maps was introduced. The performance of presented model also compared to the U-Net and AlexNet models. BenTaieb's proposed method by including class-specific spatial priors were able to achieve a more accurate segmentation network.

In a study conducted by Koyun and Yildirim [110], an unsupervised nuclei segmentation using a cycle-consistent generative adversarial networks proposed for nuclei segmentation on H&E-stained histopathology images. Segmentation maps are generated based on the proposed CycleGAN method and randomly generated labels. Patches of size of 50×50 extracted from images consists of different morphology of nucleus. The proposed architecture was an U-Net encoder-decoder architecture with nine residual connections between the encoder and decoder parts. The shape of the generator part of the proposed CycleGAN was changed to generate different regular and irregular nuclei. Two post-processing methods such as Otsu thresholding were applied to optimize the produced results. Authors discussed that the performance of the proposed network is sensitive to contrast and illumination variations of the input images.

In a similar study conducted by Mahmood et al. [136], a dual generative adversarial network were adopted for multi-organ nuclei segmentation from histopathological images. The synthetically generated pathology images from proposed model were combined with real input images to train CNNs and perform final nuclei segmentation. The backbone architecture designed using an encoder-decoder archi-

tecture similar to U-Net with skip connections. The proposed model by using an adversarial pipeline with larger receptive field was able to capture more global information in comparison with standard CNNs. The proposed model was trained on patches of 256×256 of H&E-stained slides of histopathological images from different organs such as breast, ovary, esophagus, liver, kidney, prostate, bladder, colorectal and stomach.

Zeng et al. [232] proposed a modified U-Net for nuclei segmentation in histopathology images. For stain normalization of H&E-stained images, Macenko et al. [135] method employed by authors. The proposed Residual-Inception-Channel attention-UNet (RICUNet) architecture can identify different types of cell shapes and scales. The presented model inspired by studies of Chen et al. [54] and Yu et al. [227], which was applied on nuclei segmentation of different organs such as kidney, prostate, breast, liver, stomach colon and bladder, consisting of both benign and diseased tissue samples. In Chen et al. [54], a multi-task learning framework employed to segment the nucleus and cell contour simultaneously. Yu et al. [227] employed CAB (Channel-Attention-Block) module in up-sampling part. The features from cell contour acts as auxiliary features to different dense and overlapped cells and assist to reduce errors at the object level. In the proposed U-Net model, convolutional layers were replaced with Residual-Inception-blocks.

Qu et al. [167] proposed a deep learning-based model for both nuclei segmentation and classification simultaneously on a small lung cancer histopathological dataset. The transfer learning strategy was used to improve the performance of the proposed model. Image patches of size 250×250 with overlap extracted from the original images. Different data augmentation methods, i.e. horizontal and vertical flip, transformation, rotation also used to increase the training samples size and improve the performance of the presented model. The proposed network consists of residual modules without the average pooling and fully connected layers which is able to extract both nucleus features and spatial distributions simultaneously. To further improve the segmentation performance, the cross-entropy loss and perceptual loss [104] are combined together. Qu's proposed model achieve better accuracy than U-Net and FCN models.

2.3.3 Approaches Based on Permissioned Blockchain

2.3.3.1 Off-Chain Storage of Medical Data

Liang et al. [128] used a Blockchain network for integrated data sharing and collaboration in mobile healthcare applications. The presented user-centric personal health data sharing system includes six entities, namely user, wearable devices, healthcare provider, insurance company, the cloud database and Blockchain network. Authors employed Hyperledger Fabric [47] Blockchain network for data access protection between peers and the shared ledger. A tree-based data structure and batching method were adopted to handle large data sets of personal health data collected from mobile applications.

Blockchain network was used for three purposes i) as a health data integrity protection collected from both wearable devices and healthcare providers. ii) as a decentralized permission management between healthcare provider and health insurance company to get a permission from the data owner, and iii) as a distributed access control policies to ensures stability.

Sun et al. [196] proposed a decentralized attribute-based signature (DABS) scheme for secure sharing of electronic health records (EHR) in a healthcare Blockchain system to provide a privacy-preserving verification service. The presented privacy-preserving model can verify the identity of the signer and the authenticity of EHR data without exposing the identity of the signer. Also, an on-chain and off-chain collaborative storage model was developed for secure storage and verification of EHR data. To address the issues of limited storage capacity and computational resources of Blockchain, a combination of Blockchain and off-chain storage was suggested.

Ramani et al. [172] designed an Ethereum-based Blockchain system for a secure and efficient data accessibility mechanism for healthcare systems. A smart contract is developed to manage access control decisions of the patient's healthcare information. If an unauthorized entity request to have access the system, the smart contract check the access level and deny the request. The two main operations in the presented system is i) retrieve operation and ii) append/add operation of the medical data through Blockchain. Both doctor and patient can retrieve the data. But for appending the data to the block, the doctor can only update the data along with patients' permission.

Wang et al. [214] used a Blockchain-based searchable symmetric encryption and attribute-based encryption techniques to ensure the privacy and integrity of personal health records. The hash values of encrypted personal health records are stored in Blockchain, and the related index set is stored in a smart contract to provide fine-grained access control and protect the personal health records sharing system. Compared with the existing similar schemes, the new scheme using Blockchain for key management allows patients to distribute attribute private key, which can further improve the efficiency of data integrity verification.

In another study done by Chakraborty et al. [51], a secure healthcare framework using Blockchain technology proposed to support healthcare applications, making medical data sharing and access secure and auditable. The proposed framework consists of different modules including Blockchain, IoT and machine learning. Blockchain system employed for storing and maintaining the patients' data for access control management. The Machine Learning part is used to forecast potential anomalies.

Nguyen et al. [153] designed a novel EHRs sharing framework that combines Blockchain and decentralized interplanetary file system (IPFS) for secure EHRs sharing of cloud-based e-health platforms. The proposed Ethereum Blockchain approach is able to provide a trustworthy access control mechanism to reliably exchange medical data among mobile users and healthcare providers while preserving sensitive health information against potential threats. The performance of the proposed method was

evaluated by implementing a prototype on the Amazon cloud to address critical challenges of current EHRs sharing systems.

Dubovitskaya et al. [71] proposed a Blockchain-based framework for a secure EMR data exchange and management of cancer patients. The prototype of the proposed framework was implemented on a Permissioned Blockchain network on radiation oncology department for sharing clinical data between healthcare providers to evaluate the privacy, security, availability and detailed access control over EMR data. Chaincode written in Go programming language was used for verification of the access control rights such as read, write or share operations and maintain metadata and access control policy and a cloud service to record patients' healthcare data.

Novo [154], have proposed a Blockchain-based architecture for fully distributed access control management in IoT devices. The proposed architecture consists of different components, including wireless sensor networks, managers, agent node, smart contract, Blockchain network and management hubs. Policies are managed by smart contracts. The smart contract, after validation of the defined policy, answers the requested query through a management hub.

Xiao et al. [220] proposed a cross-organizational medical data sharing framework, named EMRShare, using a Permissioned Blockchain technology to facilitate sensitive healthcare data sharing and manage privacy and trust issue of the electronic medical records in healthcare environment. A Hyperledger composer implementation provided by authors to resolve the trust issue between participating parties and facilitate the medical data sharing between patients, clinicians and researchers, insurance agent and government. A comparative analysis of existing studies and the proposed EMRShare approach also provided. In EMRShare framework, a variety of participants including patients, clinicians and researchers are involved.

A Blockchain-based secret data sharing model is proposed by a study conducted by Thwin et al. [202] using a proxy re-encryption technique to support privacy and confidentiality concerns for personal health record system. Thwin's work also analyzed different Blockchain systems and highlighted different challenges and drawbacks that exist in the existing Blockchain systems such as limited storage, privacy, consent revocation, performance, energy consumption and scalability.

2.3.3.2 On-Chain Storage of Medical Data

Azaria et al. [33] proposed a novel, decentralized record management system, MedRec, for medical data management and data access using a Permissioned Blockchain network. In this system, each block stores data ownership and viewership permissions in a private, peer-to-peer network. The proposed framework facilitates authentication management, confidentiality, and data sharing of sensitive medical data. In order to anonymize medical data access, a proof-of-work incentive was employed for both clinical and research use cases. An Ethereum Blockchain's smart contract carry out policies to automate and track

the state of transactions such as viewership rights, adding new records to the network, data retrieval instructions, recording patient-provider relationships, etc.

Based on the study of MedRec, Yang and Yang [224] proposed a Blockchain-based approach using signcryption and attribute-based authentication methods to enable the secure data healthcare sharing. A symmetric key followed by an encrypted attribute key set employed to encrypt patient's electronic health records. In order to have access to data, the signature should be verified by a user and perform key decryption and EHRs decryption. In the proposed approach, in order to provide both data confidentiality and data authenticity, signcryption which is a combination of encryption and signature was introduced. In this method, data is first encrypted and then signed.

Oliveira et al. [63] adopted a hybrid Blockchain-based method to secure electronic medical records by combining the advantages of Blockchain and public key infrastructure. In Oliveira's method, electronic medical records access control is patient-centric where a patient shares the decryption key only with trusted healthcare professionals. The scalability of the proposed method was investigated through simulations on health applications. The identification and authentication of system users (patient and physician) conducted using digital certificates provided by an official certification authority. In the proposed hybrid system, asymmetric keys supported by a PKI and secret session keys are used to store medical records in a Blockchain. The results of this study showed that the time for adding a new data in Blockchain remains low even when the number of nodes in the network increases.

Rajput et al. [171] proposed an Emergency Access Control Management System called EACMS based on a Permissioned based Blockchain using Hyperledger Composer network. The proposed framework provide privacy protection and security policies for the patient's personal health records in emergency condition. The smart contacts employed to support secure data item access and control personal health records permissions. The performance of the proposed framework simulated and evaluated based on response time, privacy, security, accessibility and compared with the traditional emergency access system.

Xu et al. [223] designed a Blockchain-enabled decentralized capability-based (BlendCAC) for access control management of IoT devices. An identity-based capability token management strategy was employed in the proposed BlendCAC scheme to support access control management of resource-constrained IoT devices. Registration, propagation and revocation of the access authorization is given to the system using a smart contract. A prototype of the proposed BlendCAC implemented in a physical IoT by a private Ethereum Blockchain network.

Pal et al. [159] discussed a secure, flexible and fine-grained delegation model by designing a Blockchain-based architecture for capability-based access control in the IoT devices. The proposed access right delegation system is based on attributes to address the issue of delegation of rights from one entity to another. Access control token (delegated or not) considered as event which is a special form of

transaction. Each event is generated and linked to a smart contract. The prototype of the proposed system implemented using an Ethereum private Blockchain with three nodes consisting of one Ether miner and two peers. Zhang et al. [239] proposed a smart contract-based framework and discussed critical issues exist on smart contract-based access control systems. The proposed framework consists of multiple access control contracts including, one judge contract, and one register contract for securing control management in IoT devices. The role of judge contract is to investigate a misbehaviour-judging method. The register contract records different information including access control and misbehaviour-judging methods, and also provides functions, e.g., register, update, and delete. The prototype of the proposed method implemented based on Ethereum based Blockchain system with one desktop computer, one laptop and two Raspberry Pi single-board computers.

Alblooshi et al. [27] designed an Ethereum-based Blockchain and smart contract to provide a trusted ownership for medical IoT devices. The proposed system consists of two smart contracts, manufacturer and IoT device smart contract to manage and trace the true ownership of Medical IoT devices for protecting medical data from cybersecurity attacks and counterfeited MIoT devices. Whenever IoT device is manufactured, a manufacturer should use manufacturer smart contract to deploy IoT device smart contract. The owner of an IoT device can set rules and conditions for data access control management using the IoT device smart contract. Authors also investigated the security analysis of the proposed method against DDoS attacks, eavesdropping and replay attacks. Furthermore, the proposed decentralized scheme avoid the single point of failure problem.

Pussewalage et al. [165] introduced an attribute-based access control scheme using Blockchain for a multi-domain e-health environment. Pussewalage's proposed system integrates an attribute-based access control scheme with controlled access delegation capabilities for accessing patient healthcare information. The proposed access control scheme is able to manage attribute assignments, delegations and revocations Blockchain technology. In another work, Zhang and Poslad [238] proposed a Blockchain-based architecture called Granular Access Authorization supporting Flexible Queries (GAA-FQ) for Electronic Medical Records (EMR). Authors discussed different levels of granularity of authorization to support flexible queries and provide access control and access authentication mechanism. There is no need for a public key encryption or public key infrastructure (PKI) for the authorization, encryption and decryption, which decrease the computation time. The proposed model consists of three layers, namely user layer, agent layer and storage layer. User layer represents the network participants such as doctors, patients, data analysts and monitoring devices of health. The agent layer aggregates the queried data and also check the inquirers' access permission to authorize the access level of the user. If the user have the access right for the data and attributes, the agent layer return the requested data. Finally, in the storage layer, all of the medical data are stored in Blockchain network.

Du et al. [70] introduced a conceptual framework based on Blockchain technology and a distributed cloud for data collection, storage, retrieving and sharing system to secure medical information in a

complex network environment. In Du's proposed framework, medical data are encrypted and then stored on a distributed cloud to avoid privacy and security problems and improve the storage and sharing of sensitive medical data. In the proposed approach, users were provided with identity-based data encryption scheme. Based on the users' identity and hierarchy level, a user can encrypt the data by using a secret key and distribute it to Blockchain and only users with authorized identity set can decrypt healthcare information.

Yu et al. [229] proposed a Blockchain-based architecture (LVChain) for IoT access control and authorization to overcome the issues associated with conventional centralized architectures. The performance of the proposed model validated on home wireless self-organizing network. Authors proposed a voted-based algorithm instead of computation-intensive Proof-of-Work and Proof-of-Stake algorithms to reach the consensus. The proposed algorithm is lightweight and well suited on Bluetooth low energy (BLE) based devices. The vote-based consensus also is less dependent on computing and storage resources which is ideal for IoT devices with limited computing hardware. The security analyzes and performance of the proposed architecture measured based on different criteria such as scalability, fault tolerant, new authorization, get authorization, and off-line working.

Omar et al. [24] presented a Blockchain-based privacy preserving mechanism, MediBchain, for accountability, integrity, pseudonymity, security and privacy of healthcare data. In this system the control of the patients' private medical data returns to themselves. Blockchain hold the sensitive health data of the system's users. Each transaction in the Blockchain has an identifier. Using this transaction identifier, users can control the access of their data.

Cruz et al. [61] proposed a Role-Based Access Control using the Smart Contracts (RBAC-SC) framework to verify the authenticity of the assigned roles and user's ownership of a role. Ethereum's smart contract technology utilized as infrastructure to define roles and relationships in the proposed framework. A prototype of the smart contract was compiled and deployed on Ethereum's Testnet Blockchain.

2.3.4 Approaches Based on Consortium Blockchain

2.3.4.1 On-Chain Storage of Medical Data

Zhang and Lin [233] proposed a Blockchain-based secure and privacy-preserving data sharing for personal e-health information scheme for diagnosis improvements in e-Health systems. A combination of a private Blockchain and consortium Blockchain was used to construct the proposed scheme. For storing the personal health data, a private Blockchain was employed while the consortium Blockchain keeps records of the secure indexes for the health records. The proof-of-conformance algorithm was employed to reach a consensus for adding new blocks to the Blockchains. The results of the security analysis demonstrated that the proposed protocol could achieve security objectives.

2.3.4.2 Off-Chain Storage of Medical Data

Xia et al. [219] designed a Blockchain-based medical data-sharing model, named MeDShare, for cloud service providers. The proposed framework employed smart contracts and consisted of four layers, including 1) user layer; 2) data query layer; 3) data structuring and provenance layer; and 4) existing database infrastructure layer to provide secure auditing, data provenance, and control for medical data.

2.3.5 Approaches Based on Permissionless Blockchain

2.3.5.1 Off-Chain Storage of Medical Data

Xu et al. [222] designed a Blockchain-based privacy-preserving scheme, called Healthchain, for protecting large-scale health data such as electrocardiogram (ECG), blood pressure, temperature, and so on collected from wearable sensors and IoT devices. In Xu's approach, users can add or revoke permission to authorized doctors using a flexible key management system to determine if a doctor can have access to their healthcare data. In this method, IoT and healthcare data cannot be deleted or compromised by unauthorized parties by using two Blockchains to conduct fine-grained access control. The proposed Healthchain system for smart healthcare system composed of different components including, IoT devices, user nodes, doctor nodes, accounting nodes and storage nodes. Data owners can revoke the doctors or add authorized doctors at any time to ensure the privacy of the user and avoid medical disputes.

3 Classification of Histopathological Biopsy Images Using Ensemble of Deep Learning Networks[1]

3.1 Introduction

Breast cancer has become one of the major causes of cancer-related death worldwide in women [107]. According to the World Health Organization reports [18], in 2018, it is estimated that 627,000 women died from invasive breast cancer - that is approximately 15% of all cancer-related deaths among women and breast cancer rates are increasing in nearly every country globally. It is evident that early detection and diagnosis plays an essential role in effective treatment planning and patient care. Cancer screening using breast tissue biopsies aims to distinguish between benign or malignant lesions. However, manual assessment of large-scale histopathological images is a challenging task due to the variations in appearance, heterogeneous structure, and textures [120]. Such a manual analysis is laborious, and time intensive and often dependent on subjective human interpretation. For this reason, developing CAD systems is a possible solution for classification of Hematoxylin-Eosin (H&E) stained histological breast cancer images. In recent years, deep learning outperformed state-of-the-art methods in various fields of machine learning and medical image analysis tasks, such as classification [161], detection [91], segmentation [113], and computer-based diagnosis [137]. The merit of deep learning compared to other types of learners is its ability to obtain the performance similar to or better than human performance. Feature extraction is a critical step since the classifier performance directly depends on the quality of extracted low and high-level features. Several feature fusion methods employing pre-trained CNN models were proposed in the literature that effectively applied to medical imaging applications [161, 134, 29]. Motivated by the success of ensemble learning models in computer vision, a novel multi-model ensemble method is proposed for binary classification of breast histopathological images. The experimental results on four publicly available datasets demonstrate that the proposed ensemble method generates more accurate cancer prediction than single classifiers and widely-used machine learning algorithms.

A number of visual characteristics such as variations in sources of acquisition device, different protocols

[1]This work was published in CASCON 2019 [106]. This chapter uses text descriptions and figures from the published paper.

in stain normalization, variations in color, and heterogeneous textures in histopathological slide images can affect the performance of the deep CNNs [120]. Hence, developing a robust automated analysis tool to support the issue of data heterogeneity collected from multiple sources is a major challenge. To address this challenge, a novel three-path ensemble architecture is proposed for binary classification of breast histopathological images collected from different datasets. Figure 3.1 depicts some examples of histology images acquired from different datasets. The variability and similarity of provided datasets can be observed in this figure.

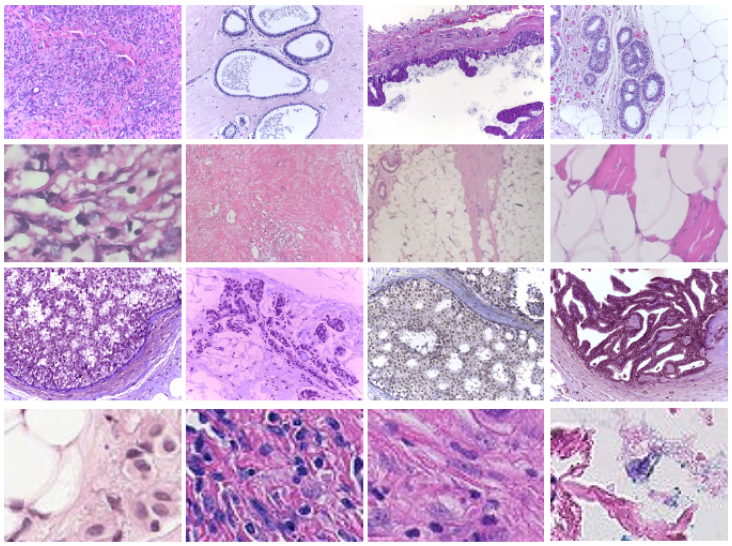

Figure 3.1: Examples of variability in tissue patterns. The histology images are adapted from [193], [209], [37], [2], [32].

The main contribution of this work is proposing a generic method that does not need handcrafted features and can be easily adapted to different datasets with the aim of reducing the generalization error and obtaining a more accurate prediction. The obtained results is compared with the traditional machine learning algorithms and also with each selected CNN individually. Experimental results showed that the proposed method outperforms both the state-of-the-art architectures and the traditional machine learning algorithms on the provided datasets. The proposed model employs three well-established pre-trained CNNs - VGG19, MobileNet, and DenseNet which aims to incorporate specific components, i.e., standard convolutions, separable convolutions, depthwise convolutions, long skip, and short-cut connections.

3.2 Methodology

In this section, the proposed methodology is discussed, then the dataset used in this study and the pre-processing steps is presented.

3.2.1 Proposed Network architecture

Few studies have been published on the application of the ensemble deep learning methods applied to breast histopathology images. Each of the adapted CNN architectures in the proposed model are constructed by different types of convolution layers in order to promote feature extraction and aggregation of fundamental information from a given input image. The entire methodology is mainly divided into six steps: collecting H&E microscopic breast cancer histology images, data pre-processing, data augmentation, feature extraction using the proposed network, classification and finally model evaluation. The quality of visual information of each input image is first improved using different pre-processing strategies. Then the training dataset size is increased with various data augmentation techniques. Once input images are prepared, they are fed into the feature extraction phase with the proposed ensemble architecture. The extracted features from each architecture are flattened together to create the final multi-view feature vector. The generated feature vector is fed into a multi-layer perceptron to classify each image into corresponding classes. Finally, the performance of the proposed method is evaluated on test images using the trained model. The performance of the proposed CNN architecture is validated on the four publicly available datasets, namely: ICIAR, BreakHis, PatchCamelyon and Bioimaging.

3.2.2 Feature extraction using transfer learning

Considering the high visual complexity of histopathological images, proper feature extraction is essential because of its impact on the performance of the classifier. However, due to the privacy issue in the medical domain, the provided datasets are not large enough to sufficiently train a CNN [96]. Aiming to tackle this challenge, a transfer learning strategy has been widely investigated to exploit the knowledge learned from cross domains instead of training a model from scratch with randomly initialized weights. In this method, knowledge learned by a dataset is transferred into the new dataset in another domain. Using a transfer learning approach, the model can learn general features from a source dataset that do not exist in the current dataset. Transfer learning has advantages such as speeding up the convergence of the network, reducing the computational power, and optimizing the network performance [132].

3.2.3 Three-path ensemble architecture for breast cancer classification

Three well-known architectures, VGG19 [189], MobileNetV2 [93] and DenseNet201 [98] are selected based on their (i) satisfying performances in different computer vision tasks (ii) usefulness towards real-time (or near real-time) applications and, (iii) feasibility of transfer learning for limited datasets. Considering that each method has shortcomings in regards to the variations of the shape and texture of the input image, inspired by the work of [142], a three-path ensemble prediction approach is proposed to make use of the advantages of the multiple classifiers to improve overall accuracy. Theses networks

are selected based on the obtained results of an exhaustive grid-search technique on different state-of-the-art architectures (i.e. InceptionV3, InceptionresNetV2, Xception, ResNet50, MobileNetV2 and DenseNet201, VGG19 and VGG16) with different combination of hyperparameters, including optimizer, learning rate, weight initialization, batch size, dropout rate to obtain the best possible performance for breast cancer detection. Figure 3.2 illustrates the proposed ensemble architecture for breast cancer classification. As demonstrated in Figure 3.2, the proposed architecture is constructed by three independent CNN architectures. The final fully connected layers of each CNN architecture are combined together to produce the final feature vector. This combination allows capturing more informative features. Therefore, it is possible to achieve a more robust accuracy.

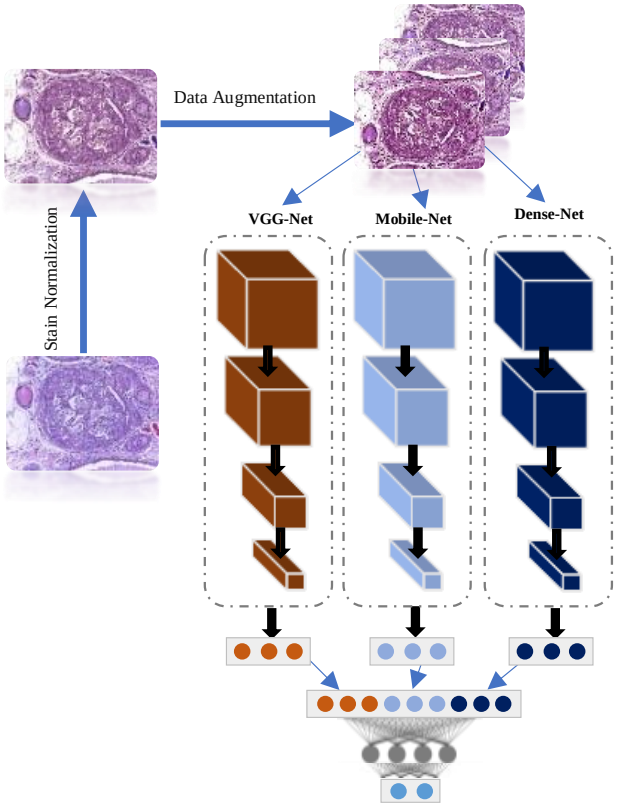

Figure 3.2: The proposed ensemble network with a three-path CNN. Histology image is adapted from [32].

VGGNet [189] was introduced by Karen Simonyan and Andrew Zisserman from Visual Geometry Group (VGG) of the University of Oxford in 2014. It achieved one of the top performances in the ImageNet Large Scale Visual Recognition Challenge (ILSVRC) 2014. The network used 3×3 convolutional layers stacked on top of each other, alternated with a max pooling layer, two 4096 nodes for fully-connected layers, and finally followed by a softmax classifier.

The MobileNet [93] architecture is the second model used for this study. MobileNet, designed by Google researchers, is mainly designed for mobile phones and embedded applications. The MobileNet

architecture was built based on depth-wise separable convolutions, followed by a pointwise convolution with a 1×1 convolution layer. In the standard convolution layer, each kernel is applied to all channels on the input image. While depthwise convolution is applied on each channel separately. This approach significantly reduces the number of parameters once is compared to standard convolutions with the same depth. MobileNet achieved inspiring performance over various applications with a fewer number of hyperparameters and computational resources.

As third feature extractor, DenseNet [98] architecture is employed. DenseNet, stands for Densely-Connected Convolutional Networks, is proposed by Huang et al. [98]. DenseNet introduces dense block, which is a sequential of convolutional layers, wherein every layer has a direct connection to all subsequent layers. This structure solves the issue of vanishing gradient and improves feature propagation by using very short connections between input and output layers throughout the network.

3.3 Experiments

This section describes the design and implementation of the proposed model.

3.3.1 Datasets description

Four benchmark datasets are used for evaluating the performance of the proposed model. BreakHis [193] dataset consisting of 7909 H&E stained microscopic images which was collected from 82 anonymous patients. The dataset is divided into benign and malignant tumor biopsies. Small patches were extracted at four magnification of ×40, ×100, ×200, and ×400. The benign tumors were classified into four subclasses which were adenosis (A), tubular adenoma (TA), phyllodes tumor (PT), and fibroadenoma (F) and the malignant tumors were also classified into four subclasses which were ductal carcinoma (DC), mucinous carcinoma (MC), lobular carcinoma (LC), and papillary carcinoma (PC).

A modified version of the Patch Camelyon (PCam) benchmark dataset [209, 37], publicly available at [6], consisting of benign and malignant breast tumor biopsies is also used to evaluate the performance of the proposed classification model. The dataset consists of 327,680 microscopy images with 96× 96-pixel size patches extracted from the whole-slide images with a binary label indicating the presence of metastatic tissue. The modified version of this database is used since the original Patch Camelyon database contained duplicated images.

Additionally, two other datasets, the Bioimaging 2015 [2] challenge dataset and the ICIAR 2018 [32] dataset, are used in this work. The ICIAR 2018 dataset, available as part of the BACH challenge, was an extended version of the Bioimaging 2015 dataset. Both datasets consisted of 24 bits RGB H&E stained breast histology images and extracted from whole slide image biopsies, with a pixel size of 0.42 μm × 0.42 μm acquired with 200× magnification. Each image is classified into four different classes,

namely: normal tissues, benign lesions, in situ carcinomas and invasive carcinomas. The Bioimaging dataset contained 249 microscopy training images and 36 microscopy testing images in total, equally distributed among the four classes. The ICIAR dataset contained 100 images in each category, i.e., in a total of 400 training images. In order to create the binary database from these two datasets, normal and benign classes are grouped into the benign category and the in situ and invasive classes into the malignant category.

3.3.2 Data preparation and pre-processing techniques

Different data preparation techniques such as data augmentation, stain-normalization and image normalization strategies have been adopted to optimize the training process. In the following, each of them briefly is explained.

3.3.2.1 Data augmentation

Due to the limited size of the input samples, training the CNN is prone to over-fitting leading to low detection rate [122]. One solution to alleviate this issue is the data augmentation technique in which the aim is to generate more training data from the existing training set. Different data augmentation techniques, such as horizontal flipping, rotating and zooming are applied to datasets to create more training samples. The data augmentation parameters utilized for all datasets are presented in Table 3.1. Examples of histopathological images after the augmentation are shown in Figure 3.3.

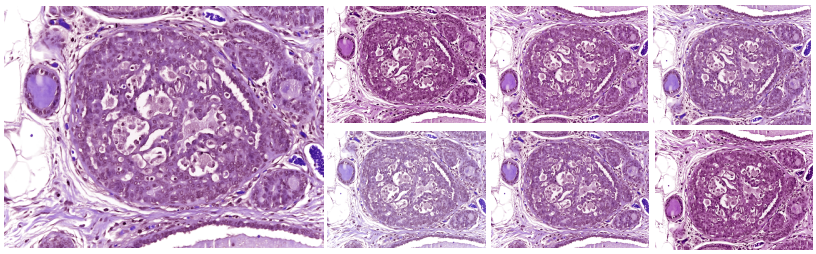

Figure 3.3: Images obtained after data augmentation techniques. The histology image is adapted from [32].

3.3.2.2 Stain-normalization

The tissue slices are stained by Haematoxylin and Eosin (H&E) to differentiate between nuclei stained with purple color as well as other tissue structures stained with pink and red color to help pathologists analyze the shape of nuclei, density, variability and overall tissue structure. However, H&E staining variability between acquired images exists due to the different staining protocols, scanners and raw materials which is a common problem with histological image analysis. Therefore, stain-normalization

of H&E stained histology slides is a necessary step to reduce the color variation and obtain a better color consistency prior to feeding input images into the proposed architecture. Different approaches have been proposed for stain normalization in histological images, including Macenko et al. [135], Reinhard et al. [174] and Vahadane et al. [206].

Table 3.1: Data augmentation parameters.

Parameter	**Value**
Horizontal Flip	True
Vertical Flip	True
Contrast Enhancement	True
Zoom Range	0.2
Shear Range	0.2
Rotational Range	90°
Fill Mode	Nearest

For this experiment, Macenko et al. [22] approach is applied due to its promising performance in many studies [221, 180, 25, 184] to standardize the color intensity of the tissue. Macenko method is based on a singular value decomposition (SVD). In this method, a logarithmic function [135] is used to adaptively transform color concentration of the original histopathological image into its optical density (OD) image as given in equation 1.

$$OD = -log\left(\frac{I}{I_0}\right) \tag{3.1}$$

Where OD is the matrix of optical density values, I is the image intensity in RGB space and I_0 is the illuminating intensity incident on the histological sample.

3.3.2.3 Image normalization

Another necessary pre-processing step is intensity normalization. The primary purpose of image normalization [230] is to obtain the same range of values for each input image before feeding to the CNN model which also helps to speed up the convergence of the model. Input images are normalized to the standard normal distribution by min-max normalization to the intensity range of [0, 1], which is computed as:

$$x_{norm} = \frac{x - x_{min}}{x_{max} - x_{min}} \tag{3.2}$$

where X is the pixel intensity. x_{min} and x_{max} are minimum and maximum intensity values of the input image in equation 2.

3.3.3 Experimental settings

All images were resized to 224×224 pixels using bicubic interpolation according to the input size of the selected pre-trained models. The batch size was set to 32 and all models trained for 1000 epochs. A

fully connected layer trained with the rectified linear unit (ReLU) activation function with 256 hidden neurons followed by a dropout layer with a probability of 0.5 to prevent over-fitting. The dropout layer helps to further reduce over-fitting by randomly eliminates their contribution in the training process. For Adam optimizer, $\beta 1$, $\beta 2$ and learning rate were set to 0.6, 0.8 and 0.0001, respectively. For fine-tuning, the last dense layer in all architectures is modified to output two classes corresponding to benign and malignant lesions instead of 1000 classes as was proposed for ImageNet. All pre-trained Deep CNN models are fine-tuned separately. Also, the network weights were initialized from weights trained on ImageNet. The operating system is Windows with an Intel(R) Core(TM) i7-8700K 3.7 GHz processors with 32 GB RAM. Training and testing process of the proposed architecture for this experiment is implemented in Python using Keras package with Tensorflow as the deep learning framework backend and run on Nvidia GeForce GTX 1080 Ti GPU with 11GB RAM.

3.3.4 Evaluation criteria

The performance of the proposed classification model was evaluated based on recall, precision, F1-score, and accuracy. Given the number of true positives (TP), false positives (FP), true negatives (TN) and false negatives (FN), the measures are mathematically expressed as follows:

$$Accuracy = \frac{TP + TN}{TP + TN + FP + FN} \times 100 \tag{3.3}$$

$$Precision = \frac{TP}{TP + FP} \times 100 \tag{3.4}$$

$$Recall = \frac{TP}{TP + FN} \times 100 \tag{3.5}$$

$$F1 - Score = 2 \times \frac{Recall \times Precision}{Recall + Precision} \tag{3.6}$$

3.4 Discussion

In this research, a binary classification of histopathological images using a three-path ensemble architecture with transfer learning and fine-tuning is proposed. To verify the effectiveness of the presented methodology, different comparative analyses were conducted. First, the obtained results is compared of the proposed ensemble model on the four provided datasets. Then, the comparison between proposed ensemble architecture and CNN classifiers individually is provided and finally, a comparison of the proposed ensemble architecture and machine learning algorithms is presented. In Table 3.2 and Figure 3.4, the obtained accuracy, precision, recall and F-score of the proposed approach for each

benchmark dataset is demonstrated. The proposed method on BreakHis dataset achieved the highest accuracy, precision, recall, and F-score with values of 98.13%, 98.75%, 98.54% and 98.64%, respectively.

Table 3.2: Results of accuracy, precision, recall, and F-score of the proposed method.

	Accuracy	Precision	Recall	F-score
BreakHis	98.13%	98.75%	98.54%	98.64%
PatchCamelyon*	94.64%	95.70%	95.27%	95.50%
ICIAR	95.00%	95.91%	94.00%	94.94%
Bioimaging	83.10%	92.60%	71.42%	80.64%

On the other hand, the results also demonstrate that the detection rate is worst on the Bioimaging dataset with 83.10% accuracy, 92.60% precision, 71.42% recall and 80.64% F-score. Table 3.3 and Figure 3.5 presents the performance of the single classifiers on the four datasets. Analyzing Table 3.3 and Figure 3.5, the maximum 97.42%, 96.41% and 92.40% accuracies are produced on the BreakHis dataset by DenseNet201, VGG19 and MobileNetV2 models, respectively.

Table 3.3: Results of accuracies obtained by single classifiers on four open access datasets.

	VGG19	MobileNetV2	DenseNet201
BreakHis	96.41%	92.40%	97.42%
PatchCamelyon*	90.84%	89.09%	87.84%
ICIAR	90.00%	92.00%	85.00%
Bioimaging	81.69%	78.87%	80.28%

Table 3.4: Classification results of different state-of-the-art CNN classifiers on four datasets.

	BreakHis	**PCamelyon***	**ICIAR**	**Bioimaging**
InceptionV3	87.66%	87.52%	83.00%	85.00%
Xception	86.37%	88.05%	83.00%	78.77%
ResNet50	79.48%	79.06%	80.00%	63.38%
InceptionResNetV2	92.40%	89.93%	89.00%	76.06%
VGG16	93.54%	88.39%	89.00%	83.10%

The classification results of different well-established CNN architectures, including InceptionV3, Xception, ResNet50, InceptionResNetV2 and VGG16 are summarized in Table 3.4. Analyzing Table 3.4, based on the obtained results, there is a level of variation in all results of datasets. As the results confirms the proposed architecture and each of the selected single classifiers delivered higher accuracy in all of the datasets except InceptionV3 architecture for Bioimaging dataset.

In Bioimaging dataset, the inceptionV3 network obtained 85.00% accuracy which is 1.9% lower than

result obtained by proposed architecture with 83.10% accuracy. For the sake of comparison, the performance of the proposed ensemble model is compared with the results of the previously published work for binary classification of breast cancer in Table 3.5. Referring to Table 3.5, on the BreakHis dataset, the proposed approach (98.13% accuracy) achieved a better performance compared to the methods in [193, 210, 87] with accuracies of 86.6%, 96.3% and 96.9%, respectively. On the binary classification of ICIAR dataset, the study in [180] achieved 92.5% while proposed method achieved 95%. On the binary classification of Bioimaging dataset, the proposed model obtained poor results in compare with studies of [210, 41] and only outperformed study in [31] [Arujo], which is slightly higher performance with a gap of accuracy of 0.7%. Finally, for PatchCamelyon* dataset, no study have been reported in the literature yet. To validate the performance of the proposed model, the proposed method is compared with five machine learning models, namely, Decision Tree, Random Forest, XGBoost, AdaBoost and Bagging Classifier. Table 3.6 summarizes the comparison of the performance of the state-of-the-art machine learning algorithms, i.e., Decision Tree, Random Forest, XGBoost, AdaBoost and Bagging Classifier. As given in this table, the topmost result was obtained by bagging classifier with 94.97% accuracy for BreakHis dataset. Random Forest produced 69.01% accuracy for Bioimaging dataset, which is the worst accuracy achieved in the classification of benign and malignant cases. The proposed model in the ICIAR dataset achieved 95.00% overall accuracy, which is the highest result reported in the literature for binary classification of this dataset with a gap in the accuracy of 5.00% for VGG19, 3.00% for mobileNetV2 and 10.00% for DenseNet201. The proposed model, on the same dataset, also outperforms other machine learning models by 18.00% for Decision Tree, 10.00% for Random Forest, 6.00% XGBoost, 16.00% for AdaBoost and finally 8.00% for Bagging Classifier.

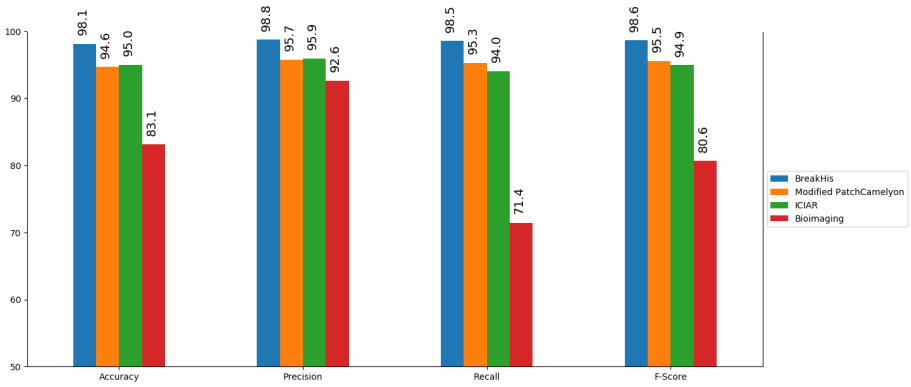

Figure 3.4: Results of accuracy, precision, recall, and F-score of the proposed method.

The largest gap is observed for Bioimaging dataset between the proposed model and Adaboost classifier, where the difference is more than 19.00%. The second most significant gap is achieved for the modified PatchCamelyon dataset between the proposed model and Decision Tree classifier, where the difference is 18.40%. The smallest gap is seen for BreakHis dataset between the proposed model and DenseNet201

architecture, where the difference is less than 1.00%. Similar conclusions can be drawn for other models. The experiment results indicate that the performance of the proposed ensemble method yields satisfactory results and outperforms both the state-of-the-art CNNs and machine learning algorithms in cancer classification on four publicly available benchmark datasets with a large gap in terms of accuracy. The proposed method is generic as it does not need handcrafted features and can be easily adapted to different detection tasks, requiring minimal pre-processing. These datasets were collected across multiple sources with different shape, textures and morphological characteristics. The transfer learning strategy has successfully transferred knowledge from the source to the target domain despite the limited dataset size of ICIAR and Bioimaging databases.

Table 3.5: Comparative analysis with presented methods in the literature.

Method	**Dataset**	**Accuracy**
Roy et al. [180]	ICIAR	92.50%
Vo et al. [210]	BreakHis	96.30%
Pratiher et al. [164]	BreakHis	98.70%
Spanhol et al. [193]	BreakHis	84.60%
Han et al. [87]	BreakHis	96.90%
Gandomkar et al. [81]	BreakHis	97.90%
Brancati et al. [41]	Bioimaging	88.90%
Arujo et al. [31]	Bioimaging	83.30%
Vo et al. [210]	Bioimaging	99.50%

Table 3.6: Comparison of classification accuracies obtained by different machine learning models.

	BreakHis	PatchCamelyon*	ICIAR	Bioimaging
Decision Tree	91.67%	76.24%	77.00%	71.83%
Random Forest	92.10%	82.54%	85.00%	69.01%
XGBoost	94.11%	87.15%	89.00%	78.87%
AdaBoost	91.82%	76.49%	79.00%	63.38%
Bagging	94.97%	88.05%	87.00%	81.69%

During the proposed approach, no over-fitting was observed to impact the classification accuracy adversely. The performance of all of the single classifier and the proposed ensemble model was poor on Bioimaging dataset. For this dataset, benign cases are confused with malignant cases since the morphology of some benign classes is more similar to malignant samples. Intuitively, the main reason is that the size of the Bioimaging dataset is not large enough for deep learning models to capture high-level features and distinguish classes from each other. Although, data augmentation strategies are employed to tackle this problem, but it will be more appropriate to collect more training data by increasing the number of samples rather than artificially increase the size of the dataset by data augmentation meth-

ods. Also, employing pre-trained models requires input images to be resized to a certain dimension which may discard discriminating information from this dataset.

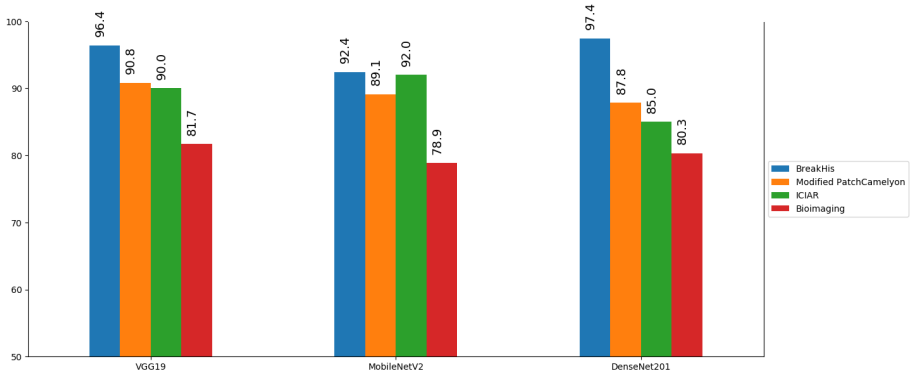

Figure 3.5: Classification accuracy of single classifiers of VGG19, MobileNetV2, DenseNet201

3.5 Conclusion

This chapter presents an ensemble-based deep learning approach for a computer-aided diagnosis of breast cancer detection. Three well-established CNNs architectures, namely VGG19, MobileNetV2 and DenseNet201 are ensembled for feature representation and extraction using different components. The combination of such various features leads to a better generalization performance than single classifiers as counterparts. The experimental results showed that the proposed model not only outperformed the individual CNN classifiers but also outperformed state-of-the-art machine learning algorithms in all the test sets of the provided datasets. The highest and lowest performances were obtained for BreakHis and Bioimaging datasets, respectively. Thus, the deep learning-based multi-model ensemble method can make full use of the local and global features at different levels and improve the prediction performance of the base architectures across different datasets.

4 A Hybrid Deep Learning Architecture for Leukemic B-lymphoblast Classification[1]

4.1 Introduction

Leukemia is a type of cancer associated with white blood cells that originates in the bone marrow and affects both children and adults. Leukemia can be divided into acute or chronic categories based on how quickly it progresses. There are four types of leukemia namely, Acute Myelogenous Leukemia (AML), Acute Lymphoblastic Leukemia (ALL), Chronic Myeloid Leukemia (CML), and Chronic Lymphocytic Leukemia (CLL) [112] [211]. The most common types of leukemia that affect young children are AML and ALL. In ALL, lymphocytes - a type of white blood cell (WBC) - do not function properly and reproduce out of control, leading to anemia [203]. This can lead to premature death if it is diagnosed in later stages or if the treatment process is delayed. Subject age is an important risk factor affecting prognosis, since the risk of developing ALL is highest in children below the age of 7-8 years. The risk then decreases until the mid-20s and begins to increase again after age 50. According to the data provided by [7], in 2018, about 5930 new cases of ALL will be diagnosed and about 1500 patients are expected to die of ALL, including both children and adults, in the United States. The risk of getting ALL is slightly higher in males than females, and higher in whites than African-Americans. However, if leukemia is diagnosed in its early stages, it is highly curable and increases the survival rate of the patients. Considering the large-scale of histopathology images, assessment of the images in a conventional way can be laborious, error-prone and hugely time-consuming since some images are highly variable in morphology which is difficult to analyze. Therefore, developing accurate and reliable approaches for Leukemia detection is important for early treatment. Numerous study results showed that with the advancement of computational capabilities, hidden trends, patterns and relationships can be discovered using the application of data mining approaches in many different areas [168, 201]. Figure 4.1 illustrates examples of ALL and healthy cells.

The signs and symptoms of ALL may range from mild symptoms such as fever, bleeding from the gums, fatigue, dizziness, and bone pain to severe life-threatening symptoms, which demonstrate the

[1]This work was published in IEEE ICTC 2018 [105]. This chapter uses text descriptions and figures from the published paper.

extent of bone marrow involvement [195, 102]. The examinations that are needed to confirm the ALL diagnosis are bone marrow aspiration and biopsy, complete blood count (CBC), and peripheral blood smear [151]. The nucleus-to-cytoplasm ratio in ALL and healthy cells are approximately 1/5 and 2/5, respectively. The healthy cells on a blood smear appear homogeneous and uniform, round-to-ovoid-shaped, small size, and with regular nuclear shape as demonstrated in Figure 4.1 (top row). ALL cells are heterogeneous in their shape and size. The shape of the ALL cells is elongated and atypical with large chromatin (a mass of genetic material). The ALL lymphoblasts vary in size and the shape of nuclei is very irregular.

Figure 4.1: Normal B-lymphoid cells (top row), leukemic B-lymphoblast cells (bottom row). The images are adapted from [4].

The details of the proposed approach are shown in Figure 4.2 and are described in the subsequent sections. Briefly, an automatic leukemic B-lymphoblast classification system using a hybrid of two Convolution Neural Network (CNN) and transfer learning is presented to extract features from each input image. Unlike previous approaches, instead of using deep features extracted from the entire pre-trained architectures, in this approach, fusing the features from specific abstraction layers can be deemed as auxiliary features lead to further improvement of the classification accuracy. In this approach features extracted from the lower levels are combined into higher dimension feature maps to help improve the discriminative capability of intermediate features and also overcome the problem of network gradient vanishing/exploding.

4.2 Materials and Methods

In this section, the proposed method is discussed, then the dataset used in this study and the pre-processing steps is presented.

4.2.1 Methodology

The approach consists of the following stages: Initially, the quality of visual information of each input image is enhanced using different pre-processing and augmentation techniques to increase the visibility

of crucial structures. Once input images are prepared, they are used in the feature extraction phase with the proposed hybrid architecture. The performance of two architectures namely, VGG16 [189] and MobileNet [93] are explored for the proposed hybrid model. VGG16 is a very simple yet effective architecture consists of 13 convolutional using 3 x 3 convolution filters followed by max pooling layers and two 4096 fully-connected layers, followed by a softmax classifier. MobileNet architecture is designed for object recognition on mobile devices. This architecture consists of depth-wise separable convolution and 1×1 point-wise convolutions. The performance of the MobileNet architecture is evaluated on ImageNet dataset and achieved an accuracy in the same level of accuracy as VGG16 with 32 times less parameters while is 27 times less computationally intensive. Since each architecture has its own shortcomings, an integrating strategy is proposed to make use of the advantages of both architectures in order to improve overall prediction accuracy. The extracted features were trained by a multi-layer perceptron to classify each image into corresponding class probabilities. Finally, the performance of the proposed architecture is evaluated on test images.

Transfer learning is a common strategy in deep learning tasks where a large dataset from a source task is used for training of a target task leading to not only overcome the problem of small datasets but also accelerate the learning process and improve the accuracy. Previous studies showed that transfer learning also has the potential to prevent over-fittings. The transfer learning approach enables us to adopt a pre-trained network that has already learned a rich set of low-level features from layers that are closer to the input image. Though the dataset is not the same, the low-level features produced by source CNN are mostly in general shapes, e.g. edges, contours and curves which are similar to the low-level features of target dataset while high-level features at the final layers concentrate on complex class-level characteristics which are needed to differentiate between classes. With the use of transfer learning, training of large CNNs can now be a more practical strategy with more promising results and significantly cost-effective by avoiding training a CNN from scratch.

4.2.2 Experimental Dataset

The dataset used for this study is based on Classification of Normal versus Malignant Cells in B-ALL White Blood Cancer Microscopic Images as part of ISBI 2019 challenge provided by SBILab which is available for the public at [4]. The images are stored with the resolution of 450×450 pixels using the 24-bit RGB color system. The size of each cell is approximately the size of 300×300 pixels. The images were annotated by experienced oncologists for the classification procedure. The methods developed by [30, 85, 73, 72, 169] are employed for segmentation and stain normalization of the provided dataset. The dataset contains a total of 76 individual subjects (47 ALL subjects and 29 Normal subjects), containing a total cells images of 7272 ALL and 3389 normal cells.

4.2.3 Data Pre-processing

4.2.3.1 Normalization

Image normalization is a process that changes the range of pixel intensity values by setting the mean of pixels to zero and variance to one. Two normalization methods are used in this experiment to compare the performance of different methods. First, the mean RGB value of all images is subtracted from the training set divided by its standard deviation to normalize the input images as suggested in [230]. All images are also normalized using ImageNet mean subtraction as a pre-processing step. The ImageNet mean is a pre-computed constant derived from ImageNet database [111].

4.2.3.2 Resizing

To remove the black margin of each image as illustrated in Figure 4.1, all images are cropped from the image center of the original size of 450×450 pixels to the appropriate size 380×380 pixels using bicubic interpolation to ensure each cell is located at the center and reduce the non-informative adjacent background regions.

4.2.3.3 Data Augmentation

CNNs demonstrated state-of-the-art performance in different tasks [57, 155, 121]. However, the performance of CNNs highly depends on training data size. Due to the data privacy issues in medical domain, collecting adequate clinical images is a challenge. To address the issue of limited dataset size and avoid over-fitting problems, various data augmentation techniques is applied to optimize the CNN performance as suggested in recent studies [163], including contrast adjustments and brightness correction, horizontal and vertical flips and intensity adjustments. The class distributions of dataset before and after data augmentation is presented in Table 4.1.

Table 4.1: Total number of class distributions before and after data augmentation.

Number of images		
Cell type	Before augmentation	After augmentation
Healthy cells	3389	27930
ALL cells	7272	53591

4.2.4 Proposed Deep CNN Architecture with Auxiliary Components

The main contribution of this study is proposing a hybrid CNN model that combines low-level features from intermediate layers in order to generate high-level discriminative feature maps for immature leukemic blast classification. In this approach, two well-established CNN architectures, namely MobileNet and VGG16 which have shown excellent performance in many computer vision tasks are used [183, 56].

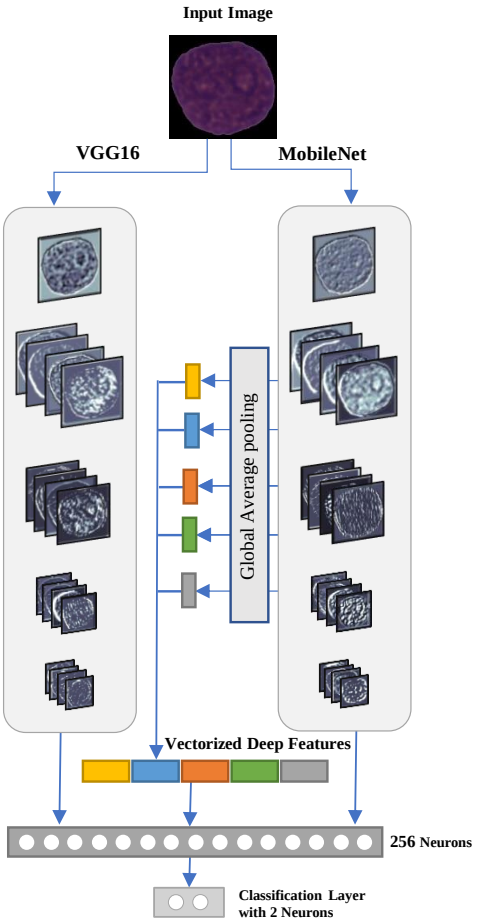

Figure 4.2: Architecture of the proposed CNN. The histology image is adapted from [4].

For the VGG16 architecture, the initial weights are obtained from weights learned from ImageNet by transfer learning strategy. As illustrated in Figure 4.2, from MobileNet architecture, features from five convolution layers are extracted. Then each of them is followed by an average pooling layer. Next, the extracted features are concatenated into a single feature vector. Thereafter, a new fully connected (FC) layer with 256 hidden units with rectified linear unit (ReLU) activation function is connected. Finally, two output neurons associating with normal and malignant cases with softmax non-linearity activation function are used at the classifier layer. These extracted features from selected intermediate layers can act as a complementary set of features to learn highly discriminative features beside the

existing extracted deep features. This approach results in detection of more complex patterns from each input image and gives higher accuracy with lower error rate. Employing very deep architecture for training limited samples could have the issues of vanishing gradients and poor local minima. The main benefit of applying a global average pooling layer is reducing the number of parameters in very deep architectures. This reduction helps to prevent getting stuck in the poor local minima in a high dimensional space which often occurs in learning from very deep CNNs. Additionally, once the number of parameters decreases, it can be ensured the gradient flow within the deep network and hence the learning process becomes stable regardless of the network depth, i.e. the number of hidden layers.

4.2.5 Evaluation Metrics

To evaluate the performance of the proposed method, three mostly used evaluation metrics namely, accuracy, sensitivity and specificity are considered. Accuracy shows the number of correctly classified ALL cases divided by the total number of test images denoting the overall correctness, is defined as:

$$Accuracy(\%) = \frac{TP + TN}{TP + TN + FP + FN} \times 100 \tag{4.1}$$

In detecting disease, sensitivity or True Positive Rate (TPR) is a measure of the proportion of true positive results to all real positives (subjects that have the disease). If cancer samples in the provided dataset are limited, the model has to be sensitive.

$$Sensitivity(\%) = \frac{TP}{TP + FN} \times 100 \tag{4.2}$$

Specificity or True Negative Rate (TNR) is a measure of the true proportion of negative results to all real negatives (subjects that do not have the disease). High specificity means that the model is good in detecting healthy cases.

$$Specificity(\%) = \frac{TN}{TN + FP} \times 100 \tag{4.3}$$

4.3 Experiment and Results

This section describes the design and implementation of the proposed model.

4.3.1 Experimental Setup

For the experiments, 70% of the images of each class are assigned to the training set, 20% to the validation set, and the remaining 10% to the test set. To obtain the optimal accuracy, several hyper-parameter tuning, using an exhaustive grid-search, is utilized. The effect of different optimizers, namely

adaptive moment estimation (Adam), stochastic gradient descent (SGD) with momentum, and root mean square propagation (RMSProp) are investigated. For SGD optimizer, the momentum term was set to 0.9. For Adam optimizer, $\beta 1$ and $\beta 2$ were set to 0.7 and 0.999, respectively. For RMSProp optimizer, rho and ϵ were set to 0.8 and None, respectively. The learning rate was set to 0.001 for the Adam optimizer and to 0.0001 for both RMSProp and SGD optimizer. The ReLU activation function and dropout [194] are utilized in the fully-connected layer with a rate of 0.4 to prevent over-fitting. The batch size was set to 32 in order to fit into the GPU memory. All models are trained for 1000 epochs. The experiment is implemented in Python using the Keras package with Tensorflow as the deep learning framework backend and run on Nvidia GeForce GTX 1080 Ti GPU with 11GB RAM.

4.3.2 Results and Discussion

The obtained results are derived from the 967 test images of the ISBI 2019 challenge which were not used in the training phase. These test set are consist of 312 normal cases and 655 ALL cases. First, the effect of image normalization and different optimizers is examined on the classification performance. The accuracy, sensitivity and specificity of the obtained results are tabulated in Table 4.2.

Table 4.2: Effects of different optimizers and image normalization techniques.

Optimizer	Normalization	Accuracy	Sensitivity	Specificity
Adam	ImageNet Mean	95.14	**95.92**	93.44
RMSProp	ImageNet Mean	93.38	94.17	91.61
SGD	ImageNet Mean	93.17	91.3	98.42
Adam	Dataset Mean	**96.17**	95.17	98.58
RMSProp	Dataset Mean	92.04	90.58	96.07
SGD	Dataset Mean	89.76	86.96	**99.53**

As the results confirm, there is a level of variation in all results when running the experiments with different optimizers and image normalization techniques. Analyzing Table 4.2, the proposed model delivered high accuracy (96.17%) on dataset mean normalization with Adam optimizer. High sensitivity (95.92%) result achieved by Adam optimizer, and ImageNet mean normalization method, and high specificity (99.53%) obtained by dataset mean normalization and SGD optimizer. Surprisingly, the worst classifier is observed by SGD optimizer and dataset mean normalization with an accuracy of 89.76%, sensitivity of 86.96%, and specificity of 99.53 (the last row in Table 4.2).

To justify the performance of the proposed approach, the performance of each architecture is individually evaluated. Table 4.3 provides the comparison of the individual VGG16 and MobileNet architectures

with the proposed model. From Table 4.3, it can be seen that the proposed method significantly outperforms the individual architectures on the provided dataset. The proposed model improves VGG16 up to 16% and MobileNet by 8.17% in terms of accuracy, which is considered significant. Moreover, the plain MobileNet architecture (88.00%) gives a better performance than VGG16 architecture (80.77%). This means the gap in accuracy is 7.23%, in favor of MobileNet. This is probably because of the benefit of the depth-wise and point-wise blocks in MobileNet compared to regular convolutional blocks in VGG16.

Table 4.3: Classification results from plain pre-trained networks and proposed model.

	Accuracy	Sensitivity	Specificity
Plain MobileNet	88	86.66	92.24
Plain VGG16	80.77	78.21	96.32
Proposed model	**96.17**	**95.17**	**98.58**

For the sake of comparison, the proposed ensemble is compared with some of the recent studies in the literature in Table 4.4. As shown in Table 4.4, the proposed approach achieves better performance compared to other studies in terms of the accuracy.

Table 4.4: The comparison of the proposed method with recent studies on leukemia detection

Dataset	Method	Accuracy	Year
DTH	Yu et al. [230]	88.50%	2017
ISBI	Mourya et al. [149]	89.62%	2018
ALL-IDB2	Singhal et al. [191]	89.72%	2014
MISP	Mohamed et al. [143]	93.00%	2018
ALL-IDB	Patel et al. [160]	93.75%	2015
IGH	Mohapatra et al. [145]	94.73%	2013
ISBI	Proposed Approach	**96.17**	2019

The experimental results in Table 4.4 confirm that the proposed ensemble, by aggregating features from intermediate layers outperforms all counterparts and achieves the highest accuracy. This indicates the important role of ensemble based deep learning in joint with highly descriptive feature. The proposed learner gains accuracy of 96.17% on the recent ISBI 2019 dataset while counterpart study at [149] from the Table 4, gains accuracy of 89.62% on the same dataset.

Although the results generated by the proposed method are encouraging, there are some limitations of the method are highlighted as follows. First, large-scale datasets are needed in training deep learning applications, and the provided training data for this study is limited. To resolve this problem, various data augmentation strategies are employed. It will be more appropriate to have access to more reliable data sources by increasing the number of samples. Also, using pre-trained networks as feature extractors requires images to be resized to a certain dimension for some architectures which may discard valuable discriminating information. The above-mentioned points will be the focus of the future directions with the aim to reduce the false positive rate and further improvement of the final accuracy.

4.4 Conclusion

We presented an automatic CNN hybrid method for classification of ALL and healthy cells. Two well-established CNNs, namely, VGG16 and MobileNet are used to extract features from multiple abstraction levels. The proposed model could extract features from chosen pre-trained and fine-tuned Deep CNNs. Fusing the features from selected intermediate layers can be regarded as an auxiliary set of features which leads to further improvement of the classification accuracy. This approach not only helps to learn more complex patterns but also addresses the issues of vanishing gradients and poor local minima by reducing the number of parameters. The obtained results suggest that combining features learned by deep models improves the performance and yield more accurate result (96.17%) than individual state-of-the-art networks. To resolve the problem of limited data size, different data augmentation techniques are employed. The transfer learning strategy was also employed to accelerate the learning process and further improve the performance of the proposed network.

5 Revisiting Deep Skip Connections and Transfer Learning for Lung Cancer Segmentation in Histology Images[1]

5.1 Introduction

Lung cancer is the leading cause of cancer-related death worldwide. Lung cancer accounts for one-quarter (26%) of all cancer-related death worldwide with over 225,000 cases, 150,000 deaths, and $12 billion in health care costs yearly in the United States. The five-year survival rate after diagnosing lung cancer is lower than other cancers varying from 4% to 17% depending on stage and type of lung malignancies and is even lower in developing or underdeveloped countries [9]. Lung cancer screening programs play an essential role in the early detection of lung cancer, effective treatment planning and improving the patient survival rate. Once lung nodules are detected, different gold standard methods such as CT image scans are performed to measure the size, shape, morphology, and location of the nodules and determine the level of malignancy of the nodules. Taking a pathological biopsy from suspicious tissue is a pre-requisite step in diagnosing the sub-type of lung cancer in routine clinical practice. The result of biopsy image analysis determines the direction of treatment planning. However, histopathology image-based assessment needs the manual inspection of pathologists, which can be time-consuming and tedious [162].

Computer-aided diagnosis (CAD) systems have the potential to be applied for lung nodules detection and provide a second opinion for image interpretation and diagnosis. Because of the dramatic increase in image modalities (e.g. MR, CT, X-ray, pathology) and the limited number of doctors, CAD systems have been proposed to assist in the clinical field by reducing the false-negative or false-positive detection rate. Recently, deep learning integrated with medical image processing has achieved great success in different tasks such as image classification, segmentation, and object detection. Convolutional neural networks (CNNs), as one of the primary parts of deep learning architectures, offer the ability to extract high-level discriminative features using a convolution kernel. Every tumor tissue slice exhibits complex

[1] An extension of this chapter is under review for publication. This chapter uses text descriptions and figures from the manuscript.

morphological structures and properties with a significant level of inter-tumor similarity and intra-tumor variability [141]. Figure 5.1 shows some examples of the provided dataset for lung tissue segmentation.

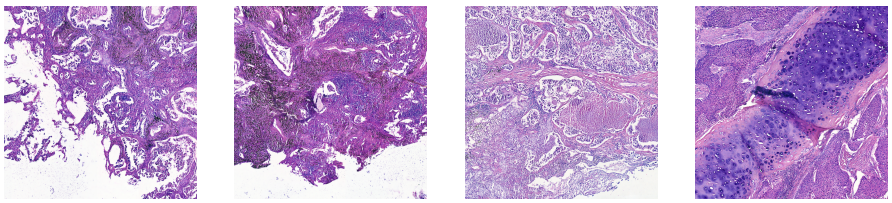

Figure 5.1: Patch images extracted from WSIs of H&E-stained lung specimens. The histology images are adapted from [126].

5.2 Motivation and Contributions

Considering the issues of manual delineation, intra- and inter-observer variability, in this work, a deep learning-based method is proposed for automatic lung carcinoma tissue segmentation. The proposed segmentation architecture is inspired by the existing deep CNN architectures. In this way, we can get a better insight into how different convolutional models can capture the high-level features and improve the performance. Thus, this study is aimed to investigate the impact of transfer learning, deep CNN modules and components in extracting high-level discriminative features in lung carcinoma tissue segmentation.

The main contributions of this work can be summarized as follows:

- To the best of our knowledge, this study is the first attempt to a CNN-based encoder-decoder with transfer learning feature extractors and skip connections for the fine-grained lung cancer tissue segmentation, which is a challenging task in practice. The presented deep CNN model contains two parts, the down-sampling part is a feature extractor utilizing transfer learning strategy to extract features from tissues, and the up-sampling part reconstructs the prediction map and segments out the region of interests.
- The performance of different state-of-the-art CNN architectures, e.g., Inception, ResNet, VGGNet, MobileNet DenseNet, InceptionResNet, SE-ResNeXt on ACDC-LungHP dataset is also investigated on the proposed encoder-decoder architecture. The impact of incorporating modules of each deep CNN feature extractor and also transfer learning are analyzes throughout a comparative study.
- The proposed model is trained on ACDC-LungHP [126] lung cancer segmentation challenge available at [1] to evaluate the performance of different deep transfer learning models. Experimental results demonstrate that shared DenseNet169 feature extractor in the encoder part of the proposed architecture achieves the state-of-the-art performance and outperforms competing deep feature extractors with a dice similarity of 82.50%, accuracy of 87.10%, precision of 83.60%, recall of 82.97%

and F1-score value of 82.63%. The integration of short and long skip connections into the proposed model helps extract more crucial contextual information and improve the performance of learners.

5.3 Materials and Methods

The proposed pipeline consists of the following stages: Initially, from each input whole-slide images (WSI), patches of the size of 1024×1024 are extracted to increase the visibility of crucial structures. Then, different augmentation techniques are applied to each patch to increase the dataset size. Once input images are prepared, they are fed into the proposed encoder-decoder architecture. The usability of a wide variety of deep CNN architectures into the encoder part of the proposed architecture is investigated in this study. The proposed encoder-decoder architecture preserves spatial information of the input image using skip connection operations such as dense modules and residual blocks to connect contextual information from the internal blocks of the encoder part to the corresponding decoder part. Since each deep CNN architecture has its own shortcomings and limitations when seeking an optimal and crucial feature, an integrating strategy of segmentation backbone architecture with deep CNN feature extractors is proposed in order to improve the overall segmentation performance. Finally, the performance of the proposed architecture is evaluated on test images.

5.3.1 Skip-connections CNN Architecture for Lung Tissue Segmentation

To achieve the best combination of feature extractor and encoder-decoder architecture with higher accuracy and lower loss value, the performance of various CNN architectures is taken into consideration. Different combinations of feature extractors such as DenseNet [98], InceptionV3 [199], InceptionResNetV2 [197], MobileNet [93], ResNet [89], SE-ResNet [94] and VGGNet [189] are designed and tested on three backbone models of FPN, U-Net and proposed encoder-decoder model. Deep CNN architectures are typically employed for different biomedical classification tasks. However, employing CNN feature extractors in encoder part of a segmentation architecture such as FPN aids in extracting spatial features and classify each pixel into cancerous or healthy classes and then the decoder part of the architecture segments complex structures in histology images. Finally, the predicted probability map is given as output. In decoder part of segmentation architectures, the pooling layers are replaced by up-sampling layers to reconstruct the predicted mask at the same dimension of the input image. Due to the GPU memory constraints, the large WSIs are patched, and the empty white patches without ROIs are discarded. The overall architecture of the proposed encoder-decoder architecture with skip-connections is illustrated in Figure 5.2. Referring to Figure 5.2, the proposed architecture consists of two parts. The encoding path (left area) is comprised of convolutions layers, followed by ReLU and max-pooling layers. To address the overfitting and vanishing gradient problems, the previous layer is merged into

the future layer using short skip connections (concatenation operation). The decoding path (right area) is comprised of up-sampling layers of convolution and ReLU layers to reconstruct feature maps [97]. Furthermore, batch normalization technique is employed in the decoder part of the proposed model to reduce the internal covariant shift. Batch normalization layers dynamically normalize the inputs of each convolutional layer. By adopting the introduced modified segmentation encoder-decoder architecture, a high dice similarity coefficient and accuracy rate are achieved for tissue segmentation of H&E lung specimens stained. With this setup, the proposed method could accurately segment cancerous regions within tissue structures with the dice similarity index of 84.10% and accuracy of 90.69%.

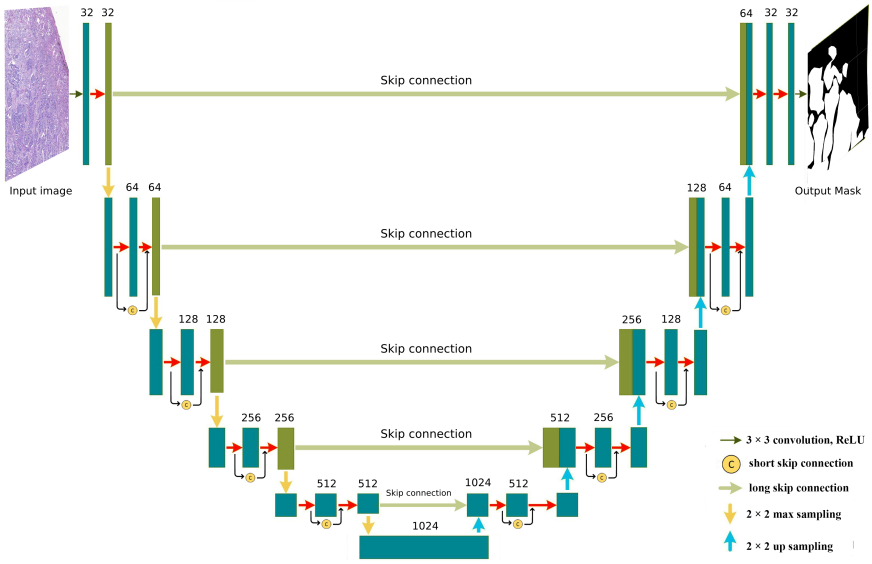

Figure 5.2: The overview of proposed skip-connections encoder-decoder CNN architecture. The histology image and the corresponding mask is adapted from [126].

The proposed pipeline is defined based on hierarchical CNNs employing skip-connections to allow an end-to-end training for fine-grained lung tissue segmentation. The proposed model first originates as a plain encoder-decoder segmentation backbone network – linearly stacked convolutional layers followed by pooling layers. In a conventional encoder-decoder deep CNN, each convolutional layer in the encoder part acts as a feature extractor, and the decoder part acts as feature reconstruction. In addition, four skip-connections are introduced in the proposed architecture to bridge the lower layers to upper layers on the basics of the backbone in order to take the characteristics of fine-grained lower-level contextual features into consideration. Also, the down-sampling layers in the encoder part are linked with the corresponding up-sampling layers using long skip connections. For further performance improvement and take advantages of transfer learning strategy, the encoder part of the proposed architecture is replaced with feature extractors, and the up-sampling layers of the decoder part are adjusted based on the encoder part. As histopathology images exhibit substantial inter-tumor similarity and intra-tumor variability, it is crucial to capture the specific and essential features with a different mechanism

in a network. Therefore, the proposed architecture consists of two types of skip connections to the network: i) based on the aforementioned considerations, short skip connections link the layers inside the encoder/decoder blocks and help exploit better discriminative visual features from intermediate layers. ii) long skip connections is used to link the encoder layers to decoder layers. Long skip connections concentrate on accurate reconstruction of the segmented masks.

5.3.1.1 Residual Units

Modern deep CNN models have become increasingly deep to capture the most important contextual information from input data and achieve higher performance. However, increasing the depth of CNN architectures causes the issue of vanishing gradients of information before reaching the initial layers of a CNN during backpropagation step. The vanishing gradient issue leads to the insensitivity of detecting fine-grained textures and boundaries [225]. To address the aforementioned issue and facilitate the training of very deep CNNs, residual units are proposed [89] to pass the gradient directly with an identity function from shallow layers to deep layers, as illustrated in Figure 5.3. A residual unit learns the residual information from multiple layers by enabling feature reuse between the input and output layers instead of directly learning information from each layer. The residual unit has been proven to be an effective approach to avoid the over-fitting and gradient disappearance and improve model performance compared with standard CNNs.

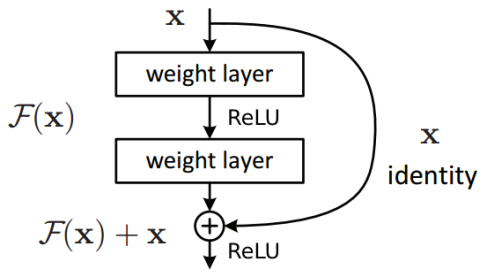

Figure 5.3: The illustration of a residual unit. The figure is adapted from [218].

5.3.1.2 Dense Blocks

The dense connections, introduced by Huang et al. [98], allow to design a deeper network with more effective information flow and prevent the problem of gradient vanishing. Moreover, dense blocks strengthen feature maps and feature propagation in subsequent layers and improve the performance of deep CNNs based on 1) bridging information flow from early layers to later layers; 2) concatenation of learnable feature maps; 3) flow of gradient information through the convolutional layers [34]. The difference between skip connections in residual units and dense blocks is the type of connection operation. The skip connections in residual units have been implemented using summation operation, while

concatenation operation is used in dense blocks to connect convolutional layers. Dense connections double the numbers of feature maps and learn-able parameters. Skip connections using concatenation operation are the key feature of the proposed architecture in this study. Figure 5.4 illustrates an example of dense block with five convolutional layers and concatenation operations to skip some of the layers from training and updating the weights.

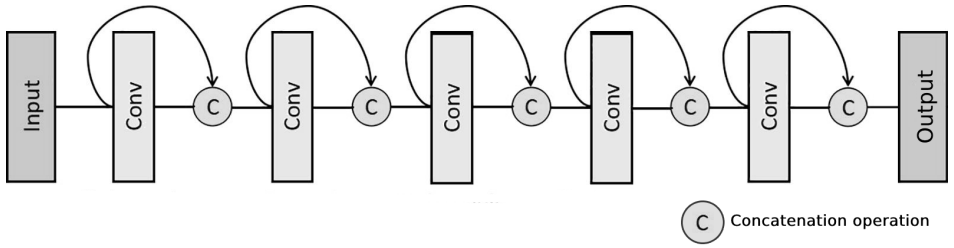

Figure 5.4: The diagram of a dense block with five convolutional layers. The figure is adapted from [68].

5.3.1.3 Batch Normalization

Batch normalization [100] is an effective normalization technique that currently plays an important role in training deep CNNs. This technique dynamically normalizes the input features of each layer, which is the output of the previous layer. The main reason to employ batch normalization is the internal covariant shift problem. The normalized data need to be fed into an activation function, which could skew the extracted feature distributions. For example, the ReLU activation function only propagates non-negative features to the subsequent layers. In other words, ReLU activation function skews the distribution to only positive features. Aiming to mitigate the aforementioned internal covariant shift, batch normalization is proposed to normalize features between non-linearities. This approach significantly improves training speed and leads to a higher performance.

5.3.2 Dataset Description

ACDC-LungHP [126] [127] dataset available at [1] is used for evaluating the performance of the proposed segmentation model in detecting and classifying lung cancer. ACDC-LungHP contains 100 WSIs divided into irregular sub-regions under 40× lenses digitized using the same scanner. The cancer regions of all WSIs have manually annotated by several qualified pathologists on tissue level for each WSI. The main goal of this challenge is to evaluate machine learning algorithms for diagnosing micro-and macro-metastases in a lymph node in H&E-stained histopathology tissue slides. Developing machine learning algorithms for automatic assessment of lung biopsy tissues could help reduce the workload of manual assessment and also prevent from subjective bias in detecting and segmenting lung carcinoma in WSIs.

5.3.3 Data Preparation and Pre-processing Techniques

5.3.3.1 Patch Extraction

An eye-fit magnification level of a WSI, as demonstrated in Figure 5.5 does not provide necessary information about tumor or healthy regions for a successful diagnosis. Therefore, a pathologist should increase the magnification level for a more detailed field of view of a WSI. For generating the dataset, a given WSI of the provided dataset with a typical size of 1 gigapixel at 20× magnification is split into patches. To this end, a number of 7447 patches for training set and 670 patches for testing set with the size of 1024×1024 pixels were extracted from 100 WSIs in total. Figure 5.6 shows the process of patch generation from an input WSI. By generating a patch with proper magnification, the machine learning algorithms can capture high-level information and patterns of tumor and non-tumor regions.

Figure 5.5: A WSI of a typical lung tissue specimen. The histology image is adapted from [126].

Figure 5.7 shows samples of 12 representative patches of tumor regions from a WSI of the provided dataset. The image on the left side shows a WSI, and the black square boxes are patch regions on the WSI. Images on the right side are selected patches. The patches with no information such as white background are removed from dataset generation process.

5.3.3.2 Data Augmentation

The performance of CNNs highly depends on the size of the training data. Due to the data privacy issues in medical domain, collecting adequate clinical images is a challenge. To this end, data augmentation techniques were used for two reasons in developing a robust method, i) to address the issue of limited dataset size and ii) to avoid over-fitting problems, as suggested in recent studies [180, 163, 183]. In this

study, data augmentation techniques including horizontal and vertical flips, random filter, and rotation were adopted only for training data subset.

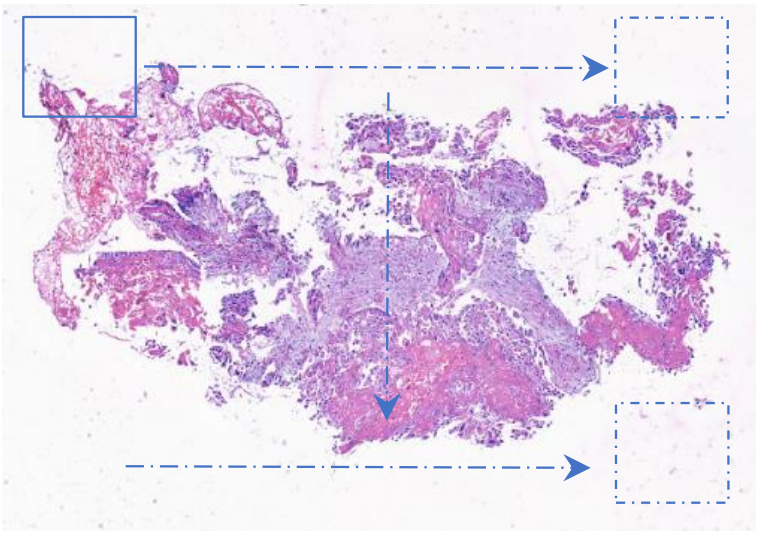

Figure 5.6: The process of patch generation from a whole slide image (WSI). The histology image is adapted from [126].

5.3.4 Experimental Settings

For CNN-based models, to minimize loss function, SGD (Stochastic Gradient Descent with momentum, proposed by [181]) is used as an optimizer with a learning rate set to 0.1, momentum set to 0.9 and decay rate set to 0.1. The SGD accepts a parameter learning rate η (default value is set to 0.01), momentum as a parameter of μ, decay parameter to decay the learning rate over the weights updates and Nesterov parameter for employing the Nesterov momentum with the following formula:

$$\eta^{(t+1)} = \frac{\eta^{(t)}}{1 + decay} \tag{5.1}$$

In training part, the mini-batch size is set to 4 images due to GPU memory limitations, and all models are trained for the maximum iteration of 50 epochs to minimize training error. The dataset has been divided into training, validation and testing sets with ratios of 70%, 20% and 10% of the total patched images, respectively. The weights for all of the feature extractors were initialized by using pre-trained ImageNet initialization. The ImageNet weight initialization approach assists in faster convergence and speeds up the training process. All experiments were run on a PC with following configuration: Intel(R) Core (TM) i7-8700K 3.7 GHz processors with 32 GB RAM. The training and testing process of the proposed architecture for this experiment is implemented in Python using Keras package with Tensorflow as deep learning framework backend and run on Nvidia GeForce GTX 1080 Ti GPU with 11GB RAM.

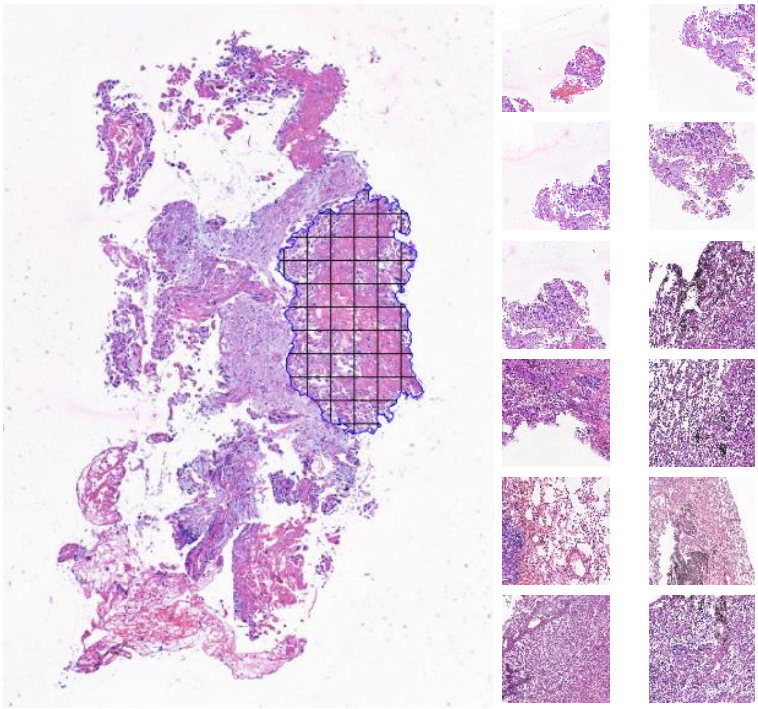

Figure 5.7: The process of patch generation from a whole slide image (WSI). The histology image is adapted from [126].

5.3.5 Evaluation Metrics

To measure the performance of the proposed method, common segmentation evaluation metrics such as dice similarity coefficient, precision, recall, f1-score were adopted to quantitatively measure similarity and difference between predicted mask from the proposed model and ground-truth mask at the pixel level.

The dice similarity coefficient measures the spatial overlap between ground truth and predicted mask produced by the proposed architecture. These metrics are computed as,

$$Dice\,(A, B) = \frac{2 \times \mid A \cap B \mid}{\mid A \mid \cup \mid B \mid} \times 100 \tag{5.2}$$

where A represents the output binary mask produced from the segmentation method, B represents the ground-truth mask, $\cup$ represents union set between A and B, and $\cap$ represents the intersection set between A and B.

Accuracy metric is used to measure the overall accuracy of the segmentation models. Given the number of true positives (TP), false positives (FP), true negatives (TN) and false negatives (FN):

$$Accuracy = \frac{TP + TN}{TP + TN + FP + FN} \times 100 \tag{5.3}$$

Precision and Recall metrics are analyzed to measure the amount of over-segmentation and under-segmentation, respectively. Precision is sensitive to over-segmentation as it is associated with a small

precision score. The recall is sensitive to under-segmentation as it is associated with results in low recall scores.

$$Precision = \frac{TP}{TP + FP} \times 100 \tag{5.4}$$

$$Recall = \frac{TP}{TP + FN} \times 100 \tag{5.5}$$

F1-score also computed as a harmonic mean of precision and recall between predicted and ground truth boundaries to evaluate the performance of the proposed approach.

$$F1 - Score = 2 \times \frac{Recall \times Precision}{Recall + Precision} \times 100 \tag{5.6}$$

5.4 Experimental Results and Discussion

Pathological examinations remain the gold standard in diagnosing of almost all types of cancers. Aiming at developing robust and automated histopathological image analysis tools, a novel deep learning-based network is presented. This study is conducted on a patch-based generated dataset over 100 WSIs of ACDC-LungHP dataset. All experiments were performed on the total numbers of 7,447 training patches and 670 testing patches extracted from the provided dataset to identify tumor regions from non-tumor regions.

Table 5.1: Comparative analysis of different feature extractors and FPN architecture.

FPN	**Dice**	**Accuracy**	**Precision**	**Recall**	**F1-score**	**MSE**
DenseNet121	80.25	88.41	82.20	81.39	80.44	0.1084
DenseNet169	**82.32**	**89.59**	80.54	87.05	**82.48**	**0.0967**
DenseNet201	<u>80.86</u>	<u>88.51</u>	82.54	82.05	<u>81.07</u>	<u>0.1066</u>
InceptionV3	79.13	87.48	80.49	81.13	79.22	0.1167
InceptionResNetV2	77.63	85.65	74.76	85.77	77.77	0.1338
MobileNet	79.10	86.84	77.49	84.70	79.14	0.1248
MobileNetV2	79.15	87.12	77.51	84.72	79.29	0.1205
ResNet18	78.96	86.21	74.47	88.60	79.05	0.1303
ResNet34	79.17	86.62	75.92	86.59	79.24	0.1257
ResNet50	80.27	87.75	77.96	86.11	80.38	0.1157
SE-ResNet18	79.37	86.52	75.33	88.17	79.42	0.1311
SE-ResNet34	78.67	86.41	75.61	86.46	78.78	0.1287
VGG16	75.76	82.38	68.32	91.17	75.83	0.1695
VGG19	74.47	82.19	69.21	87.21	74.53	0.1695

Two backbones models of FPN and U-Net in addition to the proposed encoder-decoder are considered to validate the effectiveness of the proposed approach. The main goal of this experiment is to test the generalization ability of the proposed segmentation method via a convolutional feature extractor for lung cancer tissue segmentation. Tables 5.1, 5.2 and 5.3 report the comparative analysis of 14 feature extractors on the U-Net, FPN and the proposed segmentation backbone. Overall, the results are in favor of the DenseNet architectures integrated with segmentation architectures in terms of dice similarity coefficient, accuracy and F1-score. As the results in the Table 5.3 indicate integrating the dense modules incorporated in DenseNet169 to the proposed encoder-decoder architecture is achieved more precise segmentation results from the testing images with a dice score of 84.10%. In this type of network architecture, low-level feature maps are combined with higher-level ones using concatenation skip connections (in dense modules) to precisely locate and segment ROIs more accurately. It is observed from the obtained results on ACDC-LungHP challenge dataset that the proposed approach using dense modules without extensive or task-specific pre-processing such as stain normalization achieves better performance than other state-of-the-art components on testing data. It is also inferred from these tables, the second-best result is obtained by the DenseNet201 feature extractor on FPN and U-Net architectures with an overall dice similarity coefficient of 80.86 % and 81.76%, respectively and DenseNet121 on the proposed model with 80.89% dice similarity coefficient.

Table 5.2: Comparative analysis of different feature extractors and U-Net architecture.

U-Net	**Dice**	**Accuracy**	**Precision**	**Recall**	**F1-score**	**MSE**
DenseNet121	80.08	88.21	81.11	82.24	80.16	0.1140
DenseNet169	**82.57**	**89.40**	79.06	89.13	**82.68**	**0.1019**
DenseNet201	<u>81.76</u>	<u>89.05</u>	82.51	83.32	<u>81.83</u>	<u>0.1063</u>
InceptionV3	80.38	88.17	81.00	83.01	80.52	0.1118
InceptionResNetV2	78.62	85.75	74.48	87.88	78.69	0.1361
MobileNet	79.41	87.20	77.78	85.19	79.55	0.1196
MobileNetV2	79.18	86.86	77.47	85.32	79.37	0.1227
ResNet18	79.30	86.81	76.48	86.49	79.33	0.1287
ResNet34	80.32	87.62	76.74	88.15	80.37	0.1202
ResNet50	79.41	87.04	76.32	86.33	79.47	0.1256
SE-ResNet18	79.41	86.60	75.29	88.28	79.49	0.1292
SE-ResNet34	60.59	75.47	59.16	97.76	71.59	0.3025
VGG16	74.68	80.80	66.70	91.07	74.74	0.1854
VGG19	76.52	83.22	69.86	90.54	76.62	0.1615

Comparing the first and second winners among all combinations, the performance of dense modules in

Table 5.3: Comparative analysis of different feature extractors and proposed architecture.

Proposed method	**Dice**	**Accuracy**	**Precision**	**Recall**	**F1-score**	**MSE**
DenseNet121	80.89	89.11	85.03	79.47	80.97	0.1063
DenseNet169	**84.10**	**90.69**	81.97	88.39	**84.16**	**0.0911**
DenseNet201	80.48	88.29	82.53	80.99	80.54	0.1150
InceptionV3	76.88	84.01	71.63	88.10	76.94	0.1541
InceptionResNetV2	77.47	84.13	71.94	89.01	77.51	0.1534
MobileNet	74.16	79.04	64.27	94.33	74.23	0.2012
MobileNetV2	74.46	79.44	64.65	94.36	74.53	0.1982
ResNet18	79.71	86.75	75.03	89.11	79.80	0.1282
ResNet34	79.67	86.97	75.87	87.82	79.75	0.1267
ResNet50	78.71	86.95	78.79	82.27	78.75	0.1275
SE-ResNet18	56.11	76.18	18.21	59.50	59.18	0.1821
SE-ResNet34	78.79	86.33	74.63	87.82	78.90	0.1315
VGG16	75.76	82.38	68.32	91.17	75.83	0.1695
VGG19	75.72	81.64	66.87	93.57	75.78	0.1788

DenseNet architecture is better than the rest of the feature extractors on all of the segmentation architecture backbones. In the present work, regarding state-of-the-art, a model based on deep learning and transfer learning is developed to be sufficiently reliable and generic, aiming to solve the crucial challenges posed by automated malignant tissue segmentation. During feature extraction, the state-of-the-art architectures are introduced to the encoder part of the proposed encoder-decoder architecture to benefit from transfer learning strategy. This approach, by incorporating different modules alongside standard convolution, helps retain discriminative features, which is essential for segmenting ROIs with heterogeneous textures, shapes, and sizes. Integrating modules with various convolutions such as inception, dense, separable depthwise modules in the encoder part of the segmentation model allows for multi-scale feature aggregation to improve current original segmentation architecture and achieve a more accurate segmented ROI. After feature extraction phase, the network is up-sampled from the encoded feature maps to produce the final predicted mask with localized and delineated ROIs. The deepest layers of the proposed architecture contain more crucial information at the expense of spatial resolution. Although high-level contextual and deeper information can be generated within the very deep neural network, it is crucial to avoid over-fitting and vanishing gradient descent problems, which are common issues in training deep architectures. Therefore, low-level contextual information from lower levels are directly incorporated to high-level contextual information from the upper layers to precisely delineate the tumor boundaries and avoid over-fitting and vanishing gradient issues. By

directly connecting convolution layers in dense components, an equal contribution of both low-level and high-level contextual information is ensured through skip connections. These connections in dense modules use concatenation operation to pass extracted information. Concatenating feature maps from the intermediate convolution layers of the proposed architecture demonstrates the importance and contribution of the low-level features in precise segmentation of boundaries in tissues. Also, dense modules in the pre-trained DenseNet architecture with skip connections aids in avoiding the problem of vanishing gradient descent due to the designing of deep architectures with millions of parameters. The obtained results in Table 5.3 highlight the superiority of the proposed architecture by incorporating DenseNet169 feature extractor.

5.5 Conclusion

In this research, an extensive comparative study of segmentation architectures integrated with a wide variety of well-established feature extractors is presented. The proposed approach was constructed by integrating long and short skip connections into the proposed encoder-decoder segmentation architecture in order to help exploit better discriminative visual features by allowing the flow of gradient information through the intermediate convolutional layers and achieve better performance for the segmentation of malignant regions in lung tissue histological images. Extensive experimental results on ACDC-LungHP challenge have proved the effectiveness of the proposed method using skip connections by surpassing state-of-the-art of FPN and U-Net models by a considerable margin. The obtained segmentation results show that the proposed architecture has achieved a dice similarity coefficient of 84.10%, accuracy of 90.69%, F1-score of 84.16%, and MSE rate of 0.0911. Finally, the proposed deep CNN method is inherently general and can be applied to similar segmentation tasks in histopathological image analysis. However, the performance of the segmentation model can be challenging on histopathology images with irregular shapes, noisy backgrounds and vague edge resolution. In future work, the performance of the proposed architecture can further be improved by investigating the impact of more effective modules in extracting contextual features from histological tissue images. Also, more histology images should be acquired to evaluate the effectiveness of the proposed method and applications in a clinical practice.

6 Deep Transfer Learning Based Model for Colorectal Cancer Histopathology Segmentation: A Comparative Study of Deep Pre-trained Models[1]

6.1 Introduction

Colorectal cancer (CRC), also known as colon or bowel cancer, develops from the abnormal or excessive growth of malignant cells in colon or rectum. CRC is the third most frequently cancer-related death in the United States in both men and women after lung cancer and breast cancer [207]. According to the annual report provided by the American cancer society [8], approximately 104,610 new cases of colon cancer and 43,340 new cases of rectal cancer will be diagnosed in 2020. Additionally, 51,020 patients are expected to die from colorectal cancer during 2020 in the United States. Most colorectal cancers start as abnormal tissue or benign polyps that grow in the inner linings of the intestine. Although the majority of abnormal tissue or polyps are initially benign, they might become malignant over time if left untreated. Therefore, due to the high incidence and mortality rate of colorectal cancer, detecting and removing suspicious tissues in early stages is important to prevent the risk of developing colorectal cancer. Colonoscopy is the reference method for screening and detecting polyps inside the colon. Screening and analysis of polyps or other types of abnormal tissue in colonoscopy images or videos are dependent on experienced endoscopists. When the visual inspection of a polyp demonstrates a high malignancy polyp, it should be removed immediately for pathology analysis to determine whether a polyp is benign or malignant [166].

Histopathology is the examination of thin sections of suspicious tissue through a microscope. The extracted tissues have been fixed onto glass slides and stained to reveal structures and morphological features. With the availability of whole slide scanning devices, there is a growing trend towards acquiring digitized pathology images of glass histology slides. The advent of digital pathology made tissue

[1] A manuscript describing this work is under review for publication. This chapter uses text descriptions and figures from the manuscript.

histopathology available to the application of image analysis models leading to the rise of computational pathology and assisting pathologists in their diagnostic decision making. In a conventional pathological diagnostic practice, a pathologist has to analyze thousands of tissue sections on glass slide series under the microscope to annotate structures and morphological features present in a histological slide. The manual segmentation of tumor regions is a challenging and time-consuming task. Furthermore, the visual examination of tissue slides is tedious when workloads are high. The traditional approach also lacks objectivity and is bias due to the subjective nature of the task, which inevitably leads to inter and even intra-observer variability [84, 21].

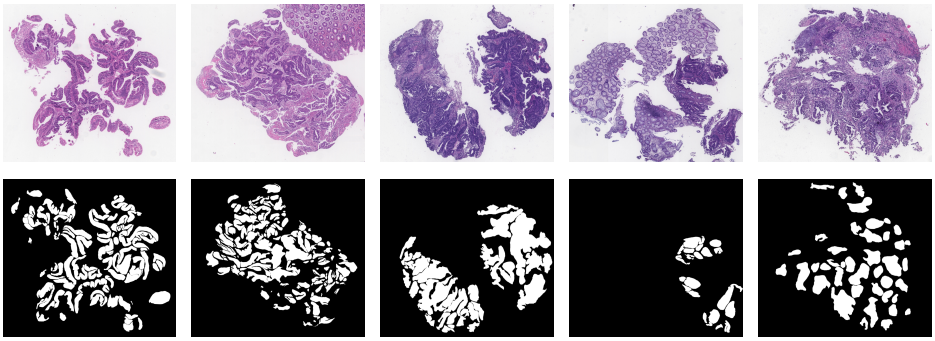

Figure 6.1: Some examples of WSIs (first row) and their corresponding manual annotated masks provided by expert pathologists (second row). The histology images are adapted from [123].

In contrast to the manual approaches, with the rise of computational pathology, pathologists would greatly benefit from the automation of pathological repetitive tasks such as segmentation. Accurate segmentation of structures such as cancerous regions, nuclei and glands are of crucial importance for a pathologist in assessing the degree of cancer malignancy and localization of tumor regions in H&E-stained slides. Therefore, automating repetitive tasks is essential in extracting visual morphological features from large scale histopathology images that would otherwise be impractical. Computer-assisted diagnosis systems and quantitative image analysis could aid in improving tissue analysis for image-based bio-marker discovery and tissue diagnosis with reproducible results. Given the increasing number of CRC cases and shortcomings of the conventional diagnosis system, the demand for developing precise and reliable segmentation algorithms is increasing progressively to assist pathologists in speeding up the diagnosis process by accurate segmentation of cancerous regions and diagnosing CRC aggressiveness, grading and scoring.

The main contributions of this research are, first, investigating the effect of modules incorporated in CNN architectures in the segmentation performance, and second, proposing a transfer learning-based fusion approach in the encoder part of segmentation backbones to train on CRC tissue segmentation and achieve excellent performance. To do so, different architectures were designed assembling multiple pre-trained CNN feature extractors on three segmentation architectures, namely U-Net, LinkNet and

FPN, to segment CRC histology segmentation effectively. In this work, the robustness of 17 deep feature extractors belonging to 7 architecture families was investigated. The properties of the selected models are given in Table 6.4. Finally, a comprehensive analysis comparing the proposed transfer learning approach on different CNN models is provided.

6.2 Materials and Methods

Deep learning architectures are formed by a sequential of convolutional layers alternated by pooling layers. This architecture is able to learn non-linear hierarchically discriminative features from input data. Different types of CNN architectures can be formulated by stacking convolutional layers. A convolution window slides over the input image and performs a convolution operation (as shown in Eq. 6.1) to extract high-level discriminative features maps.

$$Y_i^n = f\left(\sum_i^m \omega_{ij}^{n-1} * x_i^{n-1} + b_i^n\right) \tag{6.1}$$

where m is the number of feature maps, ω_{ij}^{n-1} represents the convolution filter between the i and j feature maps, x_i^{n-1} is the i^{th} map in the $(n-1)^{th}$ layer, b_i^n denotes the bias, function f denotes a nonlinear activation function, and the asterisk $(*)$ represents the convolution operator.

After generating feature maps from each convolutional layer, another layer termed as a pooling layer is used to reduce the dimensionality of the feature maps. The main idea of using a pooling layer is to reduce the model computation time and resources. If the pooling operation is removed, the amount of CNN parameters increases exponentially in the subsequent layers. Another advantage of pooling operation is to reduce the sensitivity of the model to small transformations, variations, distortions and translations in input data. The two most common pooling strategies are max-pooling and average-pooling.

After extracting features using stacked convolutions and pooling layers, fully connected (FC) layers are used to convert an extracted 2D summarized feature map into a 1D feature vector. A fully connected layer is similar to a conventional artificial neural network (ANN) or a multi-layer perceptron. The input-output operation in a neuron of the FC layer is defined in Eq. 6.2. In each neuron unit, the learned weights are multiplied by the corresponding data from the previous layer and the bias value is added. The calculated value is transmitted to the activation function before being passed to the next layer.

$$fc = f(b + \sum_i^m \omega_i x_i) \tag{6.2}$$

where f represents an activation function, w is the weight vector, x is the input feature vector of the i^{th} neuron, m is the number of feature maps, and b is the bias vector.

The final component of a deep CNN is the output layer to produce the predictive probabilities corresponding to each class. The softmax activation function is the common activation function for classification tasks. The softmax function is as follows:

$$f(x) = \frac{e^{x_i}}{\sum_{k=1}^{n} e^{n_k}} \tag{6.3}$$

where e^{x_i} is the i^{th} value in the output vector and n is the number of classes.

Figure 6.2 presents a conventional deep CNN model, consist of the input image, convolution layers followed by pooling layers and finally, fully-connected layers. In the convolution layer, also known as the feature extraction layer, a convolution kernel (yellow square) with a fixed size convolve over the input image and generate a feature map. Extracted features are fed into the next layers as input. The pooling layer is used to reduce the size of the feature maps. Finally, the fully-connected layer at the end of the network outputs the corresponding probabilities. The main idea of a CNN model is to obtain high-level features such as edge, shape, and texture directly from the input image.

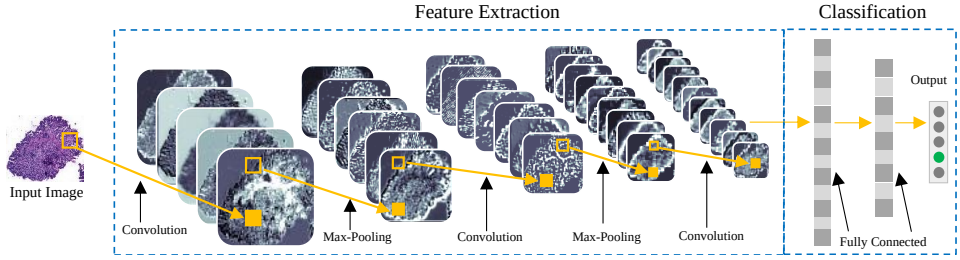

Figure 6.2: A typical convolutional neural network architecture. The histology image is adapted from [123].

6.2.1 Segmentation Architectures

In this section, a short description of each state-of-the-art CNN architectures is provided:

6.2.1.1 U-Net

U-Net, proposed by Ronneberger et al. [178] in 2015, achieved much effective segmentation result in compare with ConvNet approach and won ISBI cell tracking challenge. The contracting path or down-sampling layers of U-Net architecture learns the feature maps using alternating convolutional filters and max pooling layers. The expanding path or up-sampling layers acts as input for de-convolution process and provide precise segmentation.

6.2.1.2 LinkNet

LinkNet [64] is an efficient encoder-decoder architecture which takes the advantages of skip connections and residual blocks to address the problem of spatial information by directly connecting spatial information from the encoder to the corresponding decoder part. The encoder part of the original LinkNet uses ResNet18 to extract features from input image and the corresponding decoder part produce the predicted mask.

6.2.1.3 Feature Pyramid Network (FPN)

The main idea of FPN architecture is to combine low-level semantically strong features with high-level semantically weak features from each layer independently to produce the final pixel classification. Feature pyramids in FPN architecture are the basic component in recognition systems for detecting multi-scale objects [147].

6.2.2 Deep CNN architecture for CRC Segmentation

The main objective of this work is to explore the impacts of varying modules on the performance of deep CNN models and determine the optimal set of incorporating CNN modules and pre-trained architecture through an extensive of experiments. Hence, the performance of multiple well-established deep CNN models with various layers or specifications is investigated. In this research, 51 set combinations of pre-trained networks and segmentation architecture are designed in the down-sampling part of segmentation architecture backbones, and then a comparative study is conducted to report the results. To conduct this research, the impact of different CNN modules, e.g. squeeze-excitation (SE) incorporating into SE-ResNet (18, 34 and 50) and SE-ResNext50 models, residual blocks in ResNet (18, 34 and 50) models, dense modules in DenseNet (121, 169 and 201) models, inception modules in InceptionV3, InceptionResNetV2 model and standard convolutions in VGGNet (16 and 19) is assessed for automated CRC cancer tissue segmentation. Residual units also are incorporated in InceptionResNetV2, ResNeXt, SE-ResNeXt and SE-ResNet models. The proposed deep learning framework is based on deep convolution neural networks and includes the following two parts: the first stage is the encoder part that incorporates pre-trained deep CNN architecture to extract high-level contextual feature representations automatically from the input image. The next part of the architecture is the decoder part that up-samples the encoded image feature representations into an output predicted mask. Figure 6.3 shows the proposed fully convolutional-based feature extractor with InceptionV3 and LinkNet architecture for automatic CRC tissue segmentation and screening. The left side of this figure is the data preparation step, e.g. extracting patches from an input WSI. The right side of this figure demonstrates the proposed architecture. The encoder part of this architecture extract feature using inception modules and the decoder part of the proposed architecture produce the final mask.

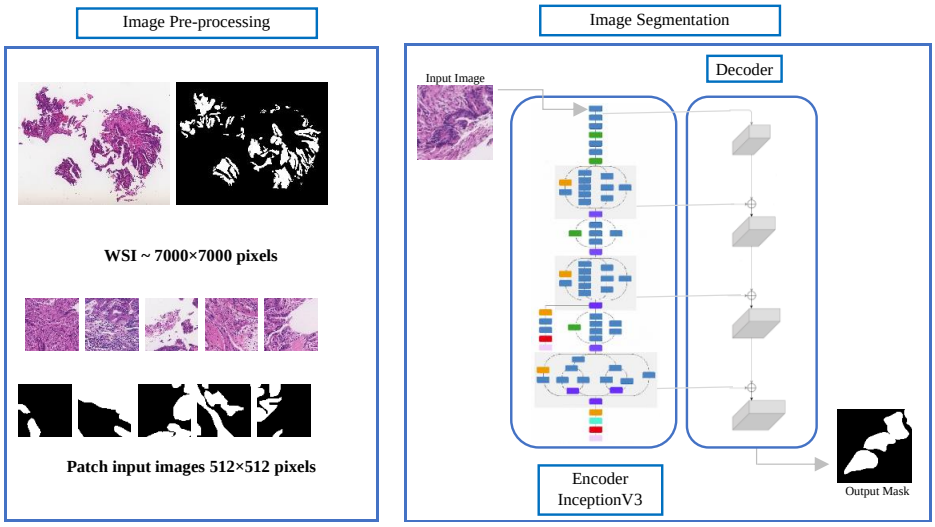

Figure 6.3: The illustration of the proposed convolutional architecture with InceptionV3 feature extractor. The histology images are adapted from [123].

The designed generic framework allows extracting discriminative features based on the end-to-end learning process of the texture and shape of normal and tumor regions and finally delineate ROIs from CRC histology slide images. Additionally, the proposed model provides a new level of feature extractors by incorporating prior knowledge already trained on the ImageNet dataset using pre-trained deep modules into the segmentation framework. As demonstrated in the Figure 6.3, the proposed architecture is composed of two separate parts. The upper part of the proposed architecture carries out feature extraction from the input layer with a resolution of 512×512 pixels. In contrast, the lower part propagates the obtained extracted features to the upper part to produce the final predicted mask. The 512×512 pixels of input images are large enough to cover the ROIs of the provided dataset with reasonable memory consumption. This approach allows to design a much deeper architecture, i.e. U-Net with 2M parameters. In contrast, the combination of DenseNet201 with UNet with the number of 26M parameters, LinkNet with the number of 1M parameters and LinkNet combined with DenseNet201 has 22M parameters to successfully accomplish the segmentation task without the problem of vanishing gradient problem.

6.2.3 Datasets Description

The image dataset used in this work for colorectal cancer segmentation is DigestPath [123] available at [5]. The dataset is consisted of a total of 250 positive colonoscopy tissue slices containing both normal and tumor regions. The size of images ranges from 3538×5736 pixels to 16054×13821 pixels extracted from the high-resolution scans of anonymous patients to evaluate the performance of the segmentation model. All of the lesions are annotated by HistoPathology Diagnostic Center together

with cooperated hospitals. All whole slide images were stained by hematoxylin and eosin and scanned at ×20. The provided H&E stained histology WSIs of colorectal tissue were highly heterogeneous in terms of shape, texture and appearance as the data were collected from 4 different medical centers in developing countries.

6.2.3.1 Patch Extraction

To conduct a successful diagnosis, the magnification level of a WSI should be adjusted for a more detailed field of view of WSI to provide necessary information about tumor or healthy regions. Due to the substantial scale of WSIs and computation limitation required to process the entire WSI at once, a patch extraction method relying on the abnormal region is employed to generate the dataset. A non-overlapping window is used to crop patches of size 512×512 pixels from each abnormal WSI (examples in Figure 6.4). Another issue with WSI processing is that abnormal regions only occupy small proportion of some WSIs compared with the healthy regions. Also, patches with less than 25% tissue sections were discarded from the generated dataset. To this end, a number of 1596 of patches for training set and 150 patches for the testing set with the size of 512×512 pixels were selected from 250 positive WSIs in total. An advantage of the proposed patch-based model is the computational efficiency that allows to train very deep CNN architectures.

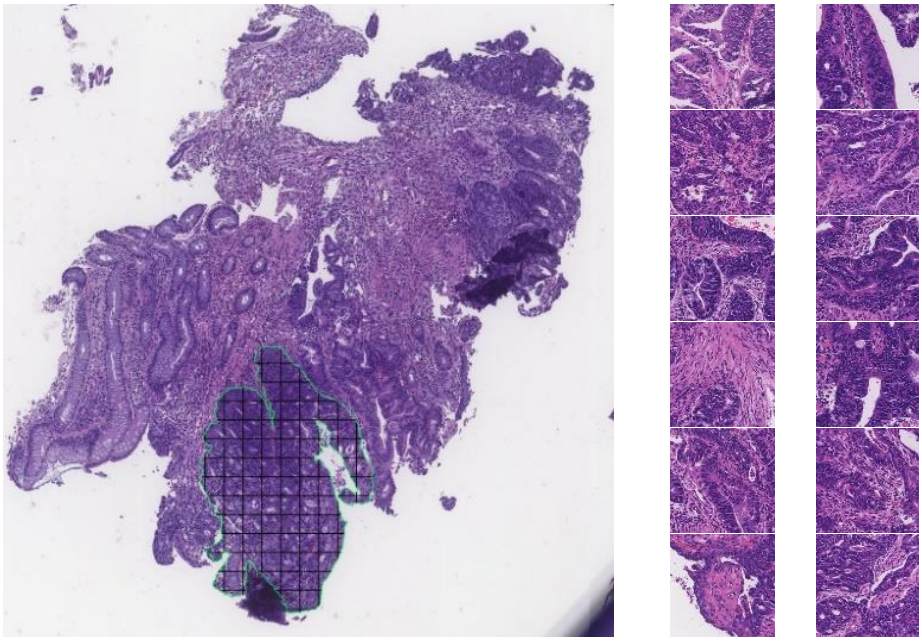

Figure 6.4: The process of patch generation from a whole slide image. The histology image is adapted from [123].

6.2.4 Experimental Settings

Training is done using SGD (Stochastic Gradient Descent with momentum, proposed by [181]) as an optimizer with a learning rate of initial rate of 0.1, momentum set to 0.9 and decay rate set to 0.1. The learning rate is the most important hyper-parameter in an optimizer when training a deep model. To set the optimal value of learning rate, this study utilizes a learning rate scheduler to facilitate the optimal convergence and avoid over-fitting during training. For this research, a grid search on discrete sets of parameters is employed to find the optimal values of optimizer and learning rate to train the architectures. The learning rate drops every two epochs during the training procedure. The SGD accepts the parameter learning rate η (default value is set to 0.01), momentum as a parameter of μ, decay parameter to decay the learning rate over the weights updates and Nesterov parameter for employing the Nesterov momentum with the following formula:

$$\eta^{(t+1)} = \frac{\eta^{(t)}}{1 + decay} \tag{6.4}$$

The mini-batch size was set to 4 images due to the GPU memory limitations, and all models were trained for 50 epochs. The dataset has been divided into training, validation and testing datasets of 70%, 20% and 10%, respectively. The weights for feature extractors were initialized by using pre-trained ImageNet initialization. The ImageNet weight initialization approach assists in faster convergence and speeds up the training process. All experiments were run on a PC with the following configuration: Intel(R) Core(TM) i7-8700K 3.7 GHz processors with 32 GB RAM. The training and testing process of the proposed architecture for this experiment is implemented in Python using Keras package with Tensorflow as the deep learning framework backend and run on Nvidia GeForce GTX 1080 Ti GPU with 11GB RAM.

6.2.5 Evaluation Metrics

To measure the performance of the proposed method for the segmentation task, common segmentation evaluation metrics such as dice similarity coefficient, precision, recall, f1-score were adopted to quantitatively measure similarity and difference between the ground-truth mask and the predicted mask produced from the segmentation model at the pixel level. The dice coefficient measures the spatial overlap between the predicted mask by the proposed architecture and ground truth. These metrics are computed by the following:

$$Dice\,(A, B) = \frac{2 \times \mid A \cap B \mid}{\mid A \mid \cup \mid B \mid} \times 100 \tag{6.5}$$

where A represents the output binary mask, produced from the segmentation method, and B represents the ground-truth mask, $\cup$ represents union set between A and B, and $\cap$ represents the intersection set between A and B.

Accuracy metric used to measure the overall accuracy of the segmentation models. Given the number of true positives (TP), false positives (FP), true negatives (TN) and false negatives (FN):

$$Accuracy = \frac{TP + TN}{TP + TN + FP + FN} \times 100 \tag{6.6}$$

Precision and recall metrics are analyzed to measure the amount of over-segmentation and under-segmentation, respectively. Precision is sensitive to over-segmentation as it is associated with a small precision score. The recall is sensitive to under-segmentation as it is associated with results in low recall scores.

$$Precision = \frac{TP}{TP + FP} \times 100 \tag{6.7}$$

$$Recall = \frac{TP}{TP + FN} \times 100 \tag{6.8}$$

F1-score also computed as a harmonic mean of precision and recall between predicted and ground truth boundaries to evaluate the performance of the proposed approach.

$$F1 - Score = 2 \times \frac{Recall \times Precision}{Recall + Precision} \times 100 \tag{6.9}$$

6.3 Comparative Experimental Results

The main objective of this experiment is to test the generalization ability of the proposed segmentation method via a convolutional feature extractor and transfer learning for early-stage colon tumor detection from small tissue slices. Different pre-trained CNN models were selected as feature extractors of the encoder part of different backbones, e.g. U-Net, LinkNet and FPN, for comparative analysis. These architectures were selected for feature extraction based on their (i) satisfying performance in medical image processing, (ii) adaptation towards real-time (or near real-time) image diagnosis support system and, (iii) feasibility of transfer learning for different computer vision tasks such as detection, segmentation and classification. Tables 6.1, 6.2 and 6.3 report the patch-based tumor segmentation results of different approaches. Overall, the results are in favor of the InceptionResNetV2 and DenseNet architectures in terms of dice similarity coefficient, accuracy and F1-score. InceptionResNetV2 combines the advantages of Inception modules with residual connections to increases convergence speed and improve performance. Analyzing Table 6.3, the topmost result of all combination was obtained by DenseNet121 feature extractor on LinkNet segmentation architecture with a maximum of 82.74% dice similarity coefficient and accuracy of 87.07%. It is also inferred from Table 6.1 that the second-best result from all combinations obtained by InceptionResNetV2 feature extractor and FPN backbone architecture with an overall dice similarity coefficient of 82.53% and accuracy of 87.10%. Based on the observations in Table 6.1, ResNet50, VGG16 and, VGG19 have the lowest segmentation accuracies, dice similarity index and F1-scores to all segmentation backbones of FPN, U-Net and LinkNet in this study. Conversely,

Table 6.1: Comparative analysis of different feature extractors and FPN segmentation architecture.

FPN	Dice	Accuracy	Precision	Recall	F1-score	MSE
DenseNet121	82.48	86.96	82.93	83.64	82.62	0.1123
DenseNet169	<u>82.50</u>	<u>87.08</u>	83.60	82.97	<u>82.63</u>	0.1120
DenseNet201	82.34	86.88	84.27	82.29	82.46	0.1148
InceptionV3	81.48	86.70	84.05	80.90	81.64	0.1152
InceptionResNetV2	**82.53**	**87.10**	82.74	84.10	**82.73**	0.1115
MobileNet	82.40	86.85	82.08	84.24	82.51	0.1151
MobileNetV2	82.12	86.59	81.21	84.82	82.34	0.1154
ResNet18	81.56	86.21	80.83	84.10	81.68	0.1211
ResNet34	82.09	86.57	81.07	84.84	82.24	0.1175
ResNet50	79.24	84.90	78.01	83.76	80.05	0.1309
ResNeXt50	81.39	86.34	82.96	81.42	81.52	0.1182
SE-ResNet18	81.63	86.24	81.34	83.58	81.78	0.1199
SE-ResNet34	81.48	86.30	82.22	82.39	81.62	0.1194
SE-ResNet50	81.39	86.86	85.94	78.87	81.55	0.1128
SE-ResNeXt50	81.05	86.60	85.85	77.97	81.19	0.1151
VGG16	80.55	83.78	73.86	90.54	80.62	0.1451
VGG19	80.68	83.85	73.38	91.59	80.80	0.1448

MobileNet, and MobileNetV2 models consistently perform better with FPN than U-Net and LinkNet networks. Also, ResNext50 and squeeze-and-excitation networks (SE-ResNet18, 34, 50, ResNext50) models, when applied in FPN architecture, are more stable than counterparts. Comparing the first and second winners among all combinations, the performance of dense modules in DenseNet architecture is slightly better (1%) than the rest of the feature extractors on the FPN backbone. Analyzing Table 6.2, among deep feature extractors, InceptionResNetV2 has the highest dice similarity score of 82.14%, accuracy of 87.03% as well as the highest F1-score of 82.27%, followed by DenseNet201 with overall dice similarity score of 82.07%, accuracy of 86.99%, as well as F1-scores of 82.12%. Though the lowest scores are obtained by Se-ResNeXt50 feature extractor, VGG19 has the worse MSE rate (0.1552).

6.4 Discussion

The segmentation of tumor epithelium in histopathology slide images is a critical step for early diagnosis in colorectal cancer. In this research, a comparative analysis of a wide variety of well-established deep

CNNs as feature extractors as part of the FPN, U-Net and LinkNet architecture is presented. The proposed framework based on encoder-decoder architectures of FPN, U-Net and LinkNet integrated with pre-trained feature extractors has the potential to overcome the current challenges of conventional segmentation methods, reducing subjectivity and the daily workload of pathologists with decent speed and accuracy. Several conclusions can be summarized based on the obtained results: i) it can be observed from the experimental results that the proposed tumor segmentation method can exploit deep convolution features and learn discriminative activation maps from the representative patches, which is less computationally expensive. Another advantage of the patch-based approach is that all of the ROIs present in an image can be cropped and be used as the input while discarding non-informative regions such as the white background.

Table 6.2: Comparative analysis of different feature extractors and U-Net segmentation architecture.

U-Net	**Dice**	**Accuracy**	**Precision**	**Recall**	**F1-score**	**MSE**
DenseNet121	81.90	86.92	85.12	80.31	81.95	0.1189
DenseNet169	81.85	86.77	84.82	80.50	81.89	0.1188
DenseNet201	<u>82.07</u>	<u>86.99</u>	83.55	82.23	<u>82.12</u>	0.1179
InceptionV3	81.84	86.76	83.12	81.97	81.91	0.1189
InceptionResNetV2	**82.14**	**87.03**	83.53	82.42	**82.27**	0.1175
MobileNet	80.43	85.38	77.49	85.58	80.63	0.1279
MobileNetV2	81.20	86.36	80.16	83.60	81.31	0.1212
ResNet18	82.16	86.76	80.57	85.30	82.23	0.1200
ResNet34	81.86	86.64	80.52	84.65	81.93	0.1217
ResNet50	81.76	86.62	83.28	81.68	81.81	0.1223
ResNeXt50	81.50	86.26	83.09	81.23	81.56	0.1247
SE-ResNet18	81.66	86.53	80.82	83.97	81.73	0.1219
SE-ResNet34	82.07	87.04	82.24	83.13	82.15	0.1166
SE-ResNet50	80.43	86.32	87.43	75.78	80.56	0.1214
SE-ResNeXt50	79.18	85.65	86.47	74.49	79.34	0.1267
VGG16	81.48	85.00	75.59	90.05	81.56	0.1355
VGG19	80.05	83.02	72.13	92.05	80.14	0.1552

In this way, a patch-based method can significantly decrease the processing time of both the training and validation set. ii) It is important to be noted that architecture hyper-parameters such as the network depths and network widths can substantially impact the performance and generalizability of the networks. Table 6.4 presents the number of parameters and layers of each architecture examined in this

study. As listed in Table 6.4, developing very deep feature extractors with millions of parameters (e.g. InceptionResNetV2 integrated into U-Net with 62 million parameters) can improve deep CNN results. However, deep models with skip connections (e.g. ResNet50), which discard some layers, can decrease the performance. The trade-off curve between the number of parameters and model performance can be adjusted with strategies such as skip connection in dense and residual modules. For instance, the combination of inception module with shortcut path of residual units in InceptionResNetV2 architecture achieved the second-best result. Training of very deep architectures remains an open problem due to its adverse effect on the ability to generalize unseen test data. First, as the number of layers increases, model performance increases too fast, but after a few iterations, the performance decreases due to the gradient degradation.

Table 6.3: Comparative analysis of different feature extractors and LinkNet segmentation architecture.

LinkNet	**Dice**	**Accuracy**	**Precision**	**Recall**	**F1-score**	**MSE**
DenseNet121	**82.74**	**87.07**	82.78	84.03	**82.79**	0.1176
DenseNet169	<u>81.95</u>	<u>86.94</u>	85.13	80.58	<u>81.99</u>	0.1195
DenseNet201	81.44	86.69	85.14	79.72	81.51	0.1209
InceptionV3	81.07	86.45	83.42	80.23	81.16	0.1212
InceptionResNetV2	81.02	86.25	83.92	80.01	81.09	0.1242
MobileNet	80.88	85.68	77.72	86.30	81.07	0.1266
MobileNetV2	79.61	85.09	78.44	83.05	79.84	0.1312
ResNet18	81.21	86.33	81.90	82.28	8128	0.1252
ResNet34	77.52	86.09	79.55	84.24	81.21	0.6358
ResNet50	80.93	86.13	82.23	81.28	80.98	0.1272
ResNeXt50	81.25	86.03	82.30	81.97	81.33	0.1259
SE-ResNet18	80.73	85.98	80.20	83.08	80.82	0.1275
SE-ResNet34	81.37	86.53	80.84	83.35	81.46	0.1223
SE-ResNet50	80.78	86.50	84.95	78.39	80.88	0.1210
SE-ResNeXt50	81.68	86.93	85.22	79.58	81.80	0.1148
VGG16	79.12	81.98	71.06	91.62	79.20	0.1648
VGG19	73.48	74.56	61.01	95.47	73.56	0.2399

A major contributing factor in resolving the vanishing gradient issue and taking full advantage of performance gains of training deep models is to introduce shortcut paths that allow flowing the gradient throughout the very deep networks. Such intuitive is crucial to enable gradient-based training of very deep models in an end-to-end manner, which means effective utilization of deep features, therefore

better generalization capability. In contrast, using just standard convolutions (e.g. VGG16 or VGG19) oversimplifies the architecture that can adversely affect the performance of the automatic CRC tissue segmentation as results shown in Table 6.3. Although the proposed method achieves overall good performance on most testing images, the performance can be decreased as the histological structures of the cancerous area in some malignant cases are more challenging and severely irregular. A careful study of the obtained results shows that irregular structures in malignant regions might reduce the ability of feature extractor modules in differentiating malignant and healthy regions. For example, a deep learning model may fail in cases with irregular and high-dense structures, which is a result of high proliferation. This is a major and long-standing limitation for developing robust deep learning models in segmenting of more challenging cases in histology images. It is worthwhile to note that the careful analysis of the errors in the results shows that cases with large variation in tissue with irregular shapes, noisy background and vague edge resolution which are resulted from acquisition images from different scanners, different staining protocols, specimen acquired from patients with a different stage of disease or at different time slots. To address the issue of over- or under-segmentation of tissue segmentation tasks and further improve the overall performance, pre-processing methods can be a potential solution.

Table 6.4: Total number of parameters and layers of each deep CNN architecture.

Model	**FPN**		**U-Net**		**LinkNet**	
	# P	# L	# P	# L	# P	# L
DenseNet121	9.9	474	12.1	468	8.3	483
DenseNet169	15.7	642	19.5	636	15.6	651
DenseNet201	21.2	754	26.3	748	22.5	763
InceptionV3	25	358	29.9	352	26.2	367
InceptionResNetV2	57.5	827	62	821	57.8	836
MobileNet	6.1	134	8.3	128	4.5	143
MobileNetV2	5.2	202	8	196	4.1	211
ResNet18	13.8	133	14.3	127	11.5	142
ResNet34	23.9	205	24.4	199	21.6	214
ResNet50	26.9	237	32.5	231	28.7	246
ResNeXt50	26.4	1263	32	1257	28.2	1272
SE-ResNet18	13.9	189	14.4	183	11.6	198
SE-ResNet34	24	317	24.6	311	21.7	326
SE-ResNet50	29.4	350	35.1	344	31.3	359
SE-ResNeXt50	28.9	1374	34.5	1368	30.8	1383
VGG16	17.5	66	23.7	66	20.3	81
VGG19	22.8	69	29	69	25.6	84

6.5 Conclusion

In conclusion, this research presents a detailed comparative analysis of a wide variety of state-of-the-art deep CNNs in the encoder part of three segmentation backbones. The method is fast in analyzing batches of images as it is based on transfer learning strategy and patch-wise extraction method from colorectal cancer histology WSIs with heterogeneous shape and texture. The transfer learning strategy helps accelerate the learning process and further improve the performance of the proposed network. The extensive comparative evaluation demonstrated the state-of-the-art performance achieved by Densenet121 integrated by the LinkNet model with dice similarity score of 82.74%, accuracy of 87.07% as well as the highest F1-score of 82.79%. The second-best result is obtained by Inception-ResNetV2 pre-trained model with dice similarity score of 82.53%, accuracy of 87.10% as well as the highest F1-score of 82.73%. Overall, comparing all of the feature extractors and segmentation backbone models, FPN and U-Net models tend to produce more stable results and are (almost) equivalent. Compared to conventional methods, where extensive pre-processing methods are used to increase the performance, the proposed approach avoids task-specific pre-processing method or data augmentation in order to improve the generalization ability. Furthermore, the proposed framework could be adopted to analyze complex problems with laboratory-dependent staining protocols, heterogeneous textures, and scanner-dependent intensity inhomogeneity. As a future direction, the proposed approach could be extended to different segmentation tasks on histology slide images. Another interesting direction could be the applications of deep CNNs on temporal histology data with LSTM or recurrent networks. Moreover, the performance of the proposed framework could further be improved by reducing the noise using specific stain normalization techniques.

7 Fine-grained Decentralized Access Control Management

7.1 Introduction

Management of access control and privacy preservation of PHR data is a crucial requirement, yet it is very challenging to solve all the security and privacy issues due to the wide range of data providers and users and also fragmented and diverse nature of electronic medical data. A variety of studies in the literature have shown that the use of Blockchain technology and smart contracts as a distributed data structure can help manage (store, query, share and verify) of medical data. Blockchain inherently offers features such as data integrity, transparency, non-repudiation and resistance to modification of data.

There have been extensive studies in the literature on the effect of Blockchain technology integrated with different access control scheme or data encryption methods to maintain a secure data sharing and management without relying on any third-party involvement. A flexible access right delegation using attribute-based access control scheme is proved to be an effective solution for access control management in large-scale and dynamic healthcare environment. Given the fact that the distributed ledger of Blockchain provides an immutable access log of transactions, no research in the field of computer-aided diagnosis systems discussed establishing data provenance through Blockchain which is an interesting research direction. Establishing data provenance is often challenging as data access in healthcare environment has become more complex. This complexity requires a precise system to track the medical data life-cycle where the process of patient's care and diagnosis need the data being accessed by different departments and users. A medical data owner needs to be aware of and be able to access the provenance data, including history of transaction (how data is used), and data movements through one user to another (who used data) to further enhance the trustworthiness of decision making as well as the security of the access control scheme. Furthermore, due to the limited storage capacity and computational resources of Blockchain, a variety of studies proposed an off-chain database to store actual medical data. However, most of these databases are located in the cloud or healthcare data center which are centralized. None of the studies in the literature considered NoSQL databases such as Apache Cassandra as a possible solution to the issues resulted from the centralized nature of the

current database systems such as single point of failure, scalability and data access traffic. Apache Cassandra is a distributed high-performance and massively scalable data store that can store a large amount of data from multiple servers.

Motivated by the advantages of Blockchain technology, in this research, a PHR data sharing and access management scheme based on attribute-based access control management is proposed to achieve secure verification of data ownership, provenance and precise access authorization. The detailed overview of the proposed scheme, design, implementation and performance evaluation are presented in the following section.

7.2 Proposed Access Control Framework

In this section, the system architecture overview using an attribute-based with privacy-aware provenance is described.

The traditional method for protecting data and maintaining privacy is based on encrypting data before distributing it to data requester. The encrypted data only can be decrypted by authorized parties. However, large-scale cloud systems need a more efficient and scalable key management mechanism to distribute the pubic and private keys among authorized parties. Public/private key management has proved to be difficult due to the collision issue in large-scale cloud systems with large numbers of users. Any malfunction due to a security breach of unauthorized parties, which is often high due to the complex nature of large-scale storing, processing and sharing data, can adversely affect cloud users. Also, access credential revocation imposes additional cost as needs to re-encrypt data and re-distribute the keys among existing users in the cloud, and requires the involvement of data owner in all of the process of encryption, decryption, and key distribution.

To address the drawbacks mentioned above and motivated by the advantages of Blockchain technology, a secure PHR data sharing and access control management scheme based on a two-layer encryption approach is proposed. The proposed architecture is able to apply user-defined access policies for managing access control updates and access revocations without requiring the involvement of data owner. A combination of hierarchical identity-based and attribute-based encryption aiming for a fine-grained access control system is used to provide a dynamic read and write access and also allow access policy updates such as access revocations in cloud-based settings. Attribute-based Encryption (ABE), a public key encryption scheme, is one of the most effective approaches for providing fine-grained access control policies over user data in large-scale systems. Hierarchical identity-based encryption (HIBE) allows granting a different level of access based on user identities that are arranged in an organizational hierarchy. For example, a user with identity at a higher level in the hierarchy can delegate secret keys to its subordinates.

In ABE, a central authority issues the access keys and also verifies the associated keys and attributes for each user. ABE allows users to decrypt and access data based on a group of defined attributes associated with private keys. The data can be decrypted if the key attributes of the user match the attributes associated with the data. For example, data can only be decrypted by users with attributes satisfying ("Oncologist" AND "Lung" AND ("Ontario" OR "Saskatoon")) to impose limitation on the access of a patient data. However, employing crypto-based access control has the main problem of increasing the complexity, response time, and computational cost, which are not suitable for real-time applications in areas such as healthcare with a large number of users and operations. Introducing decentralized ABE access control using Blockchain as the second layer aids in reducing the computational cost of generating access keys from defined attributes by dividing the task among peers (a group of central authorities in decentralized ABE systems, e.g. nodes in a permissioned Blockchain) in the network. By benefiting from the transparency property of Blockchain systems, transactions recorded in the ledger cannot be modified, removed or tampered.

Permissioned Blockchains integrated with ABE are a suitable option for applications where fine-grained access control policies (delegation of different levels of access and revocation) are needed to maintain and guarantee the enforcement of access policies. The proposed scheme results in high integrity and reliability of the whole system. The proposed decentralized solution by using Ethereum Blockchain and smart contract provides distributed access control, ownership and provenance of personal and medical data. Access Control List (ACL), a mechanism offered by the identity-based access control, is used to assist data owners in defining the list of subjects (data requesters) and their associated access permissions and attributes for the objects (medical records) in the network. Then, the data owner deploys the ACL in a smart contract and distribute it into the Blockchain network. The main goal of using a distributed ACL-smart contract is to eliminate the centralized third-party validator and avoid the issue of the single point of failure problem.

7.2.1 Access Control Delegation using Attribute-Based Access Control

In this research, a Hierarchical Identity-Based integrated with Attributed-Based access control (IB-ABE) combined with Blockchain technology is used to provide a fine-grained decentralized access control management for a medical data sharing system. A view-based integration layer is also introduced to the system to allow a view to the query retrieved from cloud database. Data users (doctors, nurses, laboratory staffs, data analysts, researchers, etc.) would execute large numbers of queries over the patients' medical and personal data as a patient suffering from a chronic medical condition such as cancer has to maintain a long medical history of diagnosis, treatment process and follow-up examination whereby having access to a complete history is necessary for treatment. The main goal of using the view layer integrated with the proposed attribute-based access model is to satisfy user-specific query

requirements and process data securely. The proposed view layer-based access management model can authorize different levels of data access, while maintaining data integrity, transparency and ownership with the underlying Blockchain network.

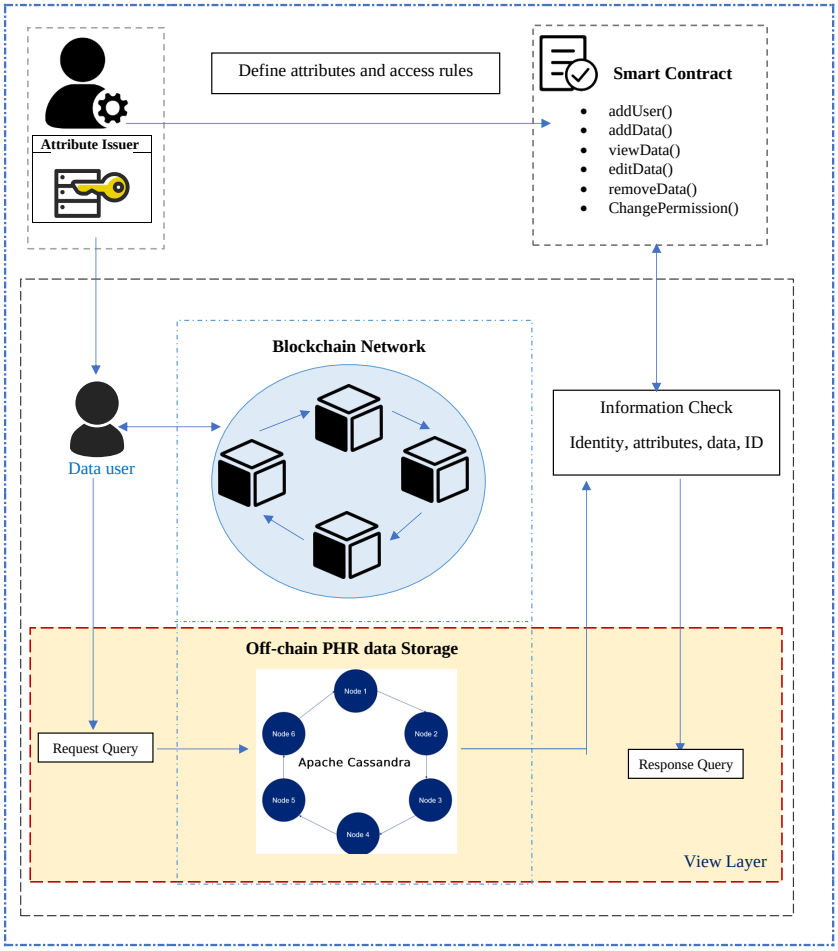

Figure 7.1: System overview.

Figure 7.1 illustrates an overview to the view layer architecture: data flows from a user that sends a query to the view layer. The user request will be sent to a module called access authorization in the view layer. The access authorization module will examine the user privileges and make a decision on what kind of access should be granted to user requests. After verifying the level of permission, authorization role and attributes of the data user, the coordinator module translates or reformulates queries into equivalent queries with respect to the data integration schema and user credential. Query processor creates the query result from NoSQL database for views in the view manager module and then return the answers to the user while satisfying all security requirements. The view layer is dedicated for managing different queries, including storing and retrieving data to support real-time query processing over the medical data and also trained deep learning models. The views are generated and maintained at the back-end, and each view may be used by several users as a shared view. The view

layer prevents improper access of unauthorized users to sensitive or confidential information based on users' corresponding credential levels. In this scenario, users with different levels of authorization are allowed to have access based on ACL and attributes defined in smart contracts to prevent a security breach. Furthermore, when a request to the database is accepted, user information and transaction information will be added to the provenance database in order to keeps track of all provenance data and transactions and the points to that data is stored in the immutable distributed ledger. Employing a private Blockchain as a secure, decentralized and distributed ledger can ensure the correctness and completeness of transactions on PHR data. Once a transaction is published to the Blockchain and confirmed as accurate, it cannot be reversed or destroyed as it is immutable.

The proposed system consists primarily of five entities, namely PHR owner, PHR requester, miners, cloud storage and private Blockchain network.

- **PHR Owner:** The patient (PHR owner) owns the PHR resources and is responsible for granting, denying and revoking the data access request from any other parties such as healthcare providers. The PHR owner deploys its own smart contract with defined ACL to manage data access. PHR owner receives requests from PHR requester demanding access to the PHRs. The PHR data is uploaded to the NoSQL database and every activity (transaction) regarding the PHR data is recorded into the Blockchain ledger.
- **PHR Requester:** In the proposed system, healthcare providers such as doctors, pharmacists, pathologists, data analysts and researchers, etc. are users in the system that request to access the PHR data. A data requester is appointed by a certain PHR owner. The data requester should obtain an access token for accessing a certain PHR resource with a specific privilege to perform diagnosis, medical test, provide medical treatment or data analysis. All data requests and access transactions are recorded on the Blockchain ledger.
- **Miners:** The miners are the nodes that manage the authorization requests and generate the requested access token based on the ACL-smart contract defined by the PHR owner. The third-party validator is replaced by minors. The miners verify access permissions of the requester. If the identity and attributes of the requester match the ACL-smart contract, the access token will be generated, and the permission to access an entity will be granted. Besides, when a transaction is created, all miner nodes need to reach a consensus before updating the distributed ledger. When the consensus is reached, the Blockchain nodes create a new block in the chain and distributed to all participant nodes in the network.
- **Blockchain Network:** The decentralized solution of this research is Ethereum Blockchain with the smart contract to govern the patient medical record and related transactions for three purposes.
  - **Data ownership:** Blockchain can provide a trusted ownership management system for PHR data by tracking the true origin of ownership using smart contracts and Public Key Infras-

tructure (PKI). Non-repudiation of data and transactions is another feature supported by Blockchain. Blockchain ensures that PHR owner and PHR user cannot deny their signature on data and transactions, respectively.

- **Anonymity and secrecy:** The identity of a user is controlled by an identity provider, as in the case of Permissionless Blockchain. The anonymity on the identification of the users associated with a transaction is provided by a PKI. The PKI maps an identity to a cryptographic primitive of public and private keys, which makes it impossible to verify the identity of an account, thus ensuring the privacy of users.
- **Data provenance:** Each of the personal and medical data access requests is processed from data owner's smart contract to ensure the permission level then return data access results. All of the access request and transaction activity by users need to be broadcasted to all miner nodes in the Blockchain network and appended to the ledger. Therefore, a PHR owner (patient) can keep track of the exchange of its PHRs and know exactly who uses its data and how, thus ensuring data provenance of individuals.

– **Cloud Database:** An off-chain storage (NoSQL Apache Cassandra) solution governed by access permissions stored on the smart contracts is employed to store the actual PHR data object. In this method, the Blockchain network only stores links to the location of data and transactions. Apache Cassandra as a distributed scalable data store can store a large amount of data from multiple servers, providing high viability. Apache Cassandra facilitates scalability by removing centralized storage constraints from the proposed system.

The following data modeling process is performed to design the database scheme:

- Analyzing system requirements
- Identifying the entities and the relationships among them (conceptual data model)
- Identifying the common queries and data access patterns (application workflow)
- Designing and structuring the database schema (logical data model)
- Optimize the schema include keys, partition sizes (physical data model)

7.2.1.1 Personal Health Records Storage

The first step is to register the system users, including patients, doctors and healthcare providers, using the registration layer. To do so, the user identity details (such as ID, social security number, and personal information), and related attributes are needed. The patient can permit his/her medical data based on the doctors' identity or attributes. Then, the public and private keys of the patient and healthcare providers can be generated using the provided information. The private key of the patient is used to encrypt the patient's information, and the public key of the patient is distributed to assigned doctor responsible for the treatment to decrypt the patient secret data. The assigned doctor and other

eligible data users are then included in the ACL. After the registration process, meta-data of the access list will be sent to the Blockchain, and the encrypted data will be sent to the off-chain cloud database and gets the pointer link of the encrypted data. The data owner's signature should be verified to ensure the user is legitimate to the system. The same process is performed to grant permission to users for the deep learning models. Whenever a new user (doctor or patient) is registered to the system, the state of associated ACL of the deep learning models should be updated.

7.2.1.2 Personal Health Records Sharing

To initiate data sharing as a new transaction, a doctor sends an access request to a patient's image data (e.g. pathology slide) in the system. The data access request is signed by the doctor's private key to ensure non-repudiation activity and trace the provenance of data. The access request is received by the access authenticator and provenance layers as the entry point for processing the access requests and registering the data provenance. The access authenticator layer first verifies the data owner's signature, and if it is valid, the process move forwards otherwise is denied. If the process is allowed, the access authenticator layer verifies doctor identity or associated attributes according to the ACL and if the identity or attribute match and is legitimate, the access is granted to the doctor to have access to the patient medical data (e.g. pathology slide). The doctor makes the diagnosis, and if there is a need for a second opinion, the doctor initiates an access request to the associated deep learning model as illustrated in Figure 7.2. The access authenticator layer again verifies doctor access to the model. If the access request to the deep learning model is legitimate, the process is accepted else denied if the access request is invalid. To manage data provenance, whenever a data sharing operation is started, an event is generated to record the process. The event record is used for tracking the provenance data to be registered as a transaction in the Blockchain and can include information such as event hash, owner public key, receiver public key, timestamp, and access type. In the second scenario, if the type of data being requested by doctors are healthcare records (e.g. laboratory reports, medical history, doctor prescriptions, and insurance information etc.), the same process will be repeated; however, an extra view layer will be employed to retrieve and filter out the patient's private and personal information from the database as illustrated in Figure 7.3. Access authenticator, provenance and view layers are smart contracts to enforce policies. At the final step, this transaction is grouped into data blocks to be mined and appended to the Blockchain by miner nodes. The data owner can track or audit the data provenance. The following provides the detailed information of the proposed attribute-based access control scheme and user's operations. The scheme consists of three datastores (attribute datastore, medical data datastore and mapping datastore) and two layers (authorization layer and provenance layer) to manage access control. The Blockchain network records the address of data stored in a NoSQL datastore and the path of medical image. The attribute data of the users are stored in the attribute datastore. Medical data datastore records the medical, personal and encrypted physical path

of the medical image file. Mapping datastore is used to store the information needed to map the actual data from NoSQL data and the pointers stored in the Blockchain. The following describes the process of each operation.

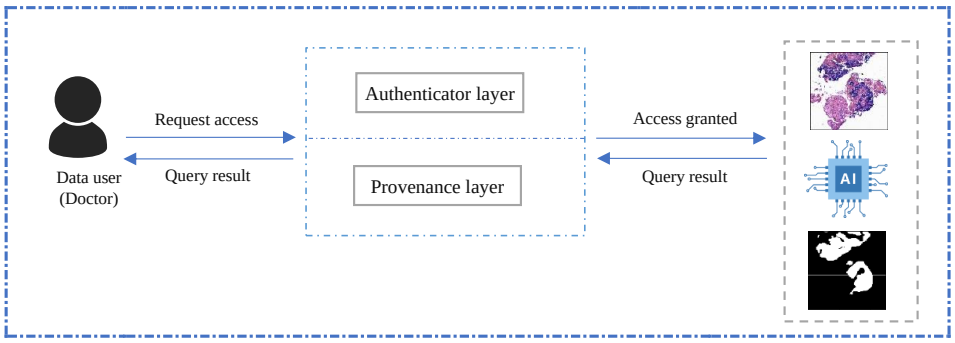

Figure 7.2: Overview of the IB-ABE framework with data access to the deep learning models.

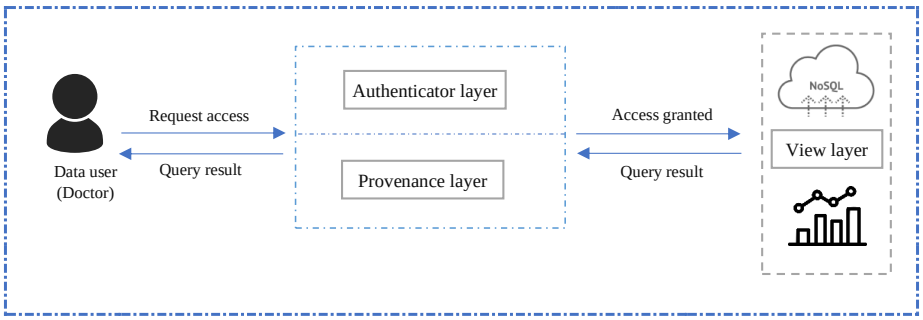

Figure 7.3: Overview of the IB-ABE framework with data access to the database.

7.2.1.3 Ciphertext-Policy Attribute-Based Encryption

The main steps of CP-ABE algorithms is described in the following [82].

1. **Setup:** To initiate, the algorithm takes the security parameter ℓ and generates the public key K_{pub} and a master secret key MK_{secret}.
2. **KeyGen:** To generate the user private key of K_{prv}, the algorithm takes the master secret key MK_{secret} and the attribute set of S.
3. **Encrypt:** The algorithm encrypts the message M with public key K_{pub} and a set of attributes S to generate the ciphertext C.
4. **Decrypt:** The algorithm takes the ciphertext C as input associated with private key of K_{prv} and the set of attributes S to outputs the plaintext of M.

7.2.1.4 Attribute Generation and Assignment

1. After successful registration of a data user to the system, user's attributes should be defined. To do so, a user should send a request of attribute assignment to the authorization layer.
2. Authorization layer verifies the identity of the user to check if the identity and its request is legitimate. This step ensures that an adversary with unauthorized identity cannot obtain attributes from the service.
3. After successful authorization, attributes are queried from the attribute datastore.
4. The attribute datastore sends the attribute set to authorization layer. The trusted authority should generate the new attribute if an associated attribute does not exist in the datastore.
5. According to the user's attribute, authorization layer generates the defined attribute private key and assign it to the user.

7.2.1.5 Access Request to Medical Data

1. The data user sends an access request to the authorization layer to access patient's medical data.
2. Authorization layer verifies the identity of the user, the digital signature, and associated attributes to ensure the legitimacy of the user access to the service. If the user is authorized, the request moves forward, otherwise is denied.
3. The authorization layer locates the data from Blockchain and uses the pointer of encrypted address to retrieve the encrypted data from NoSQL datastore.
4. Based on the access level of the data requester, the view layer needs to filter out the queried data to only return necessary information and ensure the confidentiality of the data owner. To do so, the view layer decrypt the data using the master secret key MK_{secret}.
5. According to the data requester access level, view layer encrypts the data with data requester public key and returns the encrypted data to data requester.
6. The data user decrypts the ciphertext with its private key to access data.
7. In case if a data user needs to access medical image data (e.g. pathology image) for further assessment, authorization layer verifies the access of the data requester and if passed the process moves forward by locating the data location from the Blockchain and requests the encrypted file path from the NoSQL datastore.
8. The authorization layer encrypts the file path with data requester's public key.
9. The authorization layer sends the encrypted file path to the user. The user decrypts the file with its private key.

10. To generate and record provenance data, authentication layer computes the hash value of provenance data (access log) as blockchain identifier (BId) and records it to Blockchain node along with data access transaction. The actual provenance data item is stored in NoSQL datastore with provenance identifier (PId).
11. BId and PId generated from step 10 are appended to the mapping datastore.

7.2.1.6 Data Owner Data Upload

1. After successful registration, the data owner needs to define attributes relevant to its data to generate keys.
2. The Authorization layer generates a pair of asymmetric keys (public and private), which will be used to encrypt and decrypt data.
3. The data owner encrypts the medical data and the path of medical image file by the public key.
4. The data owner uploads the ciphertext and image file path information to the authorization layer.
5. The Authorization layer stores the ciphertext into the NoSQL datastore and generate a pointer to the stored data.
6. The Authorization layer sends the generated pointers to the Blockchain nodes to store the index information.

7.2.1.7 Architectural Flow

Decentralized data provenance mechanisms with Blockchain technology and NoSQL datastore help achieve tracking the full data usage life cycle. The following explains the process flow.

1. **Register:** The first step is to register users in the system by providing the required information.
2. **Identity and Attribute Definition:** Data owner will i) select the identity of the doctor or ii) define the required attributes to grant access to its medical data.
3. **Generate Keys:** After the successful registration, the system user will receive a pair of keys, which will be used to encrypt and decrypt data for data storage and retrieval.
4. **Generate Provenance Data:** Upon of the users request to access and any operation on the medical data, authentication layer generates provenance data which will be stored in NoSQL datastore and Blockchain in the next steps.
5. **Record Provenance Data in the Blockchain:** To store provenance metadata, the SHA256 value of the provenance data item is computed and stored in the Blockchain along with a random 256 bits for the blockchain identifier (BId).

6. **Store Provenance Data in NoSQL datastore:** The actual provenance data item is stored in NoSQL datastore (e.g. Apache Cassandra). Each provenance record is also associated with a random 256 bits for provenance identifier (PId) as a unique ID, which is be used to retrieve provenance data by data owner if needed.
7. **Append Provenance Entry to Mapping File:** An entry containing mapping of BId (step 5) and PId (step 6) is appended into the mapping database.
8. **Query data provenance:** Data owners can request a query of their medical data usage to keep track of the transaction and know exactly who uses its data and how. To do so, the provenance layer authorize the user access level and if the request is legitimate, the provenance data will be retrieved from NoSQL datastore using mapping information (as shown in Figure 7.4).

7.2.2 Attribute-Based Access Control with Privacy-Aware Provenance

The proposed architecture is divided into three phases of provenance metadata generation, storage, and query to record and audit provenance data, which are described as follows.

- **Provenance data generation:** Once the data access request (via a web browser) from a health-care provider is approved by an authorization layer, metadata provenance occurs, and a permanent proof of data provenance should be recorded.
- **Provenance data storage:** Whenever a data sharing (read, write and update) transaction successfully is performed on the stored medical data, actual provenance metadata is recorded in a decentralized datastore such as Apache Cassandra, and its corresponding hash value is stored in Blockchain as a transaction.
- **Provenance data query:** Once a data owner requests for its provenance data, provenance layer maps provenance data from decentralized NoSQL datastore and the corresponding hash point from Blockchain using mapping datastore and returns the information to the data owner.

7.2.3 Attribute-Based Access Control with User Revocation

The proposed hierarchical identity-based and attribute-based encryption approach offers a way to define a flexible fine-grained access policy and encrypts the data according to the pre-defined attributes and access levels. However, a revocation mechanism should be defined to provide the possibility to revoke the issued access from the patient's data if needed. To tackle the complexity of the credential revocation operation and reduce the computational cost, a temporal access condition is proposed in the framework. The main idea is that the state of a key associated with the attributes be updated, and the new ACL be re-distributed to the network automatically. To do so, an expiration time can be assigned to the access rights by data owners to revoke data access immediately after the expiration time.

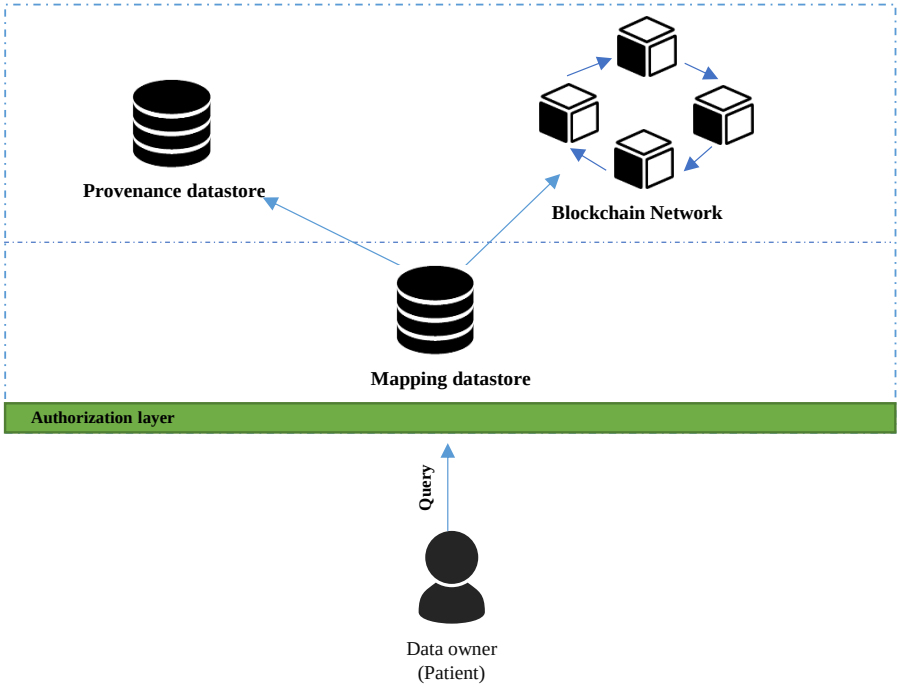

Figure 7.4: Diagram of the access revocation.

7.2.3.1 Identity Based User Revocation

Personal health data of the patients can be stored in the cloud, and access requests can take place frequently at anytime by a wide range of data users including doctors, pharmacists, researchers, EMT staff, emergency contacts where the involvement of patient as data owner is not necessary in issuing, denying or revoking all access requests. The basic idea is to revoke consent and access privileges of a user from the key generation phase. To define an access revocation policy only using attributes (e.g. "Oncologist" AND "Lung" AND ("Ontario"), it is impossible to provide a flexible and fine-grained revocation model as many users can be categorized in the same group for credential revocation. However, a precise revocation mechanism should be defined to provide the possibility to revoke the issued access to the patient's data if is needed. The trusted authority entities are responsible for issuing, revoking, and updating keys for data users in a permissioned Blockchain. Whenever a revocation operation occurs, the trusted authority should re-generate the new hash code for the revoked user and update its private key. Previous researches in the literature have addressed the revocation problem using role-based [61], attribute-based [165] and capability-based [223] revocation mechanisms. Although the previous revocation methods are a feasible solution to achieve consent revocation, it suffers from the issue of involving trusted authority and data owner. This approach also increases the computation cost and time when dataset is very large, the number of attributes is big, or the same attributes or roles shared between the revoked and non-revoked users.

7.2.3.2 Automatic Data Access Expiration

To address the above-mentioned issues, a feasible solution for credential revocation is automatic access expiration that is presented in different studies [118] [69]. The assumption is that the assigned attributes will never expire. However, users might need to access data only for a limited period of time. To tackle the complexity of the credential revocation operation and reduce the computational cost, a temporal access condition is proposed in the framework. To do so, an expiration or session time can be assigned to the access rights by data owners to revoke data access immediately after the expiration time. In this way, the expiration time can be appended to the set of attributes and be embedded in the key generation phase. When decrypting the data, the validity of the "time expiration" attribute is checked and if this attribute is still valid, the data can be decrypted and shared. The proposed "time expiration" attribute automatically updates the new ACL where no interaction between users and the trusted authority or key re-distribution is needed. It also should be noted that the revocation of a consent can only be applied for future data access requests to prohibit the key decryption of the revoked user while the data access of the previous transactions was already recorded in the ledger and is immutable. In the proposed scenario, the revocation can be achieved by executing the changePermission() function from the correspond smart contract to deny the access validity.

```
function patientProfile() public view returns(
    string memory _fullname,
    uint _birthdate,
    string memory _patientAddress,
    address _doctorAddress
)
{
    uint _id = patientIds[msg.sender];
    Patient memory p = patients[_id];
    return (
        p.name,
        p._birthdate,
        p.patientAddress,
        patientToDoctor[msg.sender]
    );
}
```

Figure 7.5: Defining smart contract rule for patient information.

7.3 Implementation and Performance Evaluation

In this section, the prototype implementation of the components of the proposed scheme is provided. Also, the performance of the proposed scheme is analyzed. The primary entities of the proposed

scheme which provides an efficient and secure mechanism are divided into four modules that should be implemented: healthcare provider, mining process, on-chain storage, and off-chain storage. All implementation has been done through a web user interface in Python, Flask, HTML, CSS, NodeJS, Redis and React. Redis allows to design a cluster of nodes and also provides the infrastructure to communicate between the Blockchain network and web interface. Python is used to develop the attribute-based encryption layer, and all of the logic for smart contract is written using the Solidity programming language. Blockchain (on-chain) module is used to store the hash of the diagnostic reports and Apache Cassandra is used as a data storage layer in a Linux node. The Blockchain is deployed on an Ubuntu Linux 16.04 LTS desktop established in the virtual machine with 4GB RAM. The implementation of encryption algorithm is based on the following configuration: Windows 10 operating system with Intel(R) Core (TM) i7-8700K 3.7 GHz processors with 32 GB RAM. The attribute-based encryption implementation is based on python cryptography libraries of pycrypto [13] and pyPEBEL [12]. Smart contracts in Ethereum framework carry out policies, enforcing rules and allows to store metadata about the permissions, ownership, and data integrity. The Solidity programming language is used to develop the smart contracts. The smart contracts are deployed on the private Ethereum client. The development environment of Remix IDE is used to test smart contracts. For dataset generation, two clinical datasets from UCI machine learning repository [17] including lung cancer dataset [16] and heart disease dataset [15] are selected for this research.

```
function getDoctorByIdentity(uint _id) public view returns(
    string memory _doctorname,
    uint _databirth,
    string memory _indentificationID,
    string memory _doctorAddress,
    address _blockchainaddress
)
{
    Practitioner memory p = practitionerList[_id];
    return (
        p.name,
        p._databirth,
        p.indentificationID,
        p.doctorAddress,
        p.blochainAddress
        );
}
```

Figure 7.6: Defining smart contract rule for restricting access.

In order to include personal patient information, synthetic data columns of patients' name, gender, date of birth, country, city, race, marital status, patient ID, admission date and ID are generated for a total number of 335 patients. Smart contracts in Ethereum framework carry out policies, enforcing

rules and allows to store metadata about the permissions, ownership, and data integrity. For example, a policy defined in a smart contract may enforce that separate transactions representing consent are sent from both patients and care providers, before granting viewing permissions to a third party. Each transaction stored in the Blockchain is cryptographically signed to protect patients' medical records stored on the system. After implementing the proposed infrastructure, the issuance of roles, attributes, user registration and management, including patients, doctors, etc. is controlled by the private Blockchain superusers and performed by using functions defined in the smart contract. The performance of the proposed scheme is evaluated to measure whether the proposed scheme is able to ensure the security and privacy requirements for a secure medical data sharing based on attribute-based access control management and Blockchain. The on-chain and off-chain exchange are experimented several times on the provided node in healthcare network. Patient nodes are triggered numerous transactions to healthcare provider nodes to test both the capacity of the network and the waiting time of each transaction to be processed and mined. The proposed scheme provides a data owner (patient) a comprehensive and credible log of the medical history. The provenance feature allows patients to be fully informed of how their medical data is being used and any modifications that is applied to it. The Blockchain immutable ledger records an auditable history of transactions between patients' data and healthcare providers. However, personal, and medical data of patient still need to be stored in local databases and managed by the system. Therefore, an external layer is proposed in the system to govern access right management. Data access management, as a layer on top of the Blockchain, enables patients to manage permission using both identity and attributes and a secure data exchange between different parties. The proposed scheme also provides features using smart contract provisions for further restrictions. To do so, metadata field such as session time is defined to set an expiration date and time for data access revocation. This specific authorization allows for confidentiality of the patients.

According to the above description, the following modules are designed in the proposed scheme:

1. **Backend Library:** The backend library facilitates the interactions between the Blockchain network and the web interface. Initiating a request triggers the smart contract. The backend library can automatically verify the access-level of the transaction by calling pre-defined functions, therefore avoid third parties of working directly with Blockchain. The backend library interacts with the Ethereum client to deal with each individual transaction with high confidence and manage the uncertainty.
2. **Registrar Contract:** The Registrar contract registers users to the system. To do so, when information of a user is first verified, this smart contract in provider node registers the user and generates a pair of public/private Ethereum address accordingly. Therefore, the owner of a valid Ethereum address has the stewardship of the data and could mange the access requests to his/her medical data. This module contains the full functionality which is needed to participate

in the system. The Ethereum client helps identifying and mapping Ethereum addresses to the top security layer in order to handle tasks such as encoding and sending transactions, updating the state of the users in the provided Blockchain network.

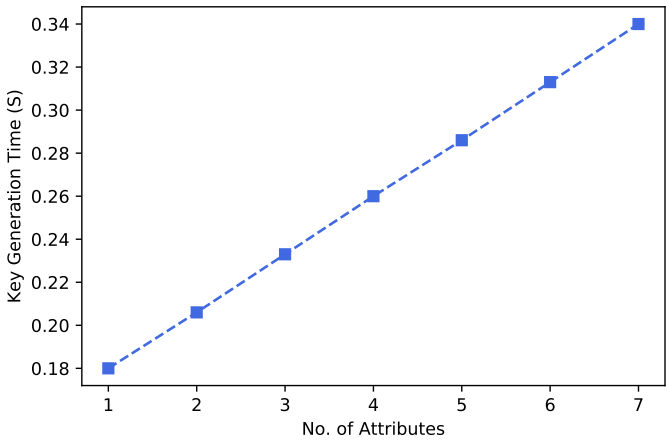

Figure 7.7: Key generation time for the implemented system.

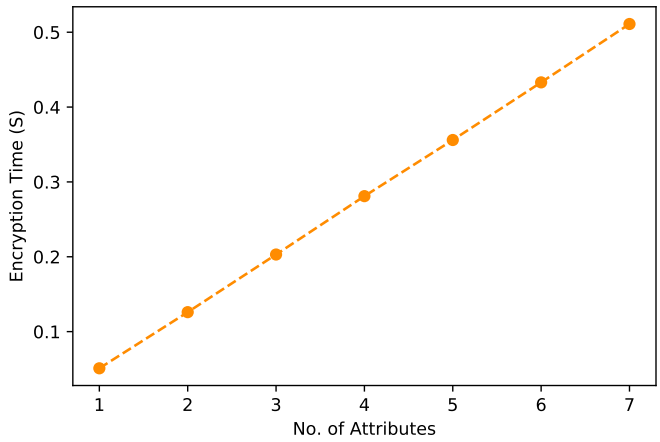

Figure 7.8: Encryption time of the implemented system.

3. **Healthcare Provider:** This module is mainly responsible for making diagnosis of patients. The diagnostic information details should be recorded to the NoSQL database. Figure. 7.5 illustrates the smart contract used by a doctor to view patient's data. Also, Figure 7.7 demonstrates the key generation time of healthcare provider e.g. doctor and the time that is needed to record diagnostic report into the datastore. Analyzing Figure.7.7, it can be seen that the encryption time is more computation-intensive than decryption time of data. The user web interface allows viewing, updating, sharing of the diagnosis information with data owner (patient) and which can

directly interact with datastore. The web interface is built using python Flask micro-framework for easy access to patients and healthcare providers.

4. **Mining Process:** The mining of blocks is the central part of decentralization in Blockchain technology as a group of mining nodes are required to execute the consensus algorithm to validate the transaction and finally create a block. Each block, which is the result of mining process, consists of a list of transactions of each patient. The time needed to mine a block and append the transaction information to the block varies based on the number of attributes. In this research, mining of a block consumes more time than generating the block for all type of transactions. The consensus mechanism used for this research is Ethereum's inherent consensus algorithm to achieve a trustworthy chain of blocks in a healthcare ecosystem. Based on this mechanism, performing a transaction requires Ether. When a miner node solves the computational puzzle, Ether can be awarded. In the Ethereum network, patients need to pay Ether to share their medical data and receive diagnosis.
5. **Off-chain storage:** An off-chain approach is used in this research to store medical and personal information on the local database nodes. The access layer on top of Blockchain network govern the permissions based on roles and attributes of the users to have access to data stored in the database. The database listens to the network for a query request. The query request should be cryptographically signed by the issuer's private key to ensure the query requester is from a legitimate user. Once a permission is allowed by the access layer, the requested query will be processed on the database and return the result to the query issuer.
6. **On-chain storage:** In the proposed framework the original data is stored in a NOSQL data-store and the hash value pointing to the data is stored in the blockchain network. Each block contains information such as timestamp from the machine internal clock, diagnostic hash pointer, patient data hash pointer, and subsequent block hash (integrity of block) (SHA-256) value. Figure 7.7, 7.8, 7.9 measure the time required for accessing a transaction by the peer nodes. Analyzing these figures, the access time increases as the number of attributes increases as expected.
7. **Re-registration** If a data owner loses or forgets his/her own private key or his/her access to the digital wallet, then the whole access to the system is also lost. In this case, the data ownership can be verified but data owner is not able to sign or manage accesses without the corresponding private key. The superuser has a global permission feature to simply delete the compromised user (associated the private and public keys) using the removeUser() function.
8. **Revocation** The revocation operation is an important part of the smart contract functions to prevent data misuse of expired accesses and also improves the flexibility of the proposed system by allowing to remove access from data.

   This operation can be conducted by executing the removeUser() function defined in smart contract. This function introduces the ability to the system to remove a user from accessing data. This

feature is based on the automate expiration time as defined in a time session to set the amount of time that a data user can access the patient's data. The revocation feature is provided using timestamp server of Ethereum to include the expiration date and time of a user or define how long an attribute associated with a user is valid. In the proposed scheme, the "sessiontime" of the addUser() function includes the expiration date and time to a data user.

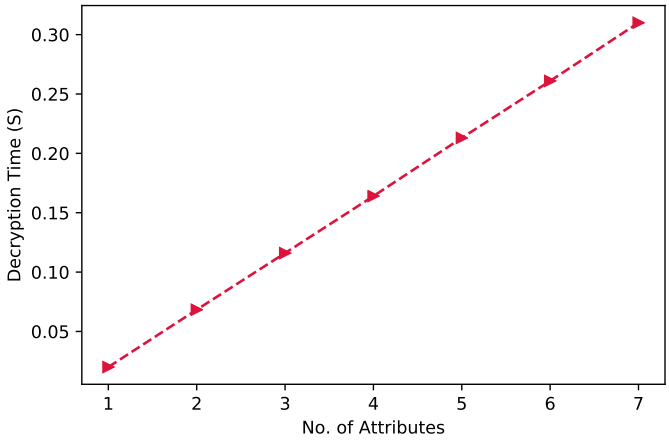

Figure 7.9: Decryption time of the implemented system.

8 Conclusion and Future work

8.1 Conclusion

To design a computer-aided diagnosis framework for automatic cancer diagnosis and grading via an ensemble of deep learning models, four case studies of different types of cancer classification and segmentation tasks, including lung, leukemia, breast and colorectal cancer, are selected to evaluate the performance of the proposed models.

An ensemble deep learning-based method is proposed using three pre-trained CNNs, namely VGG19, MobileNet, and DenseNet to extract discriminative features from the histology images. The features extracted from the proposed method are then fed into a multi-layer perceptron classifier to carry out the classification task. Different pre-processing steps, including stain-normalization, data augmentation, hyper-parameter tuning, and fine-tuning is provided to train the model. The performance of the proposed method is validated on four publicly available datasets, namely, ICIAR, BreakHis, PatchCamelyon, and Bioimaging. The proposed multi-model ensemble method obtains better predictions than single classifiers and machine learning algorithms with accuracies of 98.13%, 95.00%, 94.64% and 83.10% for BreakHis, ICIAR, PatchCamelyon and Bioimaging datasets, respectively.

In the next case study, a model is developed for computer-aided leukemia cancer diagnosis. The proposed deep learning-based method is a hybrid method using VGG16 and MobileNet architectures to distinguish between immature leukemic blasts and normal cells. Different methods such as transfer learning and various data augmentation were employed to accelerate the learning process and further improve the performance of the proposed network. Results demonstrate that the proposed model yields better prediction than individual models for Leukemic B-lymphoblast classification with 96.17% overall accuracy, 95.17% sensitivity and 98.58% specificity. Fusing the features extracted from intermediate layers, the proposed approach has the potential to improve the overall classification performance.

For lung and colorectal cancer segmentation, the proposed deep neural network is a decoder-encoder convolutional neural network employing different feature extractors models i.e. ResNet, DenseNet, InceptionV3, InceptionResNetV2 and SE-ResNeXt in the down-sampling part of the architecture. The results have shown that the proposed ensemble method using skip connections in the feature extractor part of the architecture achieved good results and significantly outperformed the baseline approaches. To perform the segmentation task for lung cancer, a CNN-based encoder-decoder architecture with

skip-connections is designed for lung cancer tissue segmentation to delineate the fine-grained structure of the histopathology images. On the proposed backbone, four skip-connections with concatenation operation are established to link the lower layers and upper layers of network. The integration of batch normalization technique helps alleviate internal covariant shift and over-fitting issues. The feasibility of transfer learning strategy of 14 state-of-the-art feature extractors are introduced to the encoder part of the proposed architecture to investigates the performance of a wide variety of deep learning-based architectures for automatically tumor segmentation of histology tissue samples. The obtained segmentation results have shown that the proposed architecture achieved a dice similarity coefficient of 84.10%, accuracy of 90.69%, F1-score of 84.16%, and MSE rate of 0.0911.

A detailed comparative analysis of a wide variety of state-of-the-art deep CNNs in the encoder part of three segmentation backbones is provided for colorectal cancer tissue segmentation. The proposed approach highlights the utility of incorporating CNN modules and transfer learning in the encoder part of a segmentation architecture for histopathology image analysis. The method is fast in analyzing batches of images as it is based on transfer learning strategy and patch-wise extraction method from colorectal cancer histology WSIs with heterogeneous shape and texture. Transfer learning strategy helps accelerate the learning process and further improve the performance of the proposed network. Experimental results demonstrate that shared DenseNet and LinkNet architecture achieves the state-of-the-art performance and outperforms other methods with a dice similarity index of 82.74%, accuracy of 87.07%, and f1-score value of 82.79%. The second-best result is obtained by InceptionResNetV2 pre-trained model on FPN architecture with dice similarity score of 82.53%, accuracy of 87.10% as well as the highest F1-score of 82.73%. Overall, comparing all of the feature extractors and segmentation backbone models, FPN and U-Net models tend to produce more stable results and are (almost) equivalent.

Motivated by the advantages of Blockchain technology in healthcare data sharing frameworks, the focus of the second part of this research is to integrate Blockchain technology in computer-aided diagnosis systems to address the problems of managing access control, authentication, provenance, and confidentiality of sensitive medical data. An attribute-base encryption with Blockchain technology is attempted to address the challenges related to access control management, provenance and data privacy of medical data. A combination of hierarchical identity and attribute-based access control mechanism using smart contract and Ethereum Blockchain is employed to securely process healthcare data without revealing sensitive information to unauthorized party. Employing a NoSQL data store could be a possible solution to address the problem of limited storage capacity and computational resources. The performance of designed infrastructure was tested and analyzed through a simulation for different transactions such as data sharing, Ether transfer, registration and mining. The performance of the proposed scheme enabled fine-grained access control for the security and privacy requirements, access revocation, anonymity, secure data provenance and traceability by an authority.

8.2 Future work

A number of interesting areas of research can be suggested for future efforts.

- Currently, deep learning based image segmentation and classification models are highly dependent on the quality of the features extracted from the input data. Different strategies such as data augmentation and transfer learning can help improve the performance of the learner. However, including more training samples is more effective than artificiality generated images by data augmentation techniques.
- Analysis of histology images is limited due to the GPU memory constraint to process large-scale whole-slide images. Therefore, the current CNN models have small receptive fields or the original resolution of WSIs are reduced to address the issue of the processing constraint. A common solution to this problem is extracting patches from the large-scale WSIs. However, generating patches from data can cause the loss of critical information. In the future, it would be interesting to investigate methods in developing efficient CNN models to process the whole-slide images without the need of patch extraction methods. It is possible that with further development these models may be deployed in real-world clinical environments.
- Due to the limitations of feature extraction methods, the impact of attention-based modules can be a potential solution for future directions to improve the quality of extracted features.
- Also, exploring the possibility of combining different image modalities i.e. mammograms, MRI and CT scans with pathology images for a more comprehensive assessment and diagnosis can be an interesting direction for the future research. Pathology shows the characteristics of the tumors, while the CT scans locate the shape, size and position of a tumor. The analysis of different imaging modalities allows to automatically identify and assess the disease diagnosis or progression.
- Furthermore, the combination of patient's genomics with imaging modalities and clinical data allows developing therapeutics expansion such as developing personalized medicine, monitoring the rate of treatment failure, managing side-effects of treatment and ultimately improving the survival rate of patients.
- Although, this research presented how different modules such as inception, dense and residual units can enhance the quality of the extracted features, it would be interesting to investigate the feature extraction methods for pixel-based localization of the tumors in H&E histopathology images.
- No study in the literature provided a real-world interpretation on how trained models and obtained features could be translated into clinical practice.
- None of the studies in the literature takes the advantage of domain knowledge to discover new features from data and help better understand the development of cancer. Therefore, analyzing quantitative deep features associated to the semantic would be an exciting research direction.

The major limitation of the proposed Blockchain network is that the configuration was implemented on a single computational node which adversely affected the time needed for key generation, encryption and decryption operations. Performing key sharing and management among multiple nodes as a possible solution could reduce data access delay.

- A real-time use case of the proposed Blockchain network as a future direction should address the patient-driven interoperability to exchange information between personal (e.g. patient's family) or/and business entities considering the requirements around secure clinical data transaction, privacy, and patient incentives for this type of data sharing.
- Future work also can address the open issue of the malicious participant tracing and anomaly detection. A fully distributed and automatic anomaly detection scheme can be developed for anomaly detection and anomaly precaution phase to respond anomalies timely and accurately in the proposed Blockchain network environment.

References

[1] ACDC-Lung. https://acdc-lunghp.grand-challenge.org/.

[2] Bioimaging 2015 dataset. http://www.bioimaging2015.ineb.up.pt/dataset.html.

[3] Cancer statistics report. https://www.who.int/news-room/fact-sheets/detail/cancer.

[4] Classification of Normal vs Malignant Cells in B-ALL White Blood Cancer Microscopic Images:ISBI 2019. URL: https://competitions.codalab.org/competitions/20429.

[5] DigestPath. https://digestpath2019.grand-challenge.org/.

[6] Histopathologic Cancer Detection. https://www.kaggle.com/c/histopathologic-cancer-detection.

[7] Key Statistics for Acute Lymphocytic Leukemia (ALL). URL: https://www.cancer.org/cancer/acute-lymphocytic-leukemia/about/key-statistics.html.

[8] Key statistics for colorectal cancer. https://www.cancer.org/cancer/colon-rectal-cancer/about/key-statistics.html.

[9] Key statistics for lung cancer. https://www.cancer.org/cancer/lung-cancer/about/key-statistics.html.

[10] Nn-svg. http://alexlenail.me/NN-SVG/index.html.

[11] PoET 1.0 Specification. https://sawtooth.hyperledger.org/docs/core/releases/latest/architecture/poet.html.

[12] Predicate Based Encryption Library. URL: https://github.com/jfdm/pyPEBEL.

[13] Python Cryptography Toolkit (pycrypto). URL: https://pypi.org/project/pycrypto/.

[14] Sawtooth. https://www.hyperledger.org/projects/sawtooth.

[15] UCI Heart Disease Data Set. URL: http://archive.ics.uci.edu/ml/datasets/heart+Disease.

[16] UCI Lung Cancer Dataset. URL: https://archive.ics.uci.edu/ml/datasets/Lung+Cancer.

[17] UCI Machine Learning Repository. URL: https://archive.ics.uci.edu/ml/datasets.php.

[18] WHO-Breast cancer. URL: https://www.who.int/cancer/prevention/diagnosis-screening/breast-cancer/en/.

[19] Systematic outperformance of 112 dermatologists in multiclass skin cancer image classification by convolutional neural networks. *European Journal of Cancer*, 2019. doi:10.1016/j.ejca.2019.06.013.

[20] PoRX: A reputation incentive scheme for blockchain consensus of IIoT. *Future Generation Computer Systems*, 2020. doi:10.1016/j.future.2019.08.005.

[21] Mohammed M Abdelsamea, Alain Pitiot, Ruta Barbora Grineviciute, Justinas Besusparis, Arvydas Laurinavicius, and Mohammad Ilyas. A cascade-learning approach for automated segmentation of tumour epithelium in colorectal cancer. *Expert Systems with Applications*, 118:539–552, 2019.

[22] Steve A. Adeshina, Adeyinka P. Adedigba, Ahmed A. Adeniyi, and Abiodun M. Aibinu. Breast cancer histopathology image classification with deep convolutional neural networks. In *14th International Conference on Electronics Computer and Computation, ICECCO 2018*, 2019. doi:10.1109/ICECCO.2018.8634690.

[23] Shubhani Aggarwal, Rajat Chaudhary, Gagangeet Singh Aujla, Neeraj Kumar, Kim Kwang Raymond Choo, and Albert Y. Zomaya. Blockchain for smart communities: Applications, challenges and opportunities, 2019. doi:10.1016/j.jnca.2019.06.018.

[24] Abdullah Al Omar, Mohammad Shahriar Rahman, Anirban Basu, and Shinsaku Kiyomoto. Medibchain: A blockchain based privacy preserving platform for healthcare data. In *International conference on security, privacy and anonymity in computation, communication and storage*, pages 534–543. Springer, 2017.

[25] Shadi Albarqouni, Christoph Baur, Felix Achilles, Vasileios Belagiannis, Stefanie Demirci, and Nassir Navab. Aggnet: deep learning from crowds for mitosis detection in breast cancer histology images. *IEEE transactions on medical imaging*, 35(5):1313–1321, 2016.

[26] Abdulkadir Albayrak and Gokhan Bilgin. A hybrid method of superpixel segmentation algorithm and deep learning method in histopathological image segmentation. In *2018 Innovations in Intelligent Systems and Applications (INISTA)*, pages 1–5. IEEE, 2018.

[27] M. Alblooshi, K. Salah, and Y. Alhammadi. Blockchain-based Ownership Management for Medical IoT (MIoT) Devices. In *Proceedings of the 2018 13th International Conference on Innovations in Information Technology, IIT 2018*, 2019. doi:10.1109/INNOVATIONS.2018.8606032.

[28] Fouzia Altaf, Syed M. S. Islam, Naveed Akhtar, and Naeem Khalid Janjua. Going Deep in Medical Image Analysis: Concepts, Methods, Challenges, and Future Directions. *IEEE Access*, 2019. arXiv:1902.05655, doi:10.1109/access.2019.2929365.

[29] Mostafa Amin-Naji, Ali Aghagolzadeh, and Mehdi Ezoji. Ensemble of cnn for multi-focus image fusion. *Information Fusion*, 51:201–214, 2019. URL: http://www.sciencedirect.com/science/article/pii/S1566253518306043, doi:https://doi.org/10.1016/j.inffus.2019.02.003.

[30] Gupta Anubha, Duggal Rahul, Gupta Ritu, Kumar Lalit, Thakkar Nisarg, and Satpathy Devprakash. GCTI-SN: Geometry-Inspired Chemical and Tissue Invariant Stain Normalization of Microscopic Medical Images.

[31] Teresa Araújo, Guilherme Aresta, Eduardo Castro, José Rouco, Paulo Aguiar, Catarina Eloy, António Polónia, and Aurélio Campilho. Classification of breast cancer histology images using convolutional neural networks. *PloS one*, 12(6):e0177544, 2017.

[32] Guilherme Aresta, Teresa Araújo, Scotty Kwok, Sai Saketh Chennamsetty, Mohammed Safwan, Varghese Alex, Bahram Marami, Marcel Prastawa, Monica Chan, Michael Donovan, et al. Bach: Grand challenge on breast cancer histology images. *Medical image analysis*, 2019.

[33] Asaph Azaria, Ariel Ekblaw, Thiago Vieira, and Andrew Lippman. MedRec: Using blockchain for medical data access and permission management. In *Proceedings - 2016 2nd International Conference on Open and Big Data, OBD 2016*, 2016. doi:10.1109/OBD.2016.11.

[34] Mohsen Azimi, Armin Dadras Eslamlou, and Gokhan Pekcan. Data-driven structural health monitoring and damage detection through deep learning: State-of-the-art review. *Sensors*, 20(10):2778, 2020.

[35] Vivek Singh Bawa and Vinay Kumar. Linearized sigmoidal activation: A novel activation function with tractable non-linear characteristics to boost representation capability. *Expert Systems with Applications*, 120:346–356, 2019.

[36] Neslihan Bayramoglu, Juho Kannala, and Janne Heikkilä. Deep learning for magnification independent breast cancer histopathology image classification. In *2016 23rd International conference on pattern recognition (ICPR)*, pages 2440–2445. IEEE, 2016.

[37] Babak Ehteshami Bejnordi, Mitko Veta, Paul Johannes Van Diest, Bram Van Ginneken, Nico Karssemeijer, Geert Litjens, Jeroen AWM Van Der Laak, Meyke Hermsen, Quirine F Manson, Maschenka Balkenhol, et al. Diagnostic assessment of deep learning algorithms for detection of lymph node metastases in women with breast cancer. *Jama*, 318(22):2199–2210, 2017.

[38] Aicha Bentaieb, Jeremy Kawahara, and Ghassan Hamarneh. Multi-loss convolutional networks for gland analysis in microscopy. In *Proceedings - International Symposium on Biomedical Imaging*, 2016. doi:10.1109/ISBI.2016.7493349.

[39] Daniel J Bernstein, Niels Duif, Tanja Lange, Peter Schwabe, and Bo-Yin Yang. High-speed high-security signatures. *Journal of cryptographic engineering*, 2(2):77–89, 2012.

[40] Danny Bradbury. The problem with Bitcoin. *Computer Fraud and Security*, 2013. doi:10.1016/S1361-3723(13)70101-5.

[41] Nadia Brancati, Maria Frucci, and Daniel Riccio. Multi-classification of breast cancer histology images by using a fine-tuning strategy. In *International Conference Image Analysis and Recognition*, pages 771–778. Springer, 2018.

[42] Titus J. Brinker, Achim Hekler, Alexander H. Enk, Carola Berking, Sebastian Haferkamp, Axel Hauschild, Michael Weichenthal, Joachim Klode, Dirk Schadendorf, Tim Holland-Letz, Christof von Kalle, Stefan Fröhling, Bastian Schilling, and Jochen S. Utikal. Deep neural networks are superior to dermatologists in melanoma image classification. *European Journal of Cancer*, 2019. doi:10.1016/j.ejca.2019.05.023.

[43] Herb Brody. Medical imaging. *Nature*, 502(7473):S81–S81, 2013.

[44] Daniel RL Brown. Sec 2: Recommended elliptic curve domain parameters. *Standars for Efficient Cryptography*, 2010.

[45] Ahmet Bugday, Adnan Ozsoy, Serdar Murat Öztaner, and Hayri Sever. Creating consensus group using online learning based reputation in blockchain networks. *Pervasive and Mobile Computing*, 59:101056, 2019.

[46] Daniel Bumblauskas, Arti Mann, Brett Dugan, and Jacy Rittmer. A blockchain use case in food distribution: Do you know where your food has been? *International Journal of Information Management*, 2019.

[47] Christian Cachin. Architecture of the hyperledger blockchain fabric. In *Workshop on distributed cryptocurrencies and consensus ledgers*, volume 310, page 4, 2016.

[48] Christian Cachin and Marko Vukolić. Blockchain consensus protocols in the wild. *arXiv preprint arXiv:1707.01873*, 2017.

[49] Nurullah Çalik, Onur Can Kurban, Ali Rıza Yilmaz, Tülay Yildirim, and Lütfiye Durak Ata. Large-scale offline signature recognition via deep neural networks and feature embedding. *Neurocomputing*, 2019.

[50] Debolina Chakraborty, Chandrasekaran Natarajan, and Amitava Mukherjee. Chapter six - advances in oral cancer detection. volume 91 of *Advances in Clinical Chemistry*, pages 181–200. Elsevier, 2019. URL: http://www.sciencedirect.com/science/article/pii/S0065242319300265, doi:https://doi.org/10.1016/bs.acc.2019.03.006.

[51] Sabyasachi Chakraborty, Satyabrata Aich, and Hee Cheol Kim. A Secure Healthcare System Design Framework using Blockchain Technology. In *International Conference on Advanced Communication Technology, ICACT*, 2019. doi:10.23919/ICACT.2019.8701983.

[52] Jongwon Chang, Jisang Yu, Taehwa Han, Hyuk Jae Chang, and Eunjeong Park. A method for classifying medical images using transfer learning: A pilot study on histopathology of breast cancer. In *2017 IEEE 19th International Conference on e-Health Networking, Applications and Services, Healthcom 2017*, 2017. doi:10.1109/HealthCom.2017.8210843.

[53] Shuchih Ernest Chang, Yi-Chian Chen, and Ming-Fang Lu. Supply chain re-engineering using blockchain technology: A case of smart contract based tracking process. *Technological Forecasting and Social Change*, 144:1–11, 2019.

[54] Hao Chen, Xiaojuan Qi, Lequan Yu, and Pheng Ann Heng. DCAN: Deep Contour-Aware Networks for Accurate Gland Segmentation. In *Proceedings of the IEEE Computer Society Conference on Computer Vision and Pattern Recognition*, 2016. arXiv:1604.02677, doi:10.1109/CVPR.2016.273.

[55] Kemeng Chen, Ning Zhang, Linda Powers, and Janet Roveda. Cell nuclei detection and segmentation for computational pathology using deep learning. In *Proceedings of the Modeling and Simulation in Medicine Symposium*, page 12. Society for Computer Simulation International, 2019.

[56] Sérgio F. Chevtchenko, Rafaella F. Vale, Valmir Macario, and Filipe R. Cordeiro. A convolutional neural network with feature fusion for real-time hand posture recognition. *Applied Soft Computing*, 73:748–766, 2018. URL: http://www.sciencedirect.com/science/article/pii/S1568494618305271, doi:https://doi.org/10.1016/j.asoc.2018.09.010.

[57] Jun-Ho Choi and Jong-Seok Lee. Embracenet: A robust deep learning architecture for multimodal classification. *Information Fusion*, 51:259–270, 2019. URL: http://www.sciencedirect.com/science/article/pii/S1566253517308242, doi:https://doi.org/10.1016/j.inffus.2019.02.010.

[58] Djork-Arné Clevert, Thomas Unterthiner, and Sepp Hochreiter. Fast and accurate deep network learning by exponential linear units (elus). *arXiv preprint arXiv:1511.07289*, 2015.

[59] Noel Codella, Veronica Rotemberg, Philipp Tschandl, M. Emre Celebi, Stephen Dusza, David Gutman, Brian Helba, Aadi Kalloo, Konstantinos Liopyris, Michael Marchetti, Harald Kittler, and Allan Halpern. Skin lesion analysis toward melanoma detection 2018: A challenge hosted by the international skin imaging collaboration (ISIC), 2019. arXiv:1902.03368.

[60] Shaen Corbet, Douglas J. Cumming, Brian M. Lucey, Maurice Peat, and Samuel A. Vigne. The destabilising effects of cryptocurrency cybercriminality. *Economics Letters*, page 108741, 2019. URL: http://www.sciencedirect.com/science/article/pii/S0165176519303714, doi:https://doi.org/10.1016/j.econlet.2019.108741.

[61] Jason Paul Cruz, Yuichi Kaji, and Naoto Yanai. RBAC-SC: Role-based access control using smart contract. *IEEE Access*, 2018. doi:10.1109/ACCESS.2018.2812844.

[62] Pierluigi Cuccuru. Beyond bitcoin: an early overview on smart contracts. *International Journal of Law and Information Technology*, 25(3):179–195, 2017.

[63] Marcela T. de Oliveira, Lucio H. A. Reis, Ricardo C. Carrano, Flavio L. Seixas, Debora C. M. Saade, Celio V. Albuquerque, Natalia C. Fernandes, Silvia D. Olabarriaga, Dianne S. V. Medeiros, and Diogo M. F. Mattos. Towards a Blockchain-Based Secure Electronic Medical Record for Healthcare Applications. 2019. doi:10.1109/icc.2019.8761307.

[64] Wenlong Deng, Yongli Mou, Takahiro Kashiwa, Sergio Escalera, Kohei Nagai, Kotaro Nakayama, Yutaka Matsuo, and Helmut Prendinger. Vision based pixel-level bridge structural damage detection using a link aspp network. *Automation in Construction*, 110:102973, 2020.

[65] Tuba Denkçeken, Murat Canpolat, Mehmet Baykara, İbrahim Başsorgun, and Anıl Aktaş-Samur. Diagnosis of pelvic lymph node metastasis in prostate cancer using single optical fiber probe. *International journal of biological macromolecules*, 90:63–67, 2016.

[66] Omar Dib, Kei-Leo Brousmiche, Antoine Durand, Eric Thea, and E Ben Hamida. Consortium blockchains: Overview, applications and challenges. *International Journal On Advances in Telecommunications*, 11(1&2), 2018.

[67] Whitfield Diffie and Martin Hellman. New directions in cryptography. *IEEE transactions on Information Theory*, 22(6):644–654, 1976.

[68] Yi Ding, Linpeng Gong, Mingfeng Zhang, Chang Li, and Zhiguang Qin. A multi-path adaptive fusion network for multimodal brain tumor segmentation. *Neurocomputing*, 2020. doi:10.1016/j.neucom.2020.06.078.

[69] Qiuxiang Dong, Dijiang Huang, Jim Luo, and Myong Kang. Achieving fine-grained access control with discretionary user revocation over cloud data. In *2018 IEEE Conference on Communications and Network Security (CNS)*, pages 1–9. IEEE, 2018.

[70] Yiwen Du, Jianwei Liu, Zhenyu Guan, and Hanwen Feng. A medical information service platform based on distributed cloud and blockchain. In *Proceedings - 3rd IEEE International Conference on Smart Cloud, SmartCloud 2018*, 2018. doi:10.1109/SmartCloud.2018.00014.

[71] Alevtina Dubovitskaya, Zhigang Xu, Samuel Ryu, Michael Schumacher, and Fusheng Wang. Secure and trustable electronic medical records sharing using blockchain. In *AMIA Annual Symposium Proceedings*, volume 2017, page 650. American Medical Informatics Association, 2017.

[72] Rahul Duggal, Anubha Gupta, Ritu Gupta, and Pramit Mallick. SD-Layer: Stain Deconvolutional Layer for CNNs in Medical Microscopic Imaging BT - Medical Image Computing and Computer-Assisted Intervention − MICCAI 2017. pages 435–443, Cham, 2017. Springer International Publishing.

[73] Rahul Duggal, Anubha Gupta, Ritu Gupta, Manya Wadhwa, and Chirag Ahuja. Overlapping Cell Nuclei Segmentation in Microscopic Images Using Deep Belief Networks. In *Proceedings of the Tenth Indian Conference on Computer Vision, Graphics and Image Processing*, ICVGIP '16, pages 82:1—-82:8, New York, NY, USA, 2016. ACM. URL: `http://doi.acm.org/10.1145/3009977.3010043`, `doi:10.1145/3009977.3010043`.

[74] Babak Ehteshami Bejnordi, Jimmy Lin, Ben Glass, Maeve Mullooly, Gretchen L. Gierach, Mark E. Sherman, Nico Karssemeijer, Jeroen Van Der Laak, and Andrew H. Beck. Deep learning-based assessment of tumor-associated stroma for diagnosing breast cancer in histopathology images. In *Proceedings - International Symposium on Biomedical Imaging*, 2017. `arXiv:1702.05803`, `doi:10.1109/ISBI.2017.7950668`.

[75] Engui Fan. Extended tanh-function method and its applications to nonlinear equations. *Physics Letters A*, 277(4-5):212–218, 2000.

[76] Leyuan Fang, Yuxuan Jin, Laifeng Huang, Siyu Guo, Guangzhe Zhao, and Xiangdong Chen. Iterative fusion convolutional neural networks for classification of optical coherence tomography images. *Journal of Visual Communication and Image Representation*, 59:327–333, 2019.

[77] Anselmo Ferreira and Gilson Giraldi. Convolutional neural network approaches to granite tiles classification. *Expert Systems with Applications*, 84:1–11, 2017.

[78] H Kamdem Fezeu, T Djotio, and R Oulad Haj Thami. Safe and irrefutable decentralized communication: Bringing non-repudiation to mesh networks. In *Proceedings of the 2nd international Conference on Big Data, Cloud and Applications*, pages 1–6, 2017.

[79] Magda Foti and Manolis Vavalis. Blockchain based uniform price double auctions for energy markets. *Applied Energy*, 254:113604, 2019.

[80] Kunihiko Fukushima. Neocognitron: A self-organizing neural network model for a mechanism of pattern recognition unaffected by shift in position. *Biological cybernetics*, 36(4):193–202, 1980.

[81] Ziba Gandomkar, Patrick C. Brennan, and Claudia Mello-Thoms. Mudern: Multi-category classification of breast histopathological image using deep residual networks. *Artificial Intelligence in Medicine*, 88:14–24, 2018. URL: `http://www.sciencedirect.com/science/article/pii/S0933365717305031`, `doi:https://doi.org/10.1016/j.artmed.2018.04.005`.

[82] Shadan Ghaffaripour and Ali Miri. Application of blockchain to patient-centric access control in medical data management systems. In *2019 IEEE 10th Annual Information Technology, Electronics and Mobile Communication Conference (IEMCON)*, pages 0190–0196. IEEE, 2019.

[83] Xavier Glorot, Antoine Bordes, and Yoshua Bengio. Deep sparse rectifier neural networks. In *Proceedings of the fourteenth international conference on artificial intelligence and statistics*, pages 315–323, 2011.

[84] Simon Graham, Hao Chen, Jevgenij Gamper, Qi Dou, Pheng-Ann Heng, David Snead, Yee Wah Tsang, and Nasir Rajpoot. Mild-net: minimal information loss dilated network for gland instance segmentation in colon histology images. *Medical image analysis*, 52:199–211, 2019.

[85] Ritu Gupta, Pramit Mallick, Rahul Duggal, Anubha Gupta, and Ojaswa Sharma. Stain Color Normalization and Segmentation of Plasma Cells in Microscopic Images as a Prelude to Development of Computer Assisted Automated Disease Diagnostic Tool in Multiple Myeloma. *Clinical Lymphoma Myeloma and Leukemia*, 17(1):e99, February 2017. URL: `https://linkinghub.elsevier.com/retrieve/pii/S2152265017304688`, `doi:10.1016/j.clml.2017.03.178`.

[86] Vibha Gupta and Arnav Bhavsar. Sequential modeling of deep features for breast cancer histopathological image classification. In *Proceedings of the IEEE Conference on Computer Vision and Pattern Recognition Workshops*, pages 2254–2261, 2018.

[87] Zhongyi Han, Benzheng Wei, Yuanjie Zheng, Yilong Yin, Kejian Li, and Shuo Li. Breast cancer multi-classification from histopathological images with structured deep learning model. *Scientific reports*, 7(1):4172, 2017.

[88] NJ Harlaar, W Kelder, A Sarantopoulos, J Bart, G Themelis, GM Van Dam, and V Ntziachristos. Real-time near infrared fluorescence (nirf) intra-operative imaging in ovarian cancer using an $\alpha v\beta 3$-integrin targeted agent. *Gynecologic oncology*, 128(3):590–595, 2013.

[89] Kaiming He, Xiangyu Zhang, Shaoqing Ren, and Jian Sun. Deep residual learning for image recognition. In *Proceedings of the IEEE Computer Society Conference on Computer Vision and Pattern Recognition*, 2016. arXiv:1512.03385, doi:10.1109/CVPR.2016.90.

[90] Cédric Hebert and Francesco Di Cerbo. Secure blockchain in the enterprise: A methodology. *Pervasive and Mobile Computing*, 2019. doi:10.1016/j.pmcj.2019.101038.

[91] P Herent, B Schmauch, P Jehanno, O Dehaene, C Saillard, C Balleyguier, J Arfi-Rouche, and S Jégou. Detection and characterization of mri breast lesions using deep learning. *Diagnostic and interventional imaging*, 100(4):219–225, 2019.

[92] Geoffrey E Hinton, Nitish Srivastava, Alex Krizhevsky, Ilya Sutskever, and Ruslan R Salakhutdinov. Improving neural networks by preventing co-adaptation of feature detectors. *arXiv preprint arXiv:1207.0580*, 2012.

[93] Andrew G. Howard, Menglong Zhu, Bo Chen, Dmitry Kalenichenko, Weijun Wang, Tobias Weyand, Marco Andreetto, and Hartwig Adam. MobileNets: Efficient Convolutional Neural Networks for Mobile Vision Applications. April 2017. URL: http://arxiv.org/abs/1704.04861, arXiv:1704.04861.

[94] Jie Hu, Li Shen, and Gang Sun. Squeeze-and-excitation networks. In *Proceedings of the IEEE conference on computer vision and pattern recognition*, pages 7132–7141, 2018.

[95] Kexin Hu, Zhenfeng Zhang, and Kaiwen Guo. Breaking the binding: Attacks on the Merkle approach to prove liabilities and its applications. *Computers & Security*, 2019. doi:10.1016/j.cose.2019.101585.

[96] Zilong Hu, Jinshan Tang, Ziming Wang, Kai Zhang, Ling Zhang, and Qingling Sun. Deep learning for image-based cancer detection and diagnosis- a survey. *Pattern Recognition*, 83:134–149, 2018.

[97] Cam-Hao Hua, Thien Huynh-The, Kiyoung Kim, Seung-Young Yu, Thuong Le-Tien, Gwang Hoon Park, Jaehun Bang, Wajahat Ali Khan, Sung-Ho Bae, and Sungyoung Lee. Bimodal learning via trilogy of skip-connection deep networks for diabetic retinopathy risk progression identification. *International journal of medical informatics*, 132:103926, 2019.

[98] Gao Huang, Zhuang Liu, Laurens Van Der Maaten, and Kilian Q Weinberger. Densely connected convolutional networks. In *Proceedings of the IEEE conference on computer vision and pattern recognition*, pages 4700–4708, 2017.

[99] Tomasz Hyla and Jerzy Pejaś. Long-term verification of signatures based on a blockchain. *Computers & Electrical Engineering*, 81:106523, 2020.

[100] Sergey Ioffe and Christian Szegedy. Batch normalization: Accelerating deep network training by reducing internal covariate shift. *arXiv preprint arXiv:1502.03167*, 2015.

[101] Karim Jabbar and Pernille Bjørn. Growing the blockchain information infrastructure. In *Proceedings of the 2017 CHI Conference on Human Factors in Computing Systems*, pages 6487–6498, 2017.

[102] José Carlos Jaime-Pérez, Gisela García-Arellano, José Luis Herrera-Garza, Luis Javier Marfil-Rivera, and David Gómez-Almaguer. Revisiting the complete blood count and clinical findings at diagnosis of childhood acute lymphoblastic leukemia: 10-year experience at a single center. *Hematology, transfusion and cell therapy*, 41(1):57–61, 2019.

[103] Mahboubeh Jannesari, Mehdi Habibzadeh, Hamidreza Aboulkheyr, Pegah Khosravi, Olivier Elemento, Mehdi Totonchi, and Iman Hajirasouliha. Breast Cancer Histopathological Image Classification: A Deep Learning Approach. In *Proceedings - 2018 IEEE International Conference on Bioinformatics and Biomedicine, BIBM 2018*, 2019. doi:10.1109/BIBM.2018.8621307.

[104] Justin Johnson, Alexandre Alahi, and Li Fei-Fei. Perceptual losses for real-time style transfer and super-resolution. In *Lecture Notes in Computer Science (including subseries Lecture Notes in Artificial Intelligence and Lecture Notes in Bioinformatics)*, 2016. arXiv:1603.08155, doi:10.1007/978-3-319-46475-6_43.

[105] Sara Hosseinzadeh Kassani, Peyman Hosseinzadeh Kassani, Michal J. Wesolowski, Kevin A. Schneider, and Ralph Deters. A Hybrid Deep Learning Architecture for Leukemic B-lymphoblast Classification. In *ICTC 2019 - 10th International Conference on ICT Convergence: ICT Convergence Leading the Autonomous Future*, 2019. arXiv:1909.11866, doi:10.1109/ICTC46691.2019.8939959.

[106] Sara Hosseinzadeh Kassani, Peyman Hosseinzadeh Kassani, Michal J. Wesolowski, Kevin A. Schneider, and Ralph Deters. Classification of histopathological biopsy images using ensemble of deep learning networks. In *CASCON 2019 Proceedings - Conference of the Centre for Advanced Studies on Collaborative Research - Proceedings of the 29th Annual International Conference on Computer Science and Software Engineering*, 2020. arXiv:1909.11870.

[107] Sana Ullah Khan, Naveed Islam, Zahoor Jan, Ikram Ud Din, and Joel J.P.C. Rodrigues. A novel deep learning based framework for the detection and classification of breast cancer using transfer learning. *Pattern Recognition Letters*, 2019. doi:10.1016/j.patrec.2019.03.022.

[108] Brady Kieffer, Morteza Babaie, Shivam Kalra, and H. R. Tizhoosh. Convolutional neural networks for histopathology image classification: Training vs. Using pre-trained networks. In *Proceedings of the 7th International Conference on Image Processing Theory, Tools and Applications, IPTA 2017*, 2018. arXiv:1710.05726, doi:10.1109/IPTA.2017.8310149.

[109] Günter Klambauer, Thomas Unterthiner, Andreas Mayr, and Sepp Hochreiter. Self-normalizing neural networks. In *Advances in neural information processing systems*, pages 971–980, 2017.

[110] Onur Can Koyun and Tulay Yildirim. Adversarial Nuclei Segmentation on H&E Stained Histopathology Images. 2019. doi:10.1109/inista.2019.8778369.

[111] Alex Krizhevsky, Ilya Sutskever, and Geoffrey E Hinton. Imagenet classification with deep convolutional neural networks. In *Advances in neural information processing systems*, pages 1097–1105, 2012.

[112] Jakkrich Laosai and Kosin Chamnongthai. Classification of acute leukemia using medical-knowledge-based morphology and cd marker. *Biomedical Signal Processing and Control*, 44:127–137, 2018. URL: http://www.sciencedirect.com/science/article/pii/S1746809418300272, doi:https://doi.org/10.1016/j.bspc.2018.01.020.

[113] Fahad Lateef and Yassine Ruichek. Survey on semantic segmentation using deep learning techniques. *Neurocomputing*, 338:321–348, 2019. URL: http://www.sciencedirect.com/science/article/pii/S092523121930181X, doi:https://doi.org/10.1016/j.neucom.2019.02.003.

[114] Yann Lecun, Yoshua Bengio, and Geoffrey Hinton. Deep learning, 2015. arXiv:1807.07987, doi:10.1038/nature14539.

[115] Yann LeCun, Bernhard E Boser, John S Denker, Donnie Henderson, Richard E Howard, Wayne E Hubbard, and Lawrence D Jackel. Handwritten digit recognition with a back-propagation network. In *Advances in neural information processing systems*, pages 396–404, 1990.

[116] Yann LeCun, Léon Bottou, Yoshua Bengio, Patrick Haffner, et al. Gradient-based learning applied to document recognition. *Proceedings of the IEEE*, 86(11):2278–2324, 1998.

[117] Han Lee and Maode Ma. Blockchain-based mobility management for 5G. *Future Generation Computer Systems*, 2019. doi:10.1016/j.future.2019.08.008.

[118] Ao Lei, Yue Cao, Shihan Bao, Dasen Li, Philip Asuquo, Haitham Cruickshank, and Zhili Sun. A blockchain based certificate revocation scheme for vehicular communication systems. *Future Generation Computer Systems*, 2019.

[119] Kai Lei, Qichao Zhang, Limei Xu, and Zhuyun Qi. Reputation-based byzantine fault-tolerance for consortium blockchain. In *2018 IEEE 24th International Conference on Parallel and Distributed Systems (ICPADS)*, pages 604–611. IEEE, 2018.

[120] Chao Li, Xinggang Wang, Wenyu Liu, Longin Jan Latecki, Bo Wang, and Junzhou Huang. Weakly supervised mitosis detection in breast histopathology images using concentric loss. *Medical Image Analysis*, 53:165–178, 2019. URL: http://www.sciencedirect.com/science/article/pii/S1361841519300118, doi:https://doi.org/10.1016/j.media.2019.01.013.

[121] Chen Li, Hao Chen, Le Zhang, Ning Xu, Dan Xue, Zhijie Hu, He Ma, and Hongzan Sun. Cervical Histopathology Image Classification Using Multilayer Hidden Conditional Random Fields and Weakly Supervised Learning. *IEEE Access*, 2019. doi:10.1109/access.2019.2924467.

[122] Hua Li, Shasha Zhuang, Deng-ao Li, Jumin Zhao, and Yanyun Ma. Benign and malignant classification of mammogram images based on deep learning. *Biomedical Signal Processing and Control*, 51:347–354, 2019.

[123] Jiahui Li, Shuang Yang, Xiaodi Huang, Qian Da, Xiaoqun Yang, Zhiqiang Hu, Qi Duan, Chaofu Wang, and Hongsheng Li. Signet Ring Cell Detection with a Semi-supervised Learning Framework. In *Lecture Notes in Computer Science (including subseries Lecture Notes in Artificial Intelligence and Lecture Notes in Bioinformatics)*, 2019. arXiv:1907.03954, doi:10.1007/978-3-030-20351-1_66.

[124] Laquan Li, Xiangming Zhao, Wei Lu, and Shan Tan. Deep learning for variational multimodality tumor segmentation in pet/ct. *Neurocomputing*, 2019. URL: http://www.sciencedirect.com/science/article/pii/S0925231219304667, doi:https://doi.org/10.1016/j.neucom.2018.10.099.

[125] Ruidong Li, Hitoshi Asaeda, Jie Li, and Xiaoming Fu. A distributed authentication and authorization scheme for in-network big data sharing. *Digital Communications and Networks*, 3(4):226–235, 2017.

[126] Zhang Li, Zheyu Hu, Jiaolong Xu, Tao Tan, Hui Chen, Zhi Duan, Ping Liu, Jun Tang, Guoping Cai, Quchang Ouyang, et al. Computer-aided diagnosis of lung carcinoma using deep learning-a pilot study. *arXiv preprint arXiv:1803.05471*, 2018.

[127] Zhang Li, Jiehua Zhang, Tao Tan, Xichao Teng, Xiaoliang Sun, Yang Li, Lihong Liu, Yang Xiao, Byungjae Lee, Yilong Li, et al. Deep learning methods for lung cancer segmentation in whole-slide histopathology images–the acdc@ lunghp challenge 2019. *arXiv preprint arXiv:2008.09352*, 2020.

[128] Xueping Liang, Juan Zhao, Sachin Shetty, Jihong Liu, and Danyi Li. Integrating blockchain for data sharing and collaboration in mobile healthcare applications. In *IEEE International Symposium on Personal, Indoor and Mobile Radio Communications, PIMRC*, 2018. doi:10.1109/PIMRC.2017.8292361.

[129] Jinhua Lin, Lin Ma, and Yu Yao. A fourier domain acceleration framework for convolutional neural networks. *Neurocomputing*, 364:254–268, 2019. URL: http://www.sciencedirect.com/science/article/pii/S0925231219309932, doi:https://doi.org/10.1016/j.neucom.2019.06.080.

[130] Yisi Liu, Xiaojun Wang, Lei Wang, and Dongliang Liu. A modified leaky relu scheme (mlrs) for topology optimization with multiple materials. *Applied Mathematics and Computation*, 352:188–204, 2019.

[131] Qinghua Lu, Xiwei Xu, Yue Liu, Ingo Weber, Liming Zhu, and Weishan Zhang. ubaas: A unified blockchain as a service platform. *Future Generation Computer Systems*, 101:564–575, 2019. URL: http://www.sciencedirect.com/science/article/pii/S0167739X18319873, doi:https://doi.org/10.1016/j.future.2019.05.051.

[132] Siyuan Lu, Zhihai Lu, and Yu-Dong Zhang. Pathological brain detection based on alexnet and transfer learning. *Journal of Computational Science*, 30:41–47, 2019. URL: http://www.sciencedirect.com/science/article/pii/S1877750318309116, doi:https://doi.org/10.1016/j.jocs.2018.11.008.

[133] Yang Lu. The blockchain: State-of-the-art and research challenges. *Journal of Industrial Information Integration*, 15:80–90, 2019. URL: http://www.sciencedirect.com/science/article/pii/S2452414X19300019, doi:https://doi.org/10.1016/j.jii.2019.04.002.

[134] Sai Ma and Fulei Chu. Ensemble deep learning-based fault diagnosis of rotor bearing systems. *Computers in Industry*, 105:143–152, 2019. URL: http://www.sciencedirect.com/science/article/pii/S0166361518304731, doi:https://doi.org/10.1016/j.compind.2018.12.012.

[135] Marc Macenko, Marc Niethammer, James S Marron, David Borland, John T Woosley, Xiaojun Guan, Charles Schmitt, and Nancy E Thomas. A method for normalizing histology slides for quantitative analysis. In *2009 IEEE International Symposium on Biomedical Imaging: From Nano to Macro*, pages 1107–1110. IEEE, 2009.

[136] Faisal Mahmood, Daniel Borders, Richard Chen, Gregory N. McKay, Kevan J. Salimian, Alexander Baras, and Nicholas J. Durr. Deep Adversarial Training for Multi-Organ Nuclei Segmentation in Histopathology Images. *IEEE Transactions on Medical Imaging*, 2019. arXiv:1810.00236, doi:10.1109/tmi.2019.2927182.

[137] Andreas Maier, Christopher Syben, Tobias Lasser, and Christian Riess. A gentle introduction to deep learning in medical image processing. *Zeitschrift für Medizinische Physik*, 29(2):86–101, 2019. URL: http://www.sciencedirect.com/science/article/pii/S093938891830120X, doi:https://doi.org/10.1016/j.zemedi.2018.12.003.

[138] Imran Makhdoom, Mehran Abolhasan, Haider Abbas, and Wei Ni. Blockchain's adoption in IoT: The challenges, and a way forward, 2019. doi:10.1016/j.jnca.2018.10.019.

[139] Angela B Mariotto, K Robin Yabroff, Yongwu Shao, Eric J Feuer, and Martin L Brown. Projections of the cost of cancer care in the united states: 2010–2020. *Journal of the National Cancer Institute*, 103(2):117–128, 2011.

[140] Nissa Mehibel and M'Hamed Hamadouche. A new approach of elliptic curve diffie-hellman key exchange. In *2017 5th International Conference on Electrical Engineering-Boumerdes (ICEE-B)*, pages 1–6. IEEE, 2017.

[141] Anna Meldo, Lev Utkin, Maxim Kovalev, and Ernest Kasimov. The natural language explanation algorithms for the lung cancer computer-aided diagnosis system. *Artificial Intelligence in Medicine*, 108:101952, 2020.

[142] Pim Moeskops, Max A Viergever, Adriënne M Mendrik, Linda S de Vries, Manon JNL Benders, and Ivana Išgum. Automatic segmentation of mr brain images with a convolutional neural network. *IEEE transactions on medical imaging*, 35(5):1252–1261, 2016.

[143] Hend Mohamed, Rowan Omar, Nermeen Saeed, Ali Essam, Nada Ayman, Taraggy Mohiy, and Ashraf AbdelRaouf. Automated detection of white blood cells cancer diseases. In *2018 First International Workshop on Deep and Representation Learning (IWDRL)*, pages 48–54. IEEE, March 2018. URL: https://ieeexplore.ieee.org/document/8358214/, doi:10.1109/IWDRL.2018.8358214.

[144] Bhabendu Kumar Mohanta, Soumyashree S Panda, and Debasish Jena. An overview of smart contract and use cases in blockchain technology. In *2018 9th International Conference on Computing, Communication and Networking Technologies (ICCCNT)*, pages 1–4. IEEE, 2018.

[145] Subrajeet Mohapatra, Dipti Patra, and Sanghamitra Satpathy. An ensemble classifier system for early diagnosis of acute lymphoblastic leukemia in blood microscopic images. *Neural Computing and Applications*, 2014. doi:10.1007/s00521-013-1438-3.

[146] Sana Moin, Ahmad Karim, Zanab Safdar, Kalsoom Safdar, Ejaz Ahmed, and Muhammad Imran. Securing IoTs in distributed blockchain: Analysis, requirements and open issues. *Future Generation Computer Systems*, 2019. doi:10.1016/j.future.2019.05.023.

[147] Shakiba Moradi, Mostafa Ghelich Oghli, Azin Alizadehasl, Isaac Shiri, Niki Oveisi, Mehrdad Oveisi, Majid Maleki, and Jan Dhooge. Mfp-unet: A novel deep learning based approach for left ventricle segmentation in echocardiography. *Physica Medica*, 67:58–69, 2019.

[148] Mahmoud Mostapha and Martin Styner. Role of deep learning in infant brain MRI analysis, 2019. doi:10.1016/j.mri.2019.06.009.

[149] Simmi Mourya, Sonaal Kant, Pulkit Kumar, Anubha Gupta, and Ritu Gupta. LeukoNet: DCT-based CNN architecture for the classification of normal versus Leukemic blasts in B-ALL Cancer. October 2018. URL: http://arxiv.org/abs/1810.07961, arXiv:1810.07961.

[150] Satoshi Nakamoto et al. Bitcoin: A peer-to-peer electronic cash system. 2008.

[151] Sujata Narayanan and Paul J Shami. Treatment of acute lymphoblastic leukemia in adults. *Critical reviews in oncology/hematology*, 81(1):94–102, 2012.

[152] Christopher Natoli and Vincent Gramoli. The balance attack or why forkable blockchains are ill-suited for consortium. In *2017 47th Annual IEEE/IFIP International Conference on Dependable Systems and Networks (DSN)*, pages 579–590. IEEE, 2017.

[153] Dinh C. Nguyen, Pubudu N. Pathirana, Ming Ding, and Aruna Seneviratne. Blockchain for Secure EHRs Sharing of Mobile Cloud Based E-Health Systems. *IEEE Access*, 2019. doi:10.1109/ACCESS.2019.2917555.

[154] Oscar Novo. Blockchain Meets IoT: An Architecture for Scalable Access Management in IoT. *IEEE Internet of Things Journal*, 2018. doi:10.1109/JIOT.2018.2812239.

[155] Ayse Betul Oktay and Anıl Gurses. Automatic detection, localization and segmentation of nanoparticles with deep learning in microscopy images. *Micron*, 120:113–119, 2019. URL: http://www.sciencedirect.com/science/article/pii/S0968432818304013, doi:https://doi.org/10.1016/j.micron.2019.02.009.

[156] Américo Oliveira, Sergio Pereira, and Carlos A Silva. Retinal vessel segmentation based on fully convolutional neural networks. *Expert Systems with Applications*, 112:229–242, 2018.

[157] Ahmet Haydar Ornek, Murat Ceylan, and Saim Ervural. Health status detection of neonates using infrared thermography and deep convolutional neural networks. *Infrared Physics & Technology*, page 103044, 2019.

[158] Patrick Orth, Carolin Peifer, Lars Goebel, Magali Cucchiarini, and Henning Madry. Comprehensive analysis of translational osteochondral repair: Focus on the histological assessment. *Progress in histochemistry and cytochemistry*, 50(3):19–36, 2015.

[159] Shantanu Pal, Tahiry Rabehaja, Michael Hitchens, Vijay Varadharajan, and Ambrose Hill. On the Design of a Flexible Delegation Model for the Internet of Things Using Blockchain. *IEEE Transactions on Industrial Informatics*, 2019. doi:10.1109/tii.2019.2925898.

[160] Nimesh Patel and Ashutosh Mishra. Automated leukaemia detection using microscopic images. *Procedia Computer Science*, 58:635–642, 2015. Second International Symposium on Computer Vision and the Internet (VisionNet'15). URL: http://www.sciencedirect.com/science/article/pii/S1877050915021936, doi:https://doi.org/10.1016/j.procs.2015.08.082.

[161] Oscar Perdomo, Hernán Rios, Francisco J. Rodríguez, Sebastián Otálora, Fabrice Meriaudeau, Henning Müller, and Fabio A. González. Classification of diabetes-related retinal diseases using a deep learning approach in optical coherence tomography. *Computer Methods and Programs in Biomedicine*, 178:181–189, 2019. URL: http://www.sciencedirect.com/science/article/pii/S0169260718318686, doi:https://doi.org/10.1016/j.cmpb.2019.06.016.

[162] Hoa Hoang Ngoc Pham, Mitsuru Futakuchi, Andrey Bychkov, Tomoi Furukawa, Kishio Kuroda, and Junya Fukuoka. Detection of lung cancer lymph node metastases from whole-slide histopathologic images using a two-step deep learning approach. *The American journal of pathology*, 189(12):2428–2439, 2019.

[163] Tri-Cong Pham, Chi-Mai Luong, Muriel Visani, and Van-Dung Hoang. Deep cnn and data augmentation for skin lesion classification. In *Asian Conference on Intelligent Information and Database Systems*, pages 573–582. Springer, 2018.

[164] Sawon Pratiher and Subhankar Chattoraj. Diving deep onto discriminative ensemble of histological hashing & class-specific manifold learning for multi-class breast carcinoma taxonomy. In *ICASSP 2019-2019 IEEE International Conference on Acoustics, Speech and Signal Processing (ICASSP)*, pages 1025–1029. IEEE, 2019.

[165] Harsha S.Gardiyawasam Pussewalage and Vladimir A. Oleshchuk. Blockchain Based Delegatable Access Control Scheme for a Collaborative E-Health Environment. In *Proceedings - IEEE 2018 International Congress on Cybermatics: 2018 IEEE Conferences on Internet of Things, Green Computing and Communications, Cyber, Physi-*

cal and Social Computing, Smart Data, Blockchain, Computer and Information Technology, iThings/GreenCom/CPSCom/SmartData/Blockchain/CIT 2018, 2018. doi:10.1109/Cybermatics_2018.2018.00214.

[166] Talha Qaiser, Yee-Wah Tsang, Daiki Taniyama, Naoya Sakamoto, Kazuaki Nakane, David Epstein, and Nasir Rajpoot. Fast and accurate tumor segmentation of histology images using persistent homology and deep convolutional features. *Medical image analysis*, 55:1–14, 2019.

[167] Hui Qu, Gregory Riedlinger, Pengxiang Wu, Qiaoying Huang, Jingru Yi, Subhajyoti De, and Dimitris Metaxas. Joint Segmentation and Fine-Grained Classification of Nuclei in Histopathology Images. 2019. doi:10.1109/isbi.2019.8759457.

[168] El-Houssainy A. Rady and Ayman S. Anwar. Prediction of kidney disease stages using data mining algorithms. *Informatics in Medicine Unlocked*, 15:100178, 2019. URL: http://www.sciencedirect.com/science/article/pii/S2352914818302387, doi:https://doi.org/10.1016/j.imu.2019.100178.

[169] Duggal Rahul, Gupta Anubha, and Ritu Gupta. Segmentation of overlapping/touching white blood cell nuclei using artificial neural networks. *CME Series on Hemato-Oncopathology, All India Institute of Medical Sciences (AIIMS)*, 2016.

[170] Mayank Raikwar, Danilo Gligoroski, and Katina Kralevska. Sok of used cryptography in blockchain. *IEEE Access*, 7:148550–148575, 2019.

[171] Ahmed Raza Rajput, Qianmu Li, Milad Taleby Ahvanooey, and Isma Masood. EACMS: Emergency Access Control Management System for Personal Health Record Based on Blockchain. *IEEE Access*, 2019. doi:10.1109/ACCESS.2019.2917976.

[172] Vidhya Ramani, Tanesh Kumar, An Bracken, Madhusanka Liyanage, and Mika Ylianttila. Secure and Efficient Data Accessibility in Blockchain Based Healthcare Systems. In *2018 IEEE Global Communications Conference, GLOBECOM 2018 - Proceedings*, 2018. doi:10.1109/GLOCOM.2018.8647221.

[173] Daniele Ravì, Charence Wong, Fani Deligianni, Melissa Berthelot, Javier Andreu-Perez, Benny Lo, and Guang-Zhong Yang. Deep learning for health informatics. *IEEE journal of biomedical and health informatics*, 21(1):4–21, 2016.

[174] Erik Reinhard, Michael Adhikhmin, Bruce Gooch, and Peter Shirley. Color transfer between images. *IEEE Computer graphics and applications*, 21(5):34–41, 2001.

[175] Ana Reyna, Cristian Martín, Jaime Chen, Enrique Soler, and Manuel Díaz. On blockchain and its integration with iot. challenges and opportunities. *Future Generation Computer Systems*, 88:173–190, 2018.

[176] Md Shamim Reza and Jinwen Ma. Imbalanced histopathological breast cancer image classification with convolutional neural network. In *International Conference on Signal Processing Proceedings, ICSP*, 2019. doi:10.1109/ICSP.2018.8652304.

[177] Stephanie Robertson, Hossein Azizpour, Kevin Smith, and Johan Hartman. Digital image analysis in breast pathology—from image processing techniques to artificial intelligence. *Translational Research*, 194:19–35, 2018.

[178] Olaf Ronneberger, Philipp Fischer, and Thomas Brox. U-net: Convolutional networks for biomedical image segmentation. In *International Conference on Medical image computing and computer-assisted intervention*, pages 234–241. Springer, 2015.

[179] F. Rosenblatt. The perceptron: A probabilistic model for information storage and organization in the brain. *Psychological Review*, 1958. doi:10.1037/h0042519.

[180] Kaushiki Roy, Debapriya Banik, Debotosh Bhattacharjee, and Mita Nasipuri. Patch-based system for classification of breast histology images using deep learning. *Computerized Medical Imaging and Graphics*, 71:90–103, 2019. URL: http://www.sciencedirect.com/science/article/pii/S0895611118302039, doi:https://doi.org/10.1016/j.compmedimag.2018.11.003.

[181] Sebastian Ruder. An overview of gradient descent optimization algorithms. *arXiv preprint arXiv:1609.04747*, 2016.

[182] Lakshmi Siva Sankar, M Sindhu, and M Sethumadhavan. Survey of consensus protocols on blockchain applications. In *2017 4th International Conference on Advanced Computing and Communication Systems (ICACCS)*, pages 1–5. IEEE, 2017.

[183] M. Santin, C. Brama, H. Théro, E. Ketheeswaran, I. El-Karoui, F. Bidault, R. Gillet, P. Gondim Teixeira, and A. Blum. Detecting abnormal thyroid cartilages on ct using deep learning. *Diagnostic and Interventional Imaging*, 100(4):251–257, 2019. URL: http://www.sciencedirect.com/science/article/pii/S2211568419300300, doi:https://doi.org/10.1016/j.diii.2019.01.008.

[184] Mukesh Saraswat and KV Arya. Automated microscopic image analysis for leukocytes identification: A survey. *Micron*, 65:20–33, 2014.

[185] M Sarıgül, BM Ozyildirim, and M Avci. Differential convolutional neural network. *Neural Networks*, 116:279–287, 2019.

[186] Yian Seo and Kyung-shik Shin. Hierarchical convolutional neural networks for fashion image classification. *Expert Systems with Applications*, 116:328–339, 2019.

[187] Wei Shao, Zhi Wang, Xiaolu Wang, Kefan Qiu, Chunfu Jia, and Chong Jiang. Lsc: Online auto-update smart contracts for fortifying blockchain-based log systems. *Information Sciences*, 2019.

[188] Rakesh Shrestha, Rojeena Bajracharya, Anish P Shrestha, and Seung Yeob Nam. A new-type of blockchain for secure message exchange in vanet. *Digital Communications and Networks*, 2019.

[189] Karen Simonyan and Andrew Zisserman. Very deep convolutional networks for large-scale image recognition. *arXiv preprint arXiv:1409.1556*, 2014.

[190] Amritraj Singh, Reza M Parizi, Qi Zhang, Kim-Kwang Raymond Choo, and Ali Dehghantanha. Blockchain smart contracts formalization: Approaches and challenges to address vulnerabilities. *Computers & Security*, page 101654, 2019.

[191] Vanika Singhal and Preety Singh. Local Binary Pattern for automatic detection of Acute Lymphoblastic Leukemia. In *2014 20th National Conference on Communications, NCC 2014*, 2014. doi:10.1109/NCC.2014.6811261.

[192] Hyun Min Song, Jiyoung Woo, and Huy Kang Kim. In-vehicle network intrusion detection using deep convolutional neural network. *Vehicular Communications*, 21:100198, 2020. URL: http://www.sciencedirect.com/science/article/pii/S2214209619302451, doi:https://doi.org/10.1016/j.vehcom.2019.100198.

[193] Fabio Alexandre Spanhol, Luiz S Oliveira, Caroline Petitjean, and Laurent Heutte. Breast cancer histopathological image classification using convolutional neural networks. In *2016 international joint conference on neural networks (IJCNN)*, pages 2560–2567. IEEE, 2016.

[194] Nitish Srivastava, Geoffrey Hinton, Alex Krizhevsky, Ilya Sutskever, and Ruslan Salakhutdinov. Dropout: a simple way to prevent neural networks from overfitting. *The Journal of Machine Learning Research*, 15(1):1929–1958, 2014.

[195] Andrew P Stein, Robin E Norris, and Jay R Shah. Pediatric acute lymphoblastic leukemia presenting with periorbital edema. *Otolaryngology Case Reports*, 9:11–14, 2018.

[196] You Sun, Rui Zhang, Xin Wang, Kaiqiang Gao, and Ling Liu. A decentralizing attribute-based signature for healthcare blockchain. In *Proceedings - International Conference on Computer Communications and Networks, ICCCN*, 2018. doi:10.1109/ICCCN.2018.8487349.

[197] Christian Szegedy, Sergey Ioffe, Vincent Vanhoucke, and Alexander A. Alemi. Inception-v4, inception-ResNet and the impact of residual connections on learning. In *31st AAAI Conference on Artificial Intelligence, AAAI 2017*, 2017. arXiv:1602.07261.

[198] Christian Szegedy, Wei Liu, Yangqing Jia, Pierre Sermanet, Scott Reed, Dragomir Anguelov, Dumitru Erhan, Vincent Vanhoucke, and Andrew Rabinovich. Going deeper with convolutions. In *Proceedings of the IEEE conference on computer vision and pattern recognition*, pages 1–9, 2015.

[199] Christian Szegedy, Vincent Vanhoucke, Sergey Ioffe, Jon Shlens, and Zbigniew Wojna. Rethinking the Inception Architecture for Computer Vision. In *Proceedings of the IEEE Computer Society Conference on Computer Vision and Pattern Recognition*, 2016. arXiv:1512.00567, doi:10.1109/CVPR.2016.308.

[200] Huimin Tang, Yong Shi, and Peiwu Dong. Public blockchain evaluation using entropy and topsis. *Expert Systems with Applications*, 117:204–210, 2019.

[201] Michael C. Thomas, Wenbo Zhu, and Jose A. Romagnoli. Data mining and clustering in chemical process databases for monitoring and knowledge discovery. *Journal of Process Control*, 67:160–175, 2018. Big Data: Data Science for Process Control and Operations. URL: http://www.sciencedirect.com/science/article/pii/S095915241730032X, doi:https://doi.org/10.1016/j.jprocont.2017.02.006.

[202] Thein Than Thwin and Sangsuree Vasupongayya. Blockchain Based Secret-Data Sharing Model for Personal Health Record System. In *ICAICTA 2018 - 5th International Conference on Advanced Informatics: Concepts Theory and Applications*, 2018. doi:10.1109/ICAICTA.2018.8541296.

[203] Thanh Tran, Oh-Heum Kwon, Ki-Ryong Kwon, Suk-Hwan Lee, and Kyung-Won Kang. Blood cell images segmentation using deep learning semantic segmentation. In *2018 IEEE International Conference on Electronics and Communication Engineering (ICECE)*, pages 13–16. IEEE, 2018.

[204] Philipp Tschandl, Cliff Rosendahl, and Harald Kittler. Data descriptor: The HAM10000 dataset, a large collection of multi-source dermatoscopic images of common pigmented skin lesions. *Scientific Data*, 2018. doi:10.1038/sdata.2018.161.

[205] Sadaqat ur Rehman, Shanshan Tu, Muhammad Waqas, Yongfeng Huang, Obaid ur Rehman, Basharat Ahmad, and Salman Ahmad. Unsupervised pre-trained filter learning approach for efficient convolution neural network. *Neurocomputing*, 365:171–190, 2019. URL: http://www.sciencedirect.com/science/article/pii/S0925231219309981, doi:https://doi.org/10.1016/j.neucom.2019.06.084.

[206] Abhishek Vahadane, Tingying Peng, Shadi Albarqouni, Maximilian Baust, Katja Steiger, Anna Melissa Schlitter, Amit Sethi, Irene Esposito, and Nassir Navab. Structure-preserved color normalization for histological images. In *2015 IEEE 12th International Symposium on Biomedical Imaging (ISBI)*, pages 1012–1015. IEEE, 2015.

[207] Yves-Rémi Van Eycke, Cédric Balsat, Laurine Verset, Olivier Debeir, Isabelle Salmon, and Christine Decaestecker. Segmentation of glandular epithelium in colorectal tumours to automatically compartmentalise ihc biomarker quantification: A deep learning approach. *Medical image analysis*, 49:35–45, 2018.

[208] Roland van Rijswijk-Deij, Anna Sperotto, and Aiko Pras. Making the case for elliptic curves in dnssec. *ACM SIGCOMM computer communication review*, 45(5):13–19, 2015.

[209] Bastiaan S Veeling, Jasper Linmans, Jim Winkens, Taco Cohen, and Max Welling. Rotation equivariant cnns for digital pathology. In *International Conference on Medical image computing and computer-assisted intervention*, pages 210–218. Springer, 2018.

[210] Duc My Vo, Ngoc-Quang Nguyen, and Sang-Woong Lee. Classification of breast cancer histology images using incremental boosting convolution networks. *Information Sciences*, 482:123–138, 2019. URL: http://www.sciencedirect.com/science/article/pii/S0020025518310466, doi:https://doi.org/10.1016/j.ins.2018.12.089.

[211] Luis H.S. Vogado, Rodrigo M.S. Veras, Flavio. H.D. Araujo, Romuere R.V. Silva, and Kelson R.T. Aires. Leukemia diagnosis in blood slides using transfer learning in cnns and svm for classification. *Engineering Applications of Artificial Intelligence*, 72:415–422, 2018. URL: http://www.sciencedirect.com/science/article/pii/S0952197618301039, doi:https://doi.org/10.1016/j.engappai.2018.04.024.

[212] Hao Wang, Shenglan Ma, Hong-Ning Dai, Muhammad Imran, and Tongsen Wang. Blockchain-based data privacy management with nudge theory in open banking. *Future Generation Computer Systems*, 2019.

[213] Licheng Wang, Xiaoying Shen, Jing Li, Jun Shao, and Yixian Yang. Cryptographic primitives in blockchains. *Journal of Network and Computer Applications*, 127:43–58, 2019.

[214] Shangping Wang, Dan Zhang, and Yaling Zhang. Blockchain-Based Personal Health Records Sharing Scheme With Data Integrity Verifiable. *IEEE Access*, 2019. doi:10.1109/access.2019.2931531.

[215] Kelvin Wong, Giancarlo Fortino, and Derek Abbott. Deep learning-based cardiovascular image diagnosis: A promising challenge. *Future Generation Computer Systems*, 2019.

[216] Chunzhi Wu, Pengcheng Jiang, Chuang Ding, Fuzhou Feng, and Tang Chen. Intelligent fault diagnosis of rotating machinery based on one-dimensional convolutional neural network. *Computers in Industry*, 108:53–61, 2019.

[217] Pengxiang Wu, Hui Qu, Jingru Yi, Qiaoying Huang, Chao Chen, and Dimitris Metaxas. Deep Attentive Feature Learning for Histopathology Image Classification. 2019. doi:10.1109/isbi.2019.8759267.

[218] Min Xia, Wan'an Liu, Ke Wang, Xu Zhang, and Yiqing Xu. Non-intrusive load disaggregation based on deep dilated residual network. *Electric Power Systems Research*, 2019. doi:10.1016/j.epsr.2019.01.034.

[219] Qi Xia, Emmanuel Boateng Sifah, Kwame Omono Asamoah, Jianbin Gao, Xiaojiang Du, and Mohsen Guizani. MeDShare: Trust-Less Medical Data Sharing among Cloud Service Providers via Blockchain. *IEEE Access*, 2017. doi:10.1109/ACCESS.2017.2730843.

[220] Zhe Xiao, Zengxiang Li, Yong Liu, Ling Feng, Weiwen Zhang, Thanarit Lertwuthikarn, and Rick Siow Mong Goh. EMRShare: A Cross-Organizational Medical Data Sharing and Management Framework Using Permissioned Blockchain. In *Proceedings of the International Conference on Parallel and Distributed Systems - ICPADS*, 2019. doi:10.1109/PADSW.2018.8645049.

[221] Hongming Xu, Cheng Lu, Richard Berendt, Naresh Jha, and Mrinal Mandal. Automated analysis and classification of melanocytic tumor on skin whole slide images. *Computerized Medical Imaging and Graphics*, 66:124–134, 2018.

[222] Jie Xu, Kaiping Xue, Shaohua Li, Hangyu Tian, Jianan Hong, Peilin Hong, and Nenghai Yu. Healthchain: A Blockchain-based Privacy Preserving Scheme for Large-scale Health Data. *IEEE Internet of Things Journal*, 2019. doi:10.1109/jiot.2019.2923525.

[223] Ronghua Xu, Yu Chen, Erik Blasch, and Genshe Chen. Blendcac: A blockchain-enabled decentralized capability-based access control for iots. In *Proceedings - IEEE 2018 International Congress on Cybermatics: 2018 IEEE Conferences on Internet of Things, Green Computing and Communications, Cyber, Physical and Social Computing, Smart Data, Blockchain, Computer and Information Technology, iThings/GreenCom/CPSCom/SmartData/Blockchain/CIT 2018*, 2018. arXiv:1804.09267, doi:10.1109/Cybermatics_2018.2018.00191.

[224] Huihui Yang and Bian Yang. A Blockchain-based Approach to the Secure Sharing of Healthcare Data. *Norwgian Information Security Conference*, 2017.

[225] Zikai Yao, Deqiang He, Yanjun Chen, Bin Liu, Jian Miao, Jianxin Deng, and Sheng Shan. Inspection of exterior substance on high-speed train bottom based on improved deep learning method. *Measurement*, page 108013, 2020.

[226] Abbas Yazdinejad, Reza M Parizi, Ali Dehghantanha, and Kim-Kwang Raymond Choo. P4-to-blockchain: A secure blockchain-enabled packet parser for software defined networking. *Computers & Security*, 88:101629, 2020.

[227] Changqian Yu, Jingbo Wang, Chao Peng, Changxin Gao, Gang Yu, and Nong Sang. Learning a Discriminative Feature Network for Semantic Segmentation. In *Proceedings of the IEEE Computer Society Conference on Computer Vision and Pattern Recognition*, 2018. arXiv:1804.09337, doi:10.1109/CVPR.2018.00199.

[228] Xinjie Yu, Huanda Lu, and Di Wu. Development of deep learning method for predicting firmness and soluble solid content of postharvest korla fragrant pear using vis/nir hyperspectral reflectance imaging. *Postharvest Biology and Technology*, 141:39–49, 2018.

[229] Yue Yu, Sheng Zhang, Chao Chen, and Xiaoxiong Zhong. LVChain: A Lightweight and Vote-based Blockchain for Access Control in the IoT. 2019. doi:10.1109/compcomm.2018.8780687.

[230] Zhen Yu, Xudong Jiang, Tianfu Wang, and Baiying Lei. Aggregating deep convolutional features for melanoma recognition in dermoscopy images. In Qian Wang, Yinghuan Shi, Heung-Il Suk, and Kenji Suzuki, editors, *Machine Learning in Medical Imaging*, pages 238–246, Cham, 2017. Springer International Publishing.

[231] Matthew D Zeiler and Rob Fergus. Visualizing and understanding convolutional networks. In *European conference on computer vision*, pages 818–833. Springer, 2014.

[232] Zitao Zeng, Weihao Xie, Yunzhe Zhang, and Yao Lu. RIC-Unet: An Improved Neural Network Based on Unet for Nuclei Segmentation in Histology Images. *IEEE Access*, 2019. doi:10.1109/ACCESS.2019.2896920.

[233] Aiqing Zhang and Xiaodong Lin. Towards secure and privacy-preserving data sharing in e-health systems via consortium blockchain. *Journal of medical systems*, 42(8):140, 2018.

[234] Lingyue Zhang, Huilin Li, Yannan Li, Yong Yu, Man Ho Au, and Baocang Wang. An efficient linkable group signature for payer tracing in anonymous cryptocurrencies. *Future Generation Computer Systems*, 2019.

[235] Peng Zhang, Douglas C. Schmidt, Jules White, and Abhishek Dubey. Chapter seven - consensus mechanisms and information security technologies. In Shiho Kim, Ganesh Chandra Deka, and Peng Zhang, editors, *Role of Blockchain Technology in IoT Applications*, volume 115 of *Advances in Computers*, pages 181–209. Elsevier, 2019. URL: http://www.sciencedirect.com/science/article/pii/S0065245819300245, doi:https://doi.org/10.1016/bs.adcom.2019.05.001.

[236] Shijie Zhang and Jong-Hyouk Lee. Analysis of the main consensus protocols of blockchain. *ICT Express*, 2019. doi:10.1016/j.icte.2019.08.001.

[237] Shijie Zhang and Jong-Hyouk Lee. Eclipse-based stake-bleeding attacks in pos blockchain systems. In *Proceedings of the 2019 ACM International Symposium on Blockchain and Secure Critical Infrastructure*, pages 67–72, 2019.

[238] Xiaoshuai Zhang and Stefan Poslad. Blockchain Support for Flexible Queries with Granular Access Control to Electronic Medical Records (EMR). In *IEEE International Conference on Communications*, 2018. doi:10.1109/ICC.2018.8422883.

[239] Yuanyu Zhang, Shoji Kasahara, Yulong Shen, Xiaohong Jiang, and Jianxiong Wan. Smart contract-based access control for the internet of things. *IEEE Internet of Things Journal*, 2019. arXiv:1802.04410, doi:10.1109/JIOT.2018.2847705.

[240] Yuanyuan Zhou, Ji Zhang, Jiao Huang, Kaifei Deng, Jianhua Zhang, Zhiqiang Qin, Zhenyuan Wang, Xiaofeng Zhang, Ya Tuo, Liqin Chen, et al. Digital whole-slide image analysis for automated diatom test in forensic cases of drowning using a convolutional neural network algorithm. *Forensic science international*, 302:109922, 2019.

[241] Xiaobin Zhu, Zun Cai, Jianjun Wu, Yuqiang Cheng, and Qiang Huang. Convolutional neural network based combustion mode classification for condition monitoring in the supersonic combustor. *Acta Astronautica*, 159:349–357, 2019.